Formability of Multi-matrix Composites

By

MARK A. TURK

Department of Aerospace Engineering
UNIVERSITY OF BRISTOL

A dissertation submitted to the University of Bristol in accordance with the requirements of the degree of DOCTOR OF PHILOSOPHY in the Faculty of Engineering.

MAY 2022

Word count: 48,396

Abstract

Multifunctionality in composites is a developing area of research which shows much promise for the production of efficient and integrated structural designs [1], [2]. Incorporating further functionality criteria on top of the basic requirement for structural strength provides a range of possibilities for weight saving. Formability of functionalized preforms has not yet been fully explored and presents the main subject of this thesis.

Most current development in multifunctional composites is focussed around functional materials. However, often functionalization, i.e. by incorporating micro/nano-additives, makes materials less compliant, handleable, or formable. An alternative approach explored in this thesis is to create multifunctional structures by separating the domains. The creation of multi-matrix structures, where two matrix materials occupy separate zones of a continuous fabric, is a relatively unexplored field with no established manufacturing process. The primary benefit is the ability to provide multifunctionality in carefully tailored regions, allowing the manufacturer to designate areas as either multifunctional or purely structural based on design requirements. This is especially relevant when the multifunctional component inhibits formability, requiring the addition of flexible 'hinges' between multifunctional regions. This thesis tackles many of the manufacturing hurdles and presents an effective technique for the creation of such structures. This work constitutes a part of the EPSRC Hub project on the manufacturing of multifunctional composites, where the contribution of this thesis focuses on the application of this technique towards enhancing the formability of structural supercapacitors This is developed in collaboration with Imperial College London, who have pioneered the development of structural supercapacitors.

Multifunctional elements tend to inhibit formability, however their introduction can also be used to improve forming if applied wisely, the modification of textile properties in regions where a defect is likely to form can lead to formability enhancement. Forming of dry fibre textile pre-forms is a commonly used technique to achieve complex shapes for light weight composite structures. Most conventional engineering fabrics can only deform through shearing. Excessive shearing often results in the formation of detrimental features, such as wrinkles, folds and fabric distortions. Modification can be achieved by the integration of patches: additional materials, such as reactive thermally-conditioned resins, tufted or stitched yarns, thermoplastic films, locally activated binder, etc. This method is simple and effective for a certain class of forming problems. Once formed the primary structural resin is added and the patch material becomes a part of the finished component. The success of the forming operation depends on the balance of properties between dry and patched materials. This thesis shows the feasibility of improving formability by local modification of preforms and explores various numerical modelling tools for optimising this process. Modification is implemented by depositing localised resin patches onto textile preforms. The technique allows for continuity of fibres throughout the preform with the additional benefit that the deposited resin can be thermally staged to the desired level of cure to tune the viscosity of the region for forming and consolidation. The location and dimensions of patches are specified through numerical modelling to inform the subsequent manufacturing process. Manufacturing trials successfully demonstrate the possibility of defect mitigation using this technique.

Dedication and Acknowledgements

The author gratefully acknowledges the support of the EPSRC through the Future Composites Manufacturing Research Hub [EP/P006701/1] which funded this project, along with the EPSRC Platform Grant [EP/P027350/1] SIMulation of new manufacturing PROcesses for Composite Structures (SIMPROCS) which funded the work that laid the foundations for this project.

Special thanks to Dr Dmitry Ivanov for constant guidance, support and enthusiasm as my lead supervisor and to Dr Jonathan Belnoue and Dr Adam Thompson for their regular input and guidance.

Thanks also to my secondary supervisor Prof Ivana Partridge and to Prof Stephen Hallett for their support and encouragement.

Thanks to my colleagues at Imperial College London; Prof Emile Greenhalgh, Prof Milo Shaffer, Dr David Anthony, Dr Sang Nguyen and Dr Maria Valkova for constructive collaboration throughout.

Thanks to Dr Michael Elkington, Dr Bethany Russell, Dr Arjun Radhakrishnan, Dr Yi Wang, Dr Caroline O'Keeffe, Hengli Cao, Dr Ian Gent, Dr Laura Pickard, Ian Chorley and Henry Redman for advice, instruction and assistance.

Author’s Declaration

The accompanying dissertation entitled ‘Formability of Multi-matrix composites’ is submitted in support for an application for the degree of Doctor of Philosophy in Engineering to the University of Bristol.

I declare that the work in this dissertation was carried out in accordance with the requirements of the University's Regulations and Code of Practice for Research Degree Programmes and that it has not been submitted for any other academic award. Except where indicated by specific reference in the text, the work is the candidate's own work. Work done in collaboration with, or with the assistance of, others, is indicated as such. Any views expressed in the dissertation are those of the author.

SIGNED: ……..... DATE: …….....

Publications

Journal Papers

1. Turk M A, Vermes B, Thompson A J, Belnoue J P H, Hallett S R and Ivanov D S. Mitigating forming defects by local modification of dry preforms Compos. Part A Appl. Sci. Manuf. 128. 2020.

2. Turk M A, Cao H, Thompson A J, Belnoue J P H, Hallett S R and Ivanov D S. A New approach to Measuring Local Properties of Preforms Enhanced for Formability. Frontiers In Materials, Mechanics of Materials. 2022.

Conference Papers

1. Turk M A, Vermes B, Thompson A J, Belnoue J P H, Hallett S R and Ivanov D S Optimising the placement of localised resin patches to enhance the formability of dry preforms Euromech Colloquium 602 Composite Manufacturing Processes Analyses, Modelling and Simulations 13 March – 15 March 2019, Lyon, France. ABSTRACT ONLY.

2. Turk M A, Vermes B, Thompson A J, Belnoue J P H, Hallett S R and Ivanov D S Characterising Fabrics with Localised Formability Enhancement ECCM19 June 22-26, 2020, Nantes, France (Virtual). ABSTRACT ONLY.

Seminars Presented

1. Turk M A, Vermes B, Thompson A J, Belnoue J P H, Hallett S R and Ivanov D S Optimising the placement of localised resin patches to enhance the formability of dry preforms Euromech Colloquium 602 Composite Manufacturing Processes Analyses, Modelling and Simulations 13 March – 15 March 2019, Lyon, France.

2. Turk M A, Vermes B, Thompson A J, Belnoue J P H, Hallett S R and Ivanov D S Characterising Local Properties of Formability Enhanced Preforms, 5 Feb 2021, Bristol Composites Institute Seminar Series.

Table of Contents

Abstract 1
Dedication and Acknowledgements 2
Author's Declaration 3
Publications 4
Table of Contents 5
List of Tables 8
List of Figures 9
Abbreviations 15
1. Introduction 16
1.1. Overview 18
1.1.1. Structural Supercapacitors 21
2. Literature Review 24
2.1. Forming Defects and Mitigation Strategies 25
2.2. Formability Modelling 26
2.2.1. Deformation Mechanisms 26
2.2.2. Modelling Approaches 27
2.3. Characterisation of Fabrics for Formability Modelling 29
2.4. Creating Multi-Matrix Composites 32
2.5. Problem Statement 34
2.6. Novelty Statement 35
2.7. Thesis Structure 36
3. Localised Formability Enhancement 38
3.1. Component Geometry 39
3.2. Experimental Trials for Preform Stabilization 40
3.2.1. Resin Conditioning 40
3.2.2. Bulk Patching Forming Trials 41
3.2.3. Line Patching Forming Trials and Model Validation 43

3.2.4. Discussion 48
3.3. Requirements for Fully Automated Dispensers for Forming 49
4. Numerical Techniques for Defect Detection 51
4.1. Model Formulation / Description 51
4.2. Defect Detection Algorithm 54
4.3. Discussion 59
5. Characterisation of Enhanced Preforms 62
5.1. Methodology 63
5.2. Non-linear Elastic Patches 66
5.2.1. Model Description 66
5.2.2. Simulation Input 67
5.2.3. Result Post-Processing 69
5.3. Viscoelastic Patches 72
5.3.1. Model Description 72
5.3.2. Result Post-Processing 73
5.4. BET Tests on Treated Fabric 78
5.4.1. BET on Preform with Deposited PLA Patches 79
5.4.2. Experiments on Visco-Elastic Patches 81
5.5. Results and Discussions 88
5.5.1. Experimental Set-up 88
5.5.2. Hypo-Elastic Model and PLA Experiments 89
5.5.3. Visco-Elastic Model and Resin Film Experiments 90
5.5.4. Discussion 91
6. Numerical Tool for Patch Placement 93
6.1. Optimisation Strategy 94
6.2. Rigid tool forming 95
6.2.1. Forming of Non-Stabilised Material 96
6.2.2. Rough Forming Optimisation using Bulk Patching 97
6.2.3. Line Patch Placement - Sequential Placement 100

6.2.4. The Effect of Patch Properties on Wrinkle Likelihood 102
6.3. Rigid Tool Forming with Experimentally Derived Properties 103
6.4. Flexible tool forming 105
6.5. Discussion 115
7. Infusion of Multi-matrix Composites 118
7.1. Motivation 119
7.2. Methodology 121
7.3. Materials 123
7.4. Barrier Method 124
7.5. Masking Method 128
7.6. C-Section Demonstrator 130
7.7. Infusion of Multi-Ply L-Section 132
7.7.1. Experimental Setup 132
7.7.2. Issues Encountered 135
7.7.3. Results 136
7.8. Discussion 137
7.9. Outlook 138
8. Conclusions and Future Work 140
8.1. Notable Achievements 140
8.2. Further Work 142
8.2.1. Modular Infusion 142
8.2.2. Structural Supercapacitors 142
8.2.3. Characterisation of Enhancements 145
8.2.4. Resin Printing 145
8.2.5. Wrinkle Detection Algorithm 146
8.2.6. Localised Formability Enhancement 146
8.3. Summary 147
Bibliography 148
Appendix A 158

List of Tables

Table 2.1: References to relevant works on formability modelling 29
Table 5.1: Polynomial coefficients for dry and patched fabric as used in simulations 68
Table 5.2: Calculated viscosity at both 50% coverage and 5% coverage firstly derived using equation 1 based on crosshead displacement and then secondly derived by averaging the pure shear zone C taking values directly from the model 76
Table 5.3: Shear Angle Measurements by Coverage Level as Measured from Videogauge Frame 84
Table 6.1: Maximum and average shear angles with various patch arrangements 113
Table 6.2: Number of wrinkles and overall weighting for the various combinations simulated 115
Table 7.1: Pros and cons of barrier and masking methods 123

List of Figures

Figure 1.1: Airbus A220 wing at the Bombardier Belfast facility with bottom cover and ribs shown, the wings for the Airbus A220 are manufactured using liquid resin infusion in combination with continuous carbon fibre reinforcement 18
Figure 1.2: Resin transfer moulding basic setup, showing the liquid resin inlet, vacuum bag edge seal and the resin outlet and vacuum application point, the dry fibre preform is clamped between the top and bottom moulds 19
Figure 1.3: A typical formability induced wrinkle occurring in the corner of the component, the top mould has been removed to allow for clear visibility and spray binder applied to hold the preform in its deformed shape. 21
Figure 1.4: The various stages of the carbon aerogel pyrolysis process utilizing carbon aerogel, left: the shape of the formable zone is masked with resin film (these are the areas where the yarns are no longer visible); centre: the sample is infused with carbon aerogel precursor; right: the sample after pyrolysis now ready for forming and further infusion of structural resin 22
Figure 2.1: Bias extension test standard design..... 31
Figure 3.1: Geometry of the a) male and b) female moulds of the component, these are machines with a small gap between the two to allow space for the fabric and are modelled on a flat plane outside the component contours..... 39
Figure 3.2: Definition of zones for introducing stabilising elements, the inner corners are zone 1, the mid-section are zone 2, the outer corners are zone 3 and the ends are zone 4..... 42
Figure 3.3: Shear map of the bulk patch injected fabrics; far left: shape formed with powder binder sample; middle left: shape formed with uncured patch sample; middle right: shape formed with low degree of cure patch sample; far right: shape formed with high degree of cure patch sample..... 43
Figure 3.4: Spray binder reference sample showing a large fold/wrinkle with the various relevant locations ‘A’-‘E’ labelled and the stamped square pattern to aid in shear measurement visible 43
Figure 3.5: Wet fabric reference sample (unstiffened) with the various relevant locations ‘A’-‘E’ labelled; note that the dyed pattern has been lost due to the presence of water which leads to the red coloration that is visible..... 44
Figure 3.6: Forming images from case study 1 a) unstiffened fabric b) stiffened with uncured resin c) low degree of cure d) high degree of cure; the laddering locations are labelled along with the wrinkle location from the high degree of cure sample; all samples have been sprayed with powder binder after the top mould is removed to preserve the deformation shape 45
Figure 3.7: Shear map of the line patch injected fabrics (low DoC), the graph is split into shear angle measurements at each corner to avoid any bias in the results and to account for the level non-symmetry 46

Figure 3.8: Forming images from case study 2 for unstiffened fabric a) full view b) corner 1 c) corner 3 d) corner 4 (rotating sample clockwise); the laddering locations are labelled along with the wrinkle locations; the sample has been sprayed with powder binder after the top mould is removed to preserve the deformation shape 47
Figure 3.9: Forming images from case study 2 for low degree of cure a) full view b) corner 1 c) corner 3 d) corner 4 (rotating sample clockwise); the wrinkle locations are labelled and the patch locations at each corner shown in blue pen; the sample has been sprayed with powder binder after the top mould is removed to preserve the deformation shape 48
Figure 3.10: Various resin printing attempts (left: no thicknener, 0.8mm needle partially pre-cured; middle: no thickener, 0.8mm needle no pre-cure; right: 2.1mm needle, thickened with silica, partially pre-cured) 50
Figure 4.1: Comparison of deformation pattern with a) 1mm mesh and b) 2mm mesh with colour plot overlay of shear angle. 54
Figure 4.2: Flowchart showing the steps of the wrinkle detection algorithm. Actions are denoted as squares and decisions are denoted as diamonds. 57
Figure 4.3: a) Down selected chains highlighted in red over deformation pattern, they can be seen to be largely clustered around visible wrinkles; note that nodes hidden behind the mould are shown through as if the mould were transparent b) close up view c) compressive stresses in x-axis d) compressive stresses in z-axis 58
Figure 5.1: Bias extension test with modified sample geometry a) schematic diagram of patch distribution; b) actual geometry of the sample with 50% coverage of PLA patches (painted). 64
Figure 5.2: Bias extension simulation with striped patches at 25% coverage 67
Figure 5.3: a) Shear stress input for dry regions b) shear stress input for patched regions (note: differing y-axis scale) 68
Figure 5.4: a) Derived patch shear stress outputs compared with patch property input a) output crosshead derived b) output based on average local strain measurements 69
Figure 5.5: Comparison of deformation pattern for a) dry fabric and b) 50% coverage at 16.5mm crosshead displacement (theoretical equivalent of 20 degrees shear angle in the pure shear zone). 70
Figure 5.6: Kelvin-Voigt model 72
Figure 5.7: Surface fit of shear stress response at various strain rates a) 50% coverage b) 5% coverage c) dry fabric 75
Figure 5.8: Bias extension test with one central stiffened strip 76
Figure 5.9: Comparison of out of plane buckling at midway point a) 50% coverage b) central stripe at the average shear of 0.277 radians 77
Figure 5.10: a) Image taken by DIC camera and b) shear map generated for 25% coverage of PLA (at 16.8 mm crosshead displacement out of 60mm) 80
Figure 5.11: PLA shear stress response at various coverage levels 81

Figure 5.12: a) Image taken by videogauge at 0% coverage b) Image taken by videogauge at 50% coverage. The red diamond outlines the approximate edges of the theoretical pure shear zone. The patch locations are indicated in white with one patch outlined 83
Figure 5.13: Shear angle measurements reading horizontally across the sample a) labels the locations measured b) charts the shear angle with grey denoting dry fabric and blue denoting patched locations. 85
Figure 5.14: Surface fit of shear stress response at 50% coverage 85
Figure 5.15: Surface fit of shear stress response at a) 100% coverage b) 0% coverage 86
Figure 5.16: Comparison of experimental and simulated results for a) 50% and b) 100% coverage at 12mm/s 88
Figure 6.1: a) Matching moulds b) top view of meshed male mould c) moulds with fabric shown between 95
Figure 6.2: Shear angle distribution in forming simulation without stabilising patches (female mould hidden): a) top view, b) side view on critical region B-B′-C′-C, note that the mould is not at full closure as mentioned in the text 96
Figure 6.3: Plot of In-plane stresses for rigid mould simulation (at 60% closure) a) no patches, x-direction (warp), b) no patches z-direction (weft) 97
Figure 6.4: Definition of zones for introducing stabilising elements, the inner corners are zone 1, the mid-section are zone 2, the outer corners are zone 3 and the ends are zone 4 98
Figure 6.5: Comparison of shear maps in a) reference (non-stabilised) and b) stabilised configurations (zone 3) at 60% closure, the critical locations are labelled and the patch locations highlighted in red 99
Figure 6.6: Comparison of shear maps in a) reference (non-stabilised) and b) bulk stabilised configurations (zone 3) at full mould closure; with the various relevant locations ‘A’-‘E’ labelled and the top mould hidden 99
Figure 6.7: a) Shear angle distribution resulting from forming simulations with stabilising line patches (patch locations hidden) b) top view with patch locations shown in red; with the various relevant locations ‘A’-‘E’ labelled and the top mould hidden 101
Figure 6.8: Plot showing the variation of maximum shear angle as shear stiffness is increased (at 60% mould closure) 103
Figure 6.9: Shear angle distribution resulting from forming simulations with experimentally derived material shear behaviour with a) unpatched fabric b) closer view of a c) stabilizing line patches (patch locations hidden) d) closer view of c with patch locations shown 104
Figure 6.10: Curved spar mould with a flat base but a curved plane for forming, all radii are chamfered to allow for smooth sliding of the fabric over the mould 106
Figure 6.11: A colour deformation plot showing dry fabric formability of double curved spar, the colour gradient depicts shear angle; various wrinkles are clearly visible a) diaphragm forming b) vacuum bag forming 108

Figure 6.12: Colour plots showing the forming outcome as a result of a) perimeter patch placement locations (averaging zone highlighted in white) and b) spot patch locations; the colour gradient depicts shear angle 110
Figure 6.13: Fabric deformation and shear map with perimeter patches; the colour gradient depicts shear angle, patch locations not shown a) without gravity b) with initial gravity only stage..... 111
Figure 6.14: Plot of In-plane stresses for vacuum bag simulation (incl. gravity) a) no patches, x-direction, b) perimeter patches x-direction, c) no patches z-direction, d) perimeter patches z-direction 111
Figure 6.15: Fabric deformation and shear map with spot patches; the colour gradient depicts shear angle, patch locations not shown a) without gravity b) with initial gravity only stage..... 112
Figure 6.16: Wrinkles highlighted on the various simulation configurations trialled a) dry fabric b) perimeter patches c) spot patches; the colour gradient depicts shear angle, patch locations not shown, images on the left not including gravity, images on the right including gravity..... 114
Figure 7.1: Structural and multifunctional zones segmented on a spar c-section, it can be seen how the multifunctional zones do not need to bend whilst the structural zones are formed around the corners 120
Figure 7.2: Resin barrier in non-crimp biaxial carbon fibre, it can be seen how the resolution has been partially lost due to the capillary forces in the fabric, the bagging film can also be faintly seen which is affixed to the barrier but not the rest of the fabric 121
Figure 7.3: PLA ‘mask’ infused into woven carbon fibre, the unmasked area can be identified by the still visible yarns, the mask is infused into both the top and bottom of the fabric. Masking tape remains around the perimeter at this stage to prevent the fabric from unravelling..... 122
Figure 7.4: Illustration of the barrier and masking methods. On the top row (barrier method), (a) fabric (grey), (b) application of barrier (red), (c) first modification/infusion to fabric (stripes), (d) second infusion (black) to fabric in, second section, or debond barrier to bagging material and infuse whole component with another media. On the bottom row (masking method), (i) fabric (grey), (ii) application of mask (blue), (iii) first modification/infusion to fabric (striped), (iv) removal of mask, (v) second infusion (black) to whole component 122
Figure 7.5: Tacky tape as barrier adhesive applied to a glass ply (a) initial arrangement, then (b) epoxy infused via resin infusion by flexible tooling (red dye used for clarity) in one region of the ply, (c) final product showing an epoxy infused region and an as-received fibre region in the opposite region. Note that the tacky tape barrier was difficult to remove as shown in (c)..... 124
Figure 7.6: Development of the barrier method. (a) epoxy used as adhesive between infusion bags, (b) demonstration of dry fabric being modified on one side of the epoxy barrier with the barrier joined to the outer infusion bagging material; with the schematic cross-sections of their respective arrangements shown below the photographs. The barrier shape was chosen to explore the resolution and spreading of the resin in right angled corners..... 125

Figure 7.7: Epoxy barrier sample demonstrating isolated zones rather than full partitioning of the fabric, the bagging film is also faintly visible with a layer on the top and bottom affixed to the barrier but not the dry fabric. The perimeter of the fabric is also masked to prevent unravelling and make transportation easier 126
Figure 7.8: (a) Barrier method modified such that the outer most bagging material and barrier are independent. Producing a fold region using a barrier method, is as follows; (i) dry fibres, (ii) barrier applied to a specific region of the fabric, (iii) infusion of the first matrix, (iv) cutting the sample to allow for specific fold line (dotted line) to be accessible, (v) side on view of the L-shaped flexible component produced 127
Figure 7.9: PLA masking sample created as a template to make two identical c-section parts, the masked areas will later form the corners of the c-section with the dry fabric exposed to the carbon aerogel. The perimeter of the fabric is also masked to prevent unravelling and make transportation easier 129
Figure 7.10: Mask method showing (a) PLA (white) hot-pressed into the fabric, (b) the fabric and PLA infused with carbon aerogel precursor, (c) carbonisation of the carbon fibre PLA showing incomplete decomposition of the PLA. (d) A more complicated PLA design was pressed into a fabric (transparent white), (e) following the same aerogel precursor procedure, (f) carbonisation and char from the PLA wiped from the surface to reveal the dry fabric surface below 130
Figure 7.11: Demonstration of the formability of carbon aerogel infused carbon fibre plies using the barrier (top) and mask (bottom) methods to create small regions as fold lines about a C-section tooling piece (radius of curvature 5 mm). Note, in the masking method the addition of duct tape was used to secure the ply to the tooling piece as residual PLA caused some resistance to folding 131
Figure 7.12: Multi-matrix trial demonstrator, this is only a proof of concept and therefore is not infused with carbon aerogel, however the partitioning between distinct formable and flat zones can be seen 132
Figure 7.13: L-Section multi-ply sample prepared for infusion, it is formed over an L-section mould with no upper mould applied, resin is infused along the long edge with distribution mesh running two thirds of the distance around the corner and the remainder travelling though the fabric only to ensure through thickness penetration before the outlet is reached 134
Figure 7.14: Labelled layup diagram, working from the tool face upwards there is firstly lower bagging film, followed by the fabric with integrated barrier-isolated-zone, followed by peel ply, followed by distribution mesh and finally upper bagging film. The upper and lower bagging film are sealed together with tacky tape 134
Figure 7.15: Test sample showing leakage into isolated zone, there is only partial intrusion of resin which is visible are the bottom edge of the corner, the remainder of the corner region remains dry. Sample shown after curing. 135

Figure 7.16: Final sample after stage 1 infusion, slight encroachment of the infused resin into the central section can be seen, however the majority of the corner region remains dry. The outline of the resin barrier can be faintly seen showing the level of ingress. Sample shown after curing. 136
Figure 8.1: Demonstrator proposal showing a spar c-section and flange intersection with structural zones planned for all curved or joint regions and flat zones kept free for the first stage of infusion. This layout demonstrates both the potential for fabric segmentation and continuous matrix joints .. 144

Abbreviations

ASTM	American Society for Testing and Materials
BET	Bias Extension Test
CAG	Carbon Aerogel
CFRP	Carbon Fibre Reinforced Polymer
CPU	Central Processing Unit
DIC	Digital Image Correlation
DOC	Degree Of Cure
FE	Finite Element
FEA	Finite Element Analysis
GFRP	Glass Fibre Reinforced Polymer
ICL	Imperial College London
NCF	Non-Crimp Fabric
Pre-Preg	Pre-impregnated Fabric
PLA	Poly Lactic Acid
RFI	Resin Film Infusion
RTM	Resin Transfer Moulding
TRL	Technology Readiness Level
VARTM	Vacuum Assisted Resin Transfer Moulding

1. Introduction

A composite is a combination of two or more materials to create a material with enhanced properties. These enhancements generally come in the form of high specific strength, improved environmental resistance or reduced cost or manufacturing time. Composites have been widely utilised in UK industry since the 1960s, however they are increasingly working their way into high-end quality critical components where they are phasing out traditionally metal components. According to the UK composites market study from 2013 "Consultation with the UK composites supply chain has shown that the UK has the opportunity to grow its current £2.3bn composite product market to £12.bn by 2030" [3].

The influence of composites on the global aerospace industry is especially noticeable, a 2018 Aerospace Technology Institute report [4] states that "Today's newest wide-body commercial aircraft platforms, the Boeing 787 and Airbus A350, are around 50% composite by weight" this is a significant increase from previous aircraft at around 20% even after extensive retrofitting. According to a Boeing article this broad incorporation of composites into the Boeing 787 "offers weight savings on average of 20 percent compared to more conventional aluminium designs." [5]. The same report [4] also claims "Aerostructures market opportunities within the 2017- 2035 timeframe are over £88 Billion, with more than 50% of the value associated with wings. Nacelles, pylons, engines and landing gears provide market opportunities of £51 Billion within the same timeframe."

The associated potential for lightweighting and significantly reduced environmental impact during operation has brought polymer composites to the fore in addressing climate change. In particular, the environmental benefits that stem from reduced emissions associated with lighter components has driven the transportation sector's interest in composites, with these materials identified as a key enabler for electrification of transportation, as highlighted by the UK target for the reduction in carbon emissions of 60% (1990 levels) by 2030 and 80% by 2050 [6]. Recently, there has been an emergence of multifunctional composites materials: structural composites which have been imbued by additional functionalities such as sensing, actuation or energy storage.

Typical composites such as carbon fibre reinforced polymer (CFRP) or glass fibre reinforced polymer (GFRP) excel in terms of strength to weight ratio where they generally outperform metals or alloys. Ceramics on the other hand can offer a higher specific strength than polymer composites though this tends to be primarily in compression and often comes at the cost of very low ductility. Therefore, for applications where weight saving is paramount such as in aerospace, polymer composites are the material of choice offering excellent strength in compression, tension, shear and torsion. However, it is worth noting that both metals and ceramics can themselves be incorporated as a composite matrix

or as fibres to utilise their unique strengths, and these in addition to polymers constitute the three main classes of composite matrix.

It is very common to rely on continuous high strength and stiffness fibres such as carbon or glass fibre running parallel to the primary loading direction to provide strength in tension and bending, whilst relying on the matrix material to provide strength in secondary directions. There are many notable exceptions to the rule however and it is not uncommon to have long or short discontinuous fibres orientated at random where alternate material properties are desired. This thesis is concerned primarily with continuous fibre biaxial woven fabrics which have higher volume fraction, better alignment with the load paths, and much better overall properties.

Continuous reinforcement can be produced by (a) laying prepregs, (b) forming of thermoplastic precursors, and (c) liquid moulding. The advantages of liquid moulding are the ability to produce large structures, reduced cost of manufacturing, high rates of fibre deposition, and long shelf life of precursors. The wings for the Airbus A220 (Figure 1.1) are manufactured using liquid resin infusion in combination with continuous carbon fibre reinforcement. The use of resin transfer moulding is of particular interest in this thesis and this process represents a significant deviation from other recent large commercial aircraft which still favour primarily prepreg and autoclave-based fabrications. The use of this technology in such a large scale and state-of -the-art application is an indicator that resin transfer moulding may well become the dominant manufacturing approach for high-rate wing production.

Figure 1.1: Airbus A220 wing at the Bombardier Belfast facility with bottom cover and ribs shown, the wings for the Airbus A220 are manufactured using liquid resin infusion in combination with continuous carbon fibre reinforcement

The National Composites Centre based in Bristol, UK is currently pursuing a £100k project called 'Modular Infusion' in association with GKN and Toray which is highly relevant to the work of this thesis and builds on some of the ideas developed. The project aim is "to demonstrate the use of a combination of multi fibre architectures, infusion strategies and multi-stage processing to simplify and de-risk infusion processing, tailor composites use within structures, and increase production rates". It is hoped that this collaboration will allow for the flow of knowledge to work its way into industrial applications.

1.1. Overview

Multi-matrix infusion and local formability enhancement are the two predominant topics of this thesis. These techniques have their basis in resin transfer moulding and focus on the desire to mitigate defects arising from the resin transfer moulding procedure. Resin transfer moulding (RTM) is the process of holding fabric and resin apart until the final stage of manufacture. Typically the fabric is formed into the desired shape using a mould and vacuum pressure, see Figure 1.2. This is controlled within a closed environment except for an inlet and outlet tube for the flow of resin. Control of resin flow is an integral part of the process, the resin is drawn through the mould with an applied vacuum until the fabric is entirely wetted, at this point the inlet is sealed but the vacuum remains, drawing out trapped air and compressing the fabric. Importantly the rigid mould allows for the application of

higher pressure at the inlet. Excess resin is drawn into a catch pot. Once the fabric has been fully wetted the vacuum pressure remains applied whilst the part is cured.

RTM is a very popular technique due to excellent versatility and quality control, it is especially successful at achieving highly controlled fibre volume fraction and low voidage. It is well suited to highly complex components and often offers shorter production cycle times than the equivalent for autoclave manufacture. Unlike many composites processes it is well suited to woven cloths. The main consideration for this process is the elimination of defects as the vacuum pressure is applied to the preform which can often be quite challenging. These defects lead to impaired material strength and therefore it is essential that they are avoided [7]. RTM is used extensively throughout this thesis.

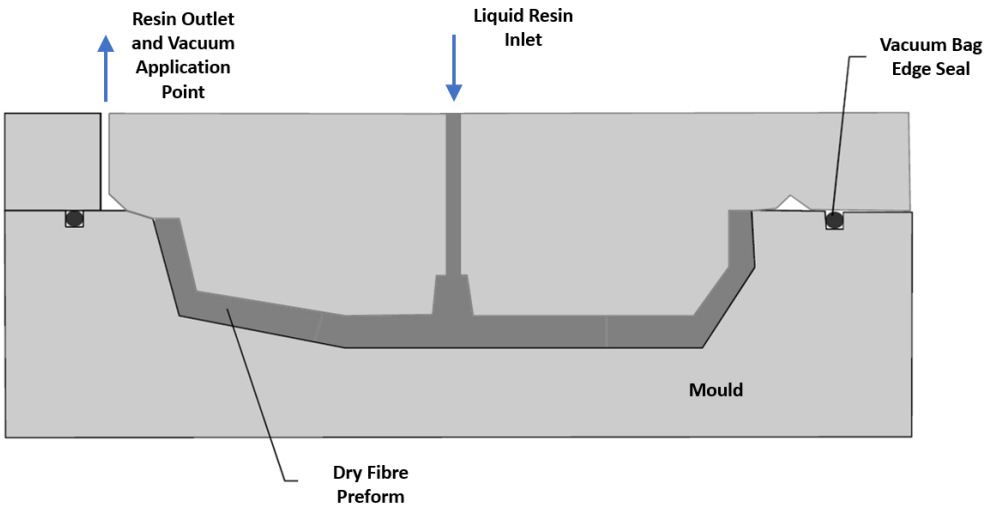

Figure 1.2: Resin transfer moulding basic setup, showing the liquid resin inlet, vacuum bag edge seal and the resin outlet and vacuum application point, the dry fibre preform is clamped between the top and bottom moulds

Resin infusion offers great advantages in rate of manufacture and cost reduction over pre-preg based techniques, though it generally results in slightly lower quality components. An integral step prior to the infusion and curing process is the forming of the reinforcement material into the final part geometry, this process is prone to various defects associated with the intrinsic properties of textile preforms: low out-of plane buckling resistance and negligible resistance to compressive stresses, minimal extensibility in the fibre directions, low initial shear stiffness and exponential stiffening at high angles of shear. Inextensibility of preforms in the fibre direction results in difficulties of forming the fabric to a complex shape without generating distortions or out-of- plane buckling of reinforcement, known as wrinkling.

There are various other associated risks with resin infusion. Firstly, there are often large flow lengths, which lead to low pressure gradients driving the flow. This leads to a risk of dry zones forming.

Secondly, there are challenges of the controlling fibre paths which often leads to the use of binder and thermoforming which carries with it the increased risk of wrinkles. Thirdly, resin infusion can result in low consolidation pressure which increases the risks of dimensional defects. In addition, the introduction of functional elements can exacerbate these problems. The material becomes less formable in the case of functional tufting, or structural tufting, or any other forms that could be used at the dry forming stage.

This variety of potential problems leads to the possible solution of modular integration of elements as discussed in the abstract, which brings the following manufacturing techniques as candidates for the solution:

1. The creation of multifunctional structures by separating the domains. Two matrix materials occupy separate zones of a continuous fabric. The primary benefit is the ability to provide multifunctionality in carefully tailored regions, allowing the manufacturer to designate areas as either multifunctional or purely structural based on design requirements. This frees up significant portions of fabric to shear freely allowing for formability.
2. The localised modification of textile properties in regions where a defect is likely to form. As mentioned, excessive shearing often results in the formation of detrimental features, such as wrinkles, folds and fabric distortions, the local modification of such regions can lead to formability enhancement. Modification can be achieved by the integration of patches: additional materials, such as reactive thermally-conditioned resins, tufted or stitched yarns, thermoplastic films, locally activated binder, etc.

The defects specifically tackled in this thesis are wrinkling (see Figure 1.3) and folding, with some problems presented by laddering also. All these defect types are relevant to the resin transfer moulding experiments presented later and inhibit preform formability.

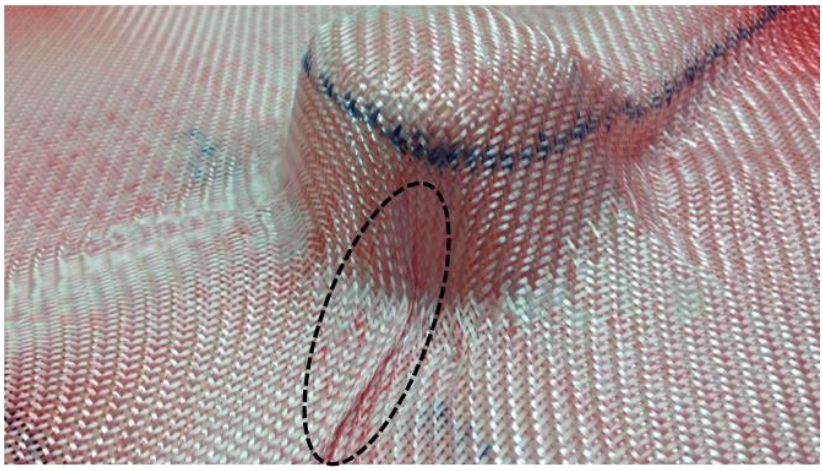

Figure 1.3: A typical formability induced wrinkle occurring in the corner of the component, the top mould has been removed to allow for clear visibility and spray binder applied to hold the preform in its deformed shape.

Formability is a general term to refer to the ability of a preform to conform to the desired shape (usually a mould) without defects occurring. Enhancing formability allows for pushing the boundaries of which geometries can be created and how reliable manufacturing processes can be [8], [9]. Computer based finite element modelling is commonly used as an ideal tool for predicting formability and identifying likely defects. Improving and refining the FEA tools available to model formability constitutes an important part of advancing composite formability as a whole.

For the purposes of this thesis a wrinkle is defined as local out-plane rotation of the fabric with respect to the geometry of the mould, around the axis perpendicular to the fibre direction. The threshold of the rotation angle is considered to be anything above $\pi/2$ radians. A fold is defined the same but the rotation around the axis aligned with the fibre direction. Out of plane fibre waviness is again the same but without exceeding the set threshold. In-plane fibre waviness is any in-plane deviation from the desired/designed fibre path. Finally buckling is not the material feature, but the process of ply buckling leading to occurrence of the wrinkle.

1.1.1. Structural Supercapacitors

An important potential application of the developed technique of modular integration of elements is the manufacture of structural supercapacitors. The idea of storing energy in structural composites is relatively new but becomes increasingly popular. The weight of batteries or capacitors can be substantially reduced or eliminated if their functions are passed to load carrying structures. This is attractive both for the emerging market of electrical vehicles and for aerospace applications where any gains in light-weighting are of paramount importance. The intrinsic architecture of composite laminates and properties of carbon fibres provide possibilities for natural incorporation of these

functions. A particularly successful development has been pursued in Imperial College London [2], [4] where the incorporation of porous aerogels with a very high specific areal density in the inter-fibre space allows for the increase of the storage functions of the composite laminates to create structural supercapacitors. These materials allow a fast storage and energy release compared to batteries and can be used for a wide range of different applications including stabilisation of power supply, power buffers to and from rechargeable batteries, and energy harvesting.

One of the central challenges facing implementation of the structural supercapacitors in a wider industrial practice is their manufacturability. Liquid aerogel precursors are infused into a textile preform using a liquid moulding process. Once foaming is completed, the preform is formed on a tool, a dielectric barrier (glass preform) is inserted between the conductive layers, and structural resin is delivered in a secondary infusion process. The problem is that the aerogels are stiff and brittle (see Figure 1.4). They make textile preform non-formable and hence, may become prohibitive for complex industrial components. The requirement of preform shearing, necessary to comply the material to a tool, presents a significant problem for manufacturing.

Figure 1.4: The various stages of the carbon aerogel pyrolysis process utilizing carbon aerogel, left: the shape of the formable zone is masked with resin film (these are the areas where the yarns are no longer visible); centre: the sample is infused with carbon aerogel precursor; right: the sample after pyrolysis now ready for forming and further infusion of structural resin

Armed with new manufacturing approaches and supported by high-fidelity numerical simulations, a major part of this thesis will attempt to tackle the problem of supercapacitor composites formability.

The solution will be centred around the idea of creating internal impermeable barriers within the textile preform prior to integrating the gel. The barriers, imprinted into fabric using the liquid resin deposition technique [11], will subdivide the textile preform into formable and non-formable domains and provide local stabilisation to eliminate excessive shearing in the forming operation. Domain boundaries and treatment will be informed by numerical simulations optimised to avoid excessive shearing, tuned to mitigate against wrinkling defects, and targeted at maximising the area of supercapacitor domains.

Significant work is required to develop design tools for the forming process, to carry out manufacturing trials, to create a design and manufacture protocol and carry out numerical simulations to assist formability. The work contained in this thesis progresses the manufacturability of structural composites with energy storage functions with the aim of raising the Technology Readiness Level (TRL) of structural supercapacitor technology to level 3 (a functional validated prototype).

2. Literature Review

This chapter presents an assessment of the current state of various topics covered in this thesis including work done thus far in the fields of formability enhancement, material characterization and multi matrix infusion. The limitations of current techniques are identified and areas of ongoing research are explored. The various formability models developed over the last 20 years are described along with their relative pros and cons, to provide a basis for the formability model used within this thesis. The three main modelling options of continuous, semi-discrete and discrete are presented and reviewed. The deformation mechanisms driving composite design are defined along with the defects commonly encountered and how engineers have tackled them. The field of formability optimisation is introduced along with the concept of localised preform modification for formability enhancement. Current techniques for material shear behaviour characterisation are detailed. Finally, the state of multifunctional composites design is considered along with the limitations restricting the ease of development, especially the problems encountered when infusing multi-matrix composites. The literature review is followed with three sections detailing the overarching problem to be tackled within this thesis, the novel methods used and the structure of the thesis.

Formability is a major aspect of composite manufacture and a key area of research for driving down cost by increasing throughput rate compared to hand layup, increasing production speed and improving component quality. Formability is the capacity within a manufacturing process to form the composite to the desired shape for the component without the introduction of defects. Depending on the complexity of the part, the properties of the preform and the nature/sequence of the forming operations this may be a trivial problem or may prove challenging or impossible. There are a wide range of manufacturing processes involved in composite manufacture, as such, the defects encountered depend heavily on the manufacturing process involved. This thesis focuses solely on the formability of dry fabric using either a mould or diaphragm forming used in combination with resin transfer moulding.

The following sections of this literature review cover the key topics of this thesis. Section 2.1 ‘Forming Defects and Mitigation Strategies’ covers the background to the technique of locally modifying material behaviour to enhance formability, which later leads on to implementing this technique in Chapter 3. Section 2.2 ‘Formability Modelling’ covers the pre-established modelling techniques used for modelling the formability of fabrics, which provided the basis for the modelling work in Chapters 4 and 6. Section 2.3 ‘ Characterisation of Fabrics for Formability Modelling’ explores established methods for characterising fabric behaviour which is then developed into a new characterisation method in Chapter 5. Finally, section 2.4 ‘Creating Multi-Matrix Composites’ provides a summary of the current state of multi-matrix composite development which is later explored in Chapter 7.

2.1.Forming Defects and Mitigation Strategies

Optimisation of the forming procedure to minimise the occurrence of defects is a developing area in composites manufacturing, which has led to a number of established methods. Broadly speaking, available techniques fall into two categories: constraining the fabric at the perimeter of the forming domain, or locally modifying the fabric at critical locations within the preform area.

Methods of fabric constraint at the perimeter include the use of: blank holders [12], [13], [14], [15] which impose a tension onto the fabric to reduce the occurrence of defects; tensioning elements [16], [17] using a series of springs that locally apply in-plane tension through clamps to the fibre preform; or flexible tracking devices [18] using a roller to apply stress to the membrane. Fabric constraint allows for the elimination of areas with compressive in-plane stresses.

Such compression can occur when fibres in an originally flat preform are formed onto a complex tool. This occurs through bending of the laminate (compressive stress in the inner plies), consolidation on curved areas / tapers leading to generation of excessive length, or forming onto double-curved surfaces etc. Fibre lengths on a formed shape may differ for each of the individual geodesic fibre paths. When the difference in neighbouring paths is significant, preform shearing takes place, but it may not always be sufficient to accommodate the length difference without causing compression. Blank holders and tensioning elements compensate for the negative stresses and allow for the obtainment of higher shear angles without wrinkling. Pre-tensioning of the fabric is effective but requires a complex system of fabric constraints and may be limited in the shapes it can efficiently handle.

Localised preform modification relies on a different mechanism. If the area where a defect is likely to occur is known, then modifying preform properties in this area can change the deformation map and drive the defect away from the critical location. Modification of the preform properties can increase buckling stiffness and prevent excessive shearing. Such gradient distribution of properties, if arranged carefully, can delocalise shearing deformations and prevent defect formation. This preform modification has been demonstrated through stitching [19], tufting [20], activation of yarns commingled with thermoplastic fibres [21], variation of weave patterns [22], and tensioning elements [17]. Local through-thickness stitching of a single - or multi-ply preform hinders the relative movement of the warp and weft fibres at the crossover points and therefore influences the shear behaviour and the formability of the fabric. The location, direction, pattern and density of the seams are all important parameters and for advanced preform formability their optimisation is necessary. It has been shown that in some cases stitches outside the shear zones have a more significant effect on drapability than those inside these zones [19]. Stitching also improves the through-thickness mechanical properties of the final composite and influences the in-plane properties in a way that

depends on a number of factors (e.g. material, stitching method, loading scenario, etc.) [23]. Likewise, tufting of multi-ply preforms was shown to have the potential to significantly reduce the wrinkling of preforms [20]. A very different approach is implemented using Jacquard weaving machines which are capable of creating fabrics with locally modified weave architectures [22]. Combining fabric weaves with different architectures in the same preform sheet leads to gradient formability characteristics. This helps to provide good stability at non-complex, mechanically critical areas and good formability at shear zones.

2.2.Formability Modelling

Modelling the formability of composites allows engineers to establish whether a textile can be formed onto a given geometric shape. Kinematic models can be used to identify geodesic paths for the shaping of the fabric onto a mould or tool [24], [25] and are very effective for demonstrating the compatibility between a certain fabric weave and the geometrical limits for its formability. However, kinematic models struggle to identify defects created during forming, necessitating the creation of more precise and accurate models based on careful assessment of textile behaviour. These models aim to answer not only if a shape is achievable but also to predict any defects likely to arise from a given formability approach. This chapter describes the common material deformation modes considered and the modelling approaches taken over approximately the last 20 years which have made significant progress towards achieving accurate textile formability modelling.

2.2.1. Deformation Mechanisms

As the primary driver behind textile deformation and defect generation in-plane shear has been the main focus of textile modelling efforts for many years [26], [27], [28], [29]. A key consideration has been how to accurately model the shear resistance of fabric as shear angle increases, whilst also incorporating the comparatively much larger tensile resistance in the fibre direction [30], [31], [32]. Textiles have very little shear resistance initially as the tows of fibres are free to slide across each other and the yarns can rotate without any need for shearing within the yarns themselves. This makes the behaviour of textiles unique and allows for the forming of complex geometries, though it significantly complicates modelling. Various approaches to the modelling of the shear resistance have been considered. Generally they focus on a material input curve which captures the exponential stiffening behaviour of textiles in shear [33]. Further consideration is also needed to account for the fact that the fibre direction changes as the textile is sheared, leading to reorientation of the directions of greatest tensile resistance. Finally, the fabric locking angle must be captured to identify the point at which further shearing is not possible due to significant contact between the tows causing compression of each individual tow until no further compression can be accommodated. These are not trivial problems with finite element analysis as no basic FEA element are individually suited to this

level of complexity. Various strategies have been explored and are provided in section 2.2.2. Experimentally shear stiffness can be characterised through the use of picture frame shear test [34], [35], the biaxial test [34] the bias extension test [35], [36], and off-axis tensile tests [37], [38], [39] as discussed in Chapter 5.

Out of plane bending plays a significantly smaller role in the creation of defects during textile forming and for this reason is often given less consideration in formability models. Textiles have very low out of plane bending resistance compared to in plane properties as the fibres which make up each individual tow are free to slide over each other. This sliding means that the fabric bending behaviour is effectively the sum of the bending behaviour of each individual fibre with the distance between the neutral axis and the upper and lower surface of each fibre being very small. Similarly to the unique in plane shear behaviour, the low out of plane bending is a beneficial property for composite formability, nevertheless it needs to be captured accurately for a reliable formability model [40], [29], [41]. The most common test for establishing out of plane properties is the ASTM cantilever bend test [42].

2.2.2. Modelling Approaches

The development of modelling capabilities to help understand and predict defect formation has been the focus of a substantial research effort. Overviews of modelling techniques for forming can be found in [43] and [44]. Homogenised constitutive equations for biaxial fabric are formulated as discrete, semi-discrete or continuous [45], with continuous models sub-divided into hypo-elastic [44] or hyper-elastic models [46], [47] and implemented in a finite-element framework for a continuous sheet of shell elements.

Continuous models treat the textile as a homogenous anisotropic material. When considered on the macro scale the behaviour is idealised though the use of a constitutive equation which aims to capture the key aspects of the textile behaviour without the computational demand of modelling the underlying interactions between tows and individual fibres. This modelling approach is the most computationally efficient but can struggle to reflect the precise deformation behaviour of composite preforms. Often continuous models rely on input properties defined by discrete models to capture deformation mechanics accurately. Continuous models can be further sub-divided into hyper-elastic and hypo-elastic. In hyper-elasticity the constitutive relations are defined through an elastic potential and stress is derived by its derivative with respect to the strain invariants. Hypo-elasticity is by contrast defined through the empirical definition of stress-strain constitutives. Hypo-elasticity may lead to violation of the energy balance and hence can be problematic. It also requires sophisticated tracking of the fibre direction, which is ensured naturally in hyper-elastic modelling.

Discrete models aim to capture the behaviour of each individual yarn. This allows for accurate modelling of the friction between yarns, slippage, compaction of yarns and yarn rotation in a unit cell.

Modelling at the meso-scale allows for highly accurate capture of textile behaviour at the cost of significant computational demand. Once a unit cell has been modelled this can be duplicated to avoid the need to model the entire fabric. Various relevant discrete models that have been developed are presented below. These models tend to be very demanding computationally but are helpful for laying the foundations for the simplifications often utilised in the continuous and semi-discrete models described earlier.

Semi-Discrete (or hybrid) models are a compromise between continuous and discrete models. The main drawbacks of a continuous model is that composites are highly anisotropic and it is near impossible to capture their behaviour accurately with a single type of finite element. Conversely discrete models are time consuming to develop and computationally demanding to run. Semi-discrete models combine two or more types of finite element in order to better approximate the behaviour of textiles, generally using one to prescribe the shear behaviour and another to model the high strength in the fibre direction. Various semi-discrete models that have been developed are referenced below, culminating in the work of Thompson [33], [48] which is the basis for the modelling work later in this thesis. Thompson superimposed Shell and Membrane elements on top of each other. Allowing for a realistic decoupling of out of plane bending behaviour and in plane shear. The shell elements carry the bending load and prescribe the tensile stiffness of the fibres whilst the membrane elements carry shear. The shear behaviour is modelled hypo-elastically using a polynomial equation.

Modelling attempts have been largely successful in capturing the in-plane rotations of the fibre directions, predictions of wrinkle sites and, more recently, the shape and size of wrinkles in single layer forming processes [14], [40], [27]. In [14] the semi-discrete approach considers the bending strain energy and the bending behaviour of the reinforcement to give a realistic description of the wrinkles. The development of such models has identified the necessity to capture the shear behaviour of the textile preform in models correctly, as it has proven to be the fundamental mechanism behind fibre re-orientation [14], [49], [50], whereas out-of-plane bending stiffness is essential to make accurate predictions of the shape and size of wrinkles [14], [40] as this mechanism can accommodate the excess material. In [40] the proper flexural behaviour is captured in the model through use of a biaxial elastic modulus which can be analytically related to the bending stiffness of the fabric. More recent modelling efforts have concentrated on including more complex deformation mechanisms into constitutive models, these include in-plane bending stiffness [41] with the tows providing resistance to changes in fibre direction within the ply; through thickness deformation [51] and the dissipative behaviour of textiles which is required to capture the effects of unloading [52] by assuming that the dissipation process is mainly related to the in-plane shear deformation. Accurate modelling of the precise fabric behaviour allows for wrinkles or other defects to be observed rather than assumed from other metrics such as shear angle. It also gives confidence that wrinkle locations and severity are realistically represented.

There exists a wealth of numerical modelling techniques that can be used for forming optimisation. Optimisation strategy can be complex when forming with a mould as the forming scenario can be highly sensitive to initial parameters. Due to the complex and highly non-linear nature of fabric behaviour during mould closure it is difficult to identify the ideal initial setup. The process therefore lends itself to optimisation through iteration with a wide variety of initial patch configurations trialled on a systematic basis. Vermes et al [53], using a discrete model inspired by Skordos et al [54], performed a systematic parametric search aimed at minimisation of the shear angle. Chapters 3 and 6 of this thesis build on the initial work reported in [53] and adapt a similar pragmatic two-step optimization strategy: at first the position of large bulk patches is selected from a short list of several likely optimum positions, then a detailed forming is considered to refine the exact geometry of patch position in the selected domain. In contrast with previous results, the optimization is performed using a 2D element approach suggested by Thompson et al [33], [48], and similar to [55]. It combines shell and membrane element formulations to present a realistic balance of bending and in-plane tensile properties of the preform. This study looks at both the conventional measure of critical deformation – shear angle [15], [16], [22], [53], [44] and a direct observation of wrinkling provided by the model. The latter is used as an independent measure of success of patch optimisation placement. The findings from the numerical study are then used to inform physical forming experiments to establish the effectiveness of patch placement for mitigating defects.

Various key developments which helped to set the precedent for current modelling approaches are outlined in Table 2.1.

Table 2.1: References to relevant works on formability modelling

Modelling Approach	**References**
Continuous	Dong [26], Peng [30] [56], Yu [31] [57], Aimene [46], Xiao [58]
Semi-Discrete	Allouai [14], Boisse [29] [49], Lin [28], Dangora [40], Harrison [41] [59], Jauffres [60], Feretti [61], Barbagallo [36], Hamila [62] [63], Xiao [64]
Discrete (Meso-Scale)	El Said [25], Boisse [45], Gatouillat [65], Thompson [66], Creech [67], Ivanov [68], Lomov [69]

2.3. Characterisation of Fabrics for Formability Modelling

The behaviour of dry fabrics prior to infusion heavily influences the resultant properties of cured composites. Fibre orientation, wrinkling and tow spreading depend both on material properties and the design of the manufacturing processes. The complexity of the problem often demands computational modelling as the tool to inform whether the envisaged strategy is optimal and guarantees a defect-free

solution. When modelling the behaviour of dry preforms in deposition and forming operations it is essential to know the shear and bending behaviour of the fabric. Effective methods for the characterisation of dry fabric are well established [34], [35], [36]. Depending on the balance of these properties simulated fabric behaves in a wide spectrum of ways from unformable paper to an unrealistically compliant pin-joint net [70]. Shear behaviour can be derived using the picture frame shear test [34], [35], the biaxial test [34] the bias extension test [35], [36], and off-axis tensile tests [37], [38], [39]. Typically, uniform fabric behaviour is assigned to the entire preform and then the forming process (fabric constraints, blank holders, sequence of operations) is optimised.

The approach, suggested by Turk et al [71], is to alter preform properties locally. It was shown that depositing resin patches in critical locations allows for the improvement of the drapability of complex geometry. Conceptually similar approaches can be implemented in terms of stitching [19], tufting [20] or other methods. This approach does not require a complex arrangement of forming operations and hence can be attractive due to its simplicity. However, the local properties of modified regions need to be known for accurate process optimisation. This adds complexity to material characterisation. Extracting a patch for testing would lead to fabric disintegration. On the other hand, there is no established procedure for measuring local properties in a heterogenous material. All the conventional testing methods either try to minimise non-uniformity of deformations in samples, as in the picture frame test, or to tailor the data processing to an assumed deformation map, as in the bias extension test.

The bias extension test is a popular method for obtaining the shear properties of a fabric [34], [35], [72], [73]. A rectangular specimen is clamped between two grips creating a diamond shaped pure shear zone in the centre from which can be derived the shear angle and shear stress. The resultant deformation field is not uniform which demands a specific conversion of both displacement and force into shear strain and shear stress. Yet, the resulting shear diagrams can be reliably obtained as evidenced by both numerical simulations and independent validation with picture frame tests [34], [35]. The advantage of BET over the picture frame test is the simplicity of implementation and absence of tensioning effects associated with clamping. This approach is also equally valid for establishing the shear behaviour of pre-impregnated fabrics despite the much higher shear stiffness characteristic of these materials [72], [74].

The conventional bias extension test involves clamping a rectangular specimen of dry fabric lengthwise between two grips. The length of the specimen is prescribed to be at least twice that of the width [72], with the orientation of the fibres at ±45°. This arrangement leads to the creation of a diamond shaped pure shear zone in the centre where deformation is close to the state of pure shear. The specimens are clamped across the full width and the clamps moved apart at a constant rate. The constraint-free boundary along the long edge ensures that the fibres are free from tension as each fibre

has at least one non-gripped end. The resultant deformation field is not uniform over the sample area which therefore demands a specific conversion of both displacement and force into shear strain and shear stress. The layout of the deformation zones are shown in Figure 2.1.

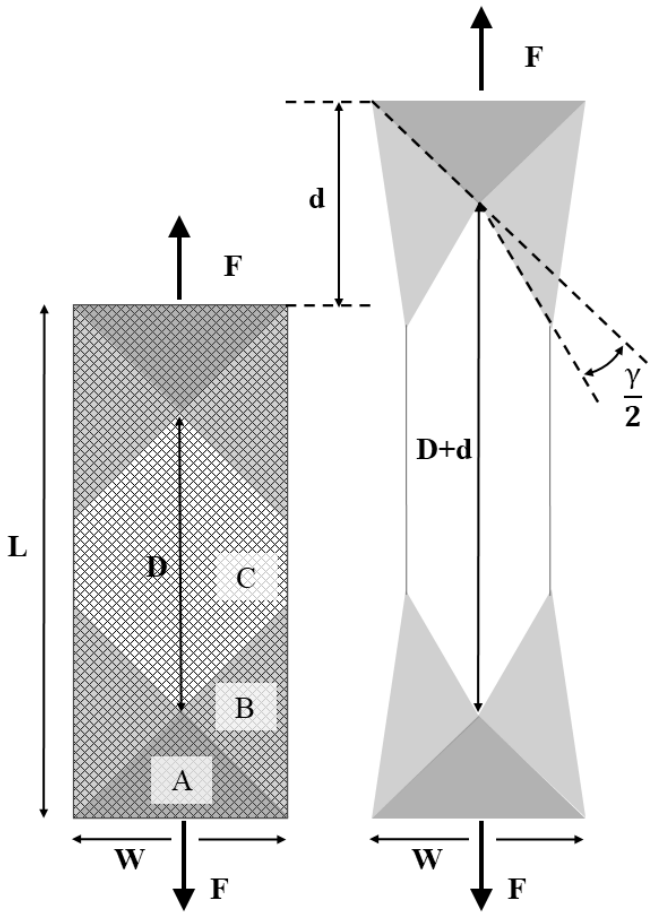

Figure 2.1: Bias extension test standard design

In a sample with uniform distribution of properties, the crosshead load and displacement of the bias extension test can be used to derive both the shear stress and shear angle respectively within the pure shear zone as detailed by Boisse et al [72]:

$$\gamma = \frac{\pi}{2} - 2Arccos\left(\frac{D+d}{\sqrt{2}D}\right) \quad (1)$$

Where γ is shear angle, D is the length of the pure shear zone (i.e. length of full sample minus width of full sample) and d denotes crosshead displacement. Shear force as a function of crosshead load is calculated incrementally based on the considerations of energy dissipated in various zones [72]:

$$F_{sh}(\gamma) = \frac{F\,D}{W(2D-W)cos\gamma}\left(cos\frac{\gamma}{2} - sin\frac{\gamma}{2}\right) - \frac{W cos^{\gamma}/_{2}}{(2D-W)cos\gamma}F_{sh}\left(\frac{\gamma}{2}\right) \quad (2)$$

Where F is the crosshead applied load and l is the width of the specimen. F_{sh} denotes the shear force within the pure shear region.

It is known that the calculation of shear stress, equation (2) and shear strain, equation (1) in BET begin to break down at large shear angles (e.g. above 40°, [35]) due to intra-ply slippage becoming a significant deformation mechanism [35], [72]. This leads to locally measured shear angle being the preferred option. As a result it is common to use optical measurements such as Digital Image Correlation (DIC) measurements rather than rely on the crosshead displacement (1) to assess the strain within the sample directly and without making assumptions on strain homogeneity. The cameras can also be a more effective way of identifying the start point of the experiment as they can track the beginning of shearing in the fabric (this is often several seconds after the crosshead begins to move due to slack in the fabric). Implementing DIC requires applying a speckle pattern on the surface of the fabric. Even though the application of paint on the surface changes the behaviour of the fabric, this gives a good idea about the specimen kinematics.

2.4. Creating Multi-Matrix Composites

Selecting the ideal matrix for a composite component or process has always being a conundrum for composites engineers [75]. Various considerations must be taken into account including the structural properties, the cost, the processability, environmental resistance and safety of manufacture. Usually the final matrix selection is based on a compromise between these factors. Naturally therefore the idea of working with multiple different matrices is desirable, removing the need for compromise and allowing the matrix to be specifically tailored to the needs of a particular region. Historically this has been tackled with the basic approach of making separate components out of different matrices and bonding them together allowing for a variety of properties and applications across the wider component [76], [77]. Aside from this the most obvious approach is to infuse additives along with the resin system allowing for a slight modification of properties, these additives can be injected or printed into local regions allowing for the desired local enhancement. Stanier et al [78] trialled this approach with local deposition of carbon nanotubes.

Due to the highly versatile nature of resin transfer moulding [79], [80] composites engineers have for a while experimented with alternative approaches attempting to infuse multiple resin systems into one continuous composite part allowing for utilisation of the best properties of each matrix. Resin transfer moulding is often prepared by hand and therefore the specifics can be manually modified during

layup. Historically most success has been had attempting to isolate different plies of the preform. Gillio et al [81] successfully trialled a technique of separating plies with a layer of adhesive polysulphone film allowing for the inner plies to be infused with Vinyl Ester as structural resin and the outer plies to be infused with Phenolic resin to provide environmental resistance against fire, smoke and toxicity. This technique has come to be known as resin film infusion (RFI) [82] with variants on the approach considered by Kruckenberg [83], Uchida et al [84] and Fiedler [85].

An alternative to separating individual plies from each other through the use of segmenting adhesive film, is to use multiple resin systems within a ply, with a partition spanning the width of the preform. This allows for a truly continuous fabric architecture despite two matrix systems being present. Krollman [75], [86] demonstrated the approach of infusing two resin systems simultaneously through different inlets and controlling the flow front of each resin system to carefully prescribe the path along which the two systems merge. This creates a zone for resin A and a zone for resin B with a narrow region between the two where the two resins meet. This is a simple and highly practical way of injecting multiple resin systems and relatively simple configurations can be manufactured effectively. The impact on voidage and other material parameters were considered across the various zones, a major drawback being that it is not possible two achieve a complex boundary path between the two regions and the resolution of the boundary is difficult to prescribe.

A development to this approach that is currently being trialled at the National Composites Centre (NCC) is to use directly applied pressure upon the preform to control resin flow paths. In implementation this is very similar to [75] except that the resins are not allowed to mix freely due to the presence of a tool pressurising the surface, preventing lateral flow across the ply. with this approach it is possible to exert greater control over the exact boundary between the two, the resins are also infused across multiple stages to allow the second resin to permeate the previously pressurised zone. This approach has higher tooling costs due to the need for a bespoke shape used for imprinting the pressurised region, however once set up it should be ideally suited to large scale production. No published works on this approach are yet available.

The idea of incorporating electrical conductivity or energy storage into composites is an area that has recently been explored [2], [87]. This field is especially relevant to the area of multi matrix infusion as the incorporation of energy storage elements into the matrix requires a far greater compromise in structural strength. This brings the need for tailored matrix properties to the forefront of development. Transferring the functions of supercapacitors into structural composites has the potential for significant weight savings which is attractive in industries where weight is a significant cost driver such as aerospace or electric vehicles.

2.5.Problem Statement

The overarching problem tackled in this thesis is what implication the insertion of functional elements has on the formability of dry preforms. Multifunctional elements have the potential to complicate and worsen formability issues but also the potential to be used for formability enhancement.

The project is broken down into two primary problems. Firstly how to improve the formability of preforms using localised enhancements:

1) Is it possible to enhance preform formability through localised enhancement? This will involve consideration of the likely defect types that are encountered and whether inhibiting shearing in carefully selected regions can reduce defect occurrence and severity.
2) What form should modifications take? Considering the practicality of resin deposition, stitching or tufting as a means to inhibit shear, as well as their subsequent removal or incorporation into the finished component.
3) Which parameters affect the effectiveness of the technique? This involves assessment of possible geometry, location and stiffness of local enhancements.
4) Can optimisation be performed using computer modelling and an optimisation algorithm? How accurately can formability be modelled and how time consuming is the optimisation process? Does the process require significant human input or can it be automated?
5) How can the properties of enhanced regions be characterised to allow for accurate modelling? Considering in particular how the shear properties of local enhancements can be calculated to allow for accurate formability modelling.

Secondly how to develop a manufacturing technique for the infusion of multi-matrix composites through resin transfer moulding:

1) How can multi-matrix composites be manufactured? This requires a detailed manufacturing procedure and an assessment of the reliability of the process. Consideration of incorporation into the manufacturing process for structural supercapacitors is also required.
2) Which techniques are cost and time efficient? A particular focus will be needed on the trade off between having a more complex process than conventional VARTM and the benefits in terms of material properties.
3) What are the applications and limitations of the manufacturing process? Considering scale of potential geometry and the potential to be applied to mass production.

2.6.Novelty Statement

This project resulted in the following novel outcomes:

1) Manufacturing trials were carried out demonstrating successful creation of resin barriers in order to segment fabrics allowing for multi matrix infusion. This method was effective for both single ply and multiple ply stacks. This opens up a range of possible novel manufacturing techniques such as tailoring the strength of certain regions without the use of traditional pad up, or alternatively creating joints with the matrix material spanning the joint.
2) Carbon Aerogel (CAG) based composite supercapacitors were trialled with partitioning allowing for formability into simple shapes. This is the first successful trial of composites used for electricity storage being formed into a shape other than a flat panel, a vital step in progressing the technology to a wider possible range of applications.
3) Experiments were carried out demonstrating that locally deposited resin patches can be used in conjunction with resin transfer moulding to pin certain regions of fabric in order to enhance formability. This process was informed in advance by formability modelling indicating the optimal arrangement.
4) An algorithm was developed to identify wrinkles from the output of formability simulations, to allow for repeated iterative model runs. The algorithm benefits from the ability of modern formability models to accurately identify specific wrinkle locations visually, whilst removing the need for human input in the iterative process. The algorithm remains in the development phase but is shown to be effective at wrinkle identification on the two geometries trialled.
5) The conventional bias extension test was successfully adapted to allow for the characterisation of local fabric enhancements. This modified procedure is simple to implement and entails only slightly more complexity than the conventional bias test. The procedure is shown to be effective primarily for viscous patches, with less successful results for high stiffness non-viscous patch material.

2.7. Thesis Structure

This thesis is structured as follows:

Chapter 2 ‘Literature Review’. An assessment of the current state of various topics covered in this thesis including work done thus far in the fields of formability enhancement, material characterization and multi matrix infusion. The limitations of current techniques are identified and areas of ongoing research are explored. The various formability models developed over the last 20 years are described along with their relative pros and cons, to provide a basis for the formability model used throughout this thesis.

Chapter 3 ‘Localised Formability Enhancement’. The concept of local formability enhancement through the introduction of deposited resin or other modifying substances is introduced. A detailed case study is presented providing the rationale behind the placement of resin patches and choice of resin parameters. Experiments are shown demonstrating the effectiveness of the concept on a specific geometry along with the other experimental details which impact formability. *Much of the content of this chapter is extracted from a paper published on this topic* [71], *also authored by myself.*

Chapter 4 ‘Numerical Techniques for Defect Detection’. This chapter explores the concept of using a computer algorithm to identify defects within a simulated formability trial. A framework for how to set up such an algorithm is established along with a demonstration of a basic algorithm which can identify the location of wrinkles within a simulation without requiring human input. This algorithm is successfully demonstrated showing how optimization would work. The further work required to turn this into a complete program is detailed.

Chapter 5 ‘Characterisation of Enhanced Preforms’. Following the demonstration of automated wrinkle identification in the previous chapter, the topic of how to characterise localised enhancements is explored. This chapter focuses specifically on attempts to characterise how resin patches behave in shear to allow for more accurate formability modelling. It seeks to investigate the feasibility of a new experimental procedure where the properties of patches, which can be highly non-linear and time-dependent, are extracted by testing a larger volume of the material. This testing will also give a deeper insight on how localised enhancements affect the macroscale behaviour. The experimental procedure is based on several elements: (a) reference testing of blank fabric, (b) detailed deformation analysis using optical methods, (c) concurrent numerical modelling. The process is analysed in a virtual environment where input (hypothetical) properties of the patch need to correspond to deduced properties from the test. Two models are explored, one for viscous materials such as stage cured resin or resin film and a second for high stiffness non-viscous materials. *The DIC experiments presented in section 5.4 were carried out by Hengli Cao, guided by myself. Much of the content of this chapter is extracted from a paper published on this topic* [88], *also authored by myself.*

Chapter 6 ‘Numerical Tool for Patch Placement’. Simulations are shown demonstrating the technique for identifying regions which may benefit from local formability enhancement to complement the various physical manufacturing trials described in Chapter 3, with the results presented demonstrating successful defect mitigation. The many considerations for optimisation of patch placement are discussed along with a detailed description of the hypo-elastic model used throughout this thesis for formability simulations. *Much of the content of this chapter is extracted from a paper published on this topic* [71]*, also authored by myself.*

Chapter 7 ‘Infusion of Multi-matrix Composites’. Two methods for the infusion of multi-matrix composites are described in detail and put through manufacturing trials. Particular emphasis is put on the production of experimental structural supercapacitors using multi-stage infusion. The limitations of the current techniques are outlined and a variety of geometries and applications are trialled with various levels of complexity. Both methods are shown to be effective and consideration is given as to how to scale up the TRL to allow for more practical large scale manufacturing. *The multi-ply L-section demonstrator shown in section 7.7 was manufactured by Henry Redman, guided by myself.*

Chapter 8 ‘Conclusions and Future Work’. The findings of the project are summarised and the objectives reviewed. The potential applications of the novel developments contained in this thesis are considered, along with any future work required to apply the findings to an industrial context.

3. Localised Formability Enhancement

This chapter explores experimentally the concept of local formability enhancement through the introduction of deposited resin or other modifying substances. A detailed case study is presented providing the rationale behind the placement of resin patches and choice of resin parameters. Experiments are shown demonstrating the effectiveness of the concept on a specific geometry along with the other practical details which impact formability. Various degrees of cure are considered along with how the characteristics of the patching material impact the forming behaviour. Successful defect mitigation is demonstrated and attempts to automate deposition are shown with a view to enabling larger scale manufacture. Later chapters explore modelling approaches with the aim of assisting the technique demonstrated here.

The hypothesis explored is that altering properties of the preform may be advantageous to defect mitigation. This technique has the potential to be a simple to implement and relatively quick method for driving out wrinkles, whilst retaining continuity of fibres and allowing the deposited resin to become a part of the finished component. Following an early study of Vermes et al [53], the main means of property modification is the introduction of resin patches by means of Liquid Resin Print [11], [89] or any similar approach. As opposed to other approaches, this has a minimal impact on the internal architecture of the reinforcements. Thermosetting fast curing resin is deposited locally into regions where high shearing is expected and then thermally staged to the desired level of cure to tune the viscosity of the region for forming and consolidation. Viscous deposited resin changes the interaction between fibres. Patched regions remain deformable but exhibit a notably stiffer or more compliant response (depending on degree of cure) compared to surrounding dry material. This affects the shear angle distribution across the component.

Localised modification of the preform is especially valuable in scenarios where creating constraints at the perimeter is either overly complex, too time consuming, or too costly, leading to disproportionate challenges for implementation and automation. Local modification on the other hand has the potential to negatively impact the internal cohesion of the structure and hence damage the mechanical properties of the finished part. There is also the potential for tufting or stitching to distort fibres leading to a reduction of the in-plane strength of the component. This approach aims to mitigate these issues whilst incorporating the formability enhancement.

Multiple process parameters of local patching need to be established to make it effective. One set of parameters relate to the geometrical position of the patches. Shape, orientation, size, location and distribution of patches all make a clear impact on the possibility of mitigating defects. An incorrect patch pattern may actually negatively affect the shear angle distribution and defect likelihood. Another set of parameters relate to the properties of the patches. Deposition of reactive resin gives the

potential to take advantage of a wide range of viscosities that can be achieved through thermal treatment and hence, tune bending/shear resistance of the fabric. As will be shown in this chapter, the patch properties do influence shear map distribution. On the other hand, the additional material parameters result in greater optimisation space but increase the complexity of optimisation. This complexity makes numerical simulations an essential part of this process, as explored in Chapter 6.

3.1. Component Geometry

The test case, chosen for this study, is a non-structural component with exaggerated geometry. Kinematic drape simulations suggest that this component is not formable [53] - independently of drape starting point and initial fabric orientation the shear angle in some locations approaches 90°. This does not however mean that the component cannot be formed in principle – it means that it is not possible to align fabric reinforcement with the geodesic lines and hence, an additional material treatment is needed. The challenge set by this study is to explore the feasibility of making such a component formable by applying stabilising elements through liquid injected resin.

The component is thin-walled and doubly symmetric as shown in Figure 3.1. It is tapered towards the centre with characteristic dimensions of approximately 230 mm in length and 30-50 mm in width. The maximum height at location A-A′ is approximately 25 mm. This geometry is chosen as it is sufficiently complex to present forming difficulties without being excessively difficult or impossible to form. The geometrical features include convex and concave corners, tapers, ramps and other double curvature features. It is envisaged that a wide range of geometries could be readily assessed using the approach to patch placement shown below.

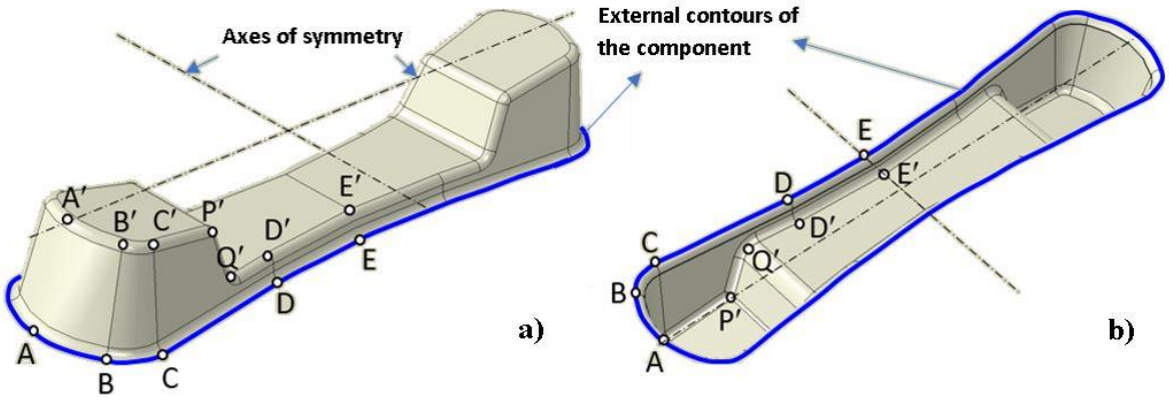

Figure 3.1: Geometry of the a) male and b) female moulds of the component, these are machines with a small gap between the two to allow space for the fabric and are modelled on a flat plane outside the component contours

The process considered for the manufacture of this component is liquid resin infusion of a dry biaxal preform. The essential driver for the choice of processing technique is to minimize manual intervention such as sequential draping operations. Hence, the infusion must be preceded by deep drawing forming and consolidation of the fabric. This chapter focuses on describing the forming process and defect mitigation for an isolated layer of material only. It is important to emphasize that defects associated with the forming of a multi-layer stack can be of a different nature (e.g. due to inter-ply/inter-tool friction [90], [91], [92], consolidation factors [93], and non-biaxial symmetry of the preform) and need to be addressed separately.

Kinematic simulations of this geometry with fabric aligned with the component symmetry axes show excessive shearing at the regions of B-B′ to C-C’ and along the concave corner P′Q′D′ (see Figure 3.1) – well above the locking angle (when the lateral interaction of sheared yarns causes out of plane buckling of fabric). As shown later, full forming simulations predict similar issues. Hence, the process requires interference in redistribution of the shear angle to mitigate the occurrence of critical defects.

3.2. Experimental Trials for Preform Stabilization

Experimental trials were carried out in a direct forming experiment using a single layer of reinforcement constrained between two rigid moulds. The Acrylonitrile Styrene Acrylate moulds of the same geometry as shown later in Figure 6.1 were manufactured using Fused Deposition Modelling technique with a resolution of 0.1 mm. A 2/2 twill E-glass reinforcement sheet of 280 g/m^2 areal density and a repeating unit length of 5 mm was chosen for trials based on its balance between formability and excessive bundle deformations. Sheets of 350 mm x 200 mm were cut from the fabric in 0°/90° fibre orientation. An ink grid of ~8.5 mm cell-size was stamped onto one side of each sheet, still in its flat undeformed state to track and visualize shear deformation. In some instances, the patch free fabric was uniformly sprayed with epoxy spray binder to maintain the deformed shape after opening of the mould. For the double contact forming, a 6 kg weight was placed on top of the male mould to close the moulds and apply the consolidation pressure. After reaching the gel-point, the male mould was removed to examine the shear pattern of the fabric, the form of which was preserved by the resin and/or the spray binder.

3.2.1. Resin Conditioning

For the preform stabilization, a fast curing epoxy resin system was chosen. The Huntsman Araldite LY3585 epoxy and the Aradur 3475 hardener were mixed in a 100:21 weight ratio. The resin was injected into the fabric at the predefined stabilization zones using fine needles to avoid fibre distortion. In the case of line patching narrow resin bands were placed at 45° to the fibre directions along lines B-B’ and C-C’ (see Figure 3.1). Deposited as narrow bands, these quickly widened due to

the capillary forces. Therefore cornflour was mixed into the resin prior to the injections in a 100:60 weight ratio of mixed resin to powder to increase its viscosity, thereby reducing the capillary effect. Thermal tuning of resin viscosity was carried out by conditioning of the injected resin using a heated flat press. At the first stage, the heated plate is brought into contact with the impregnated fabric without applying pressure. At the second stage the fabric is consolidated and transferred to forming. Duration and temperature of heating has to be chosen to ramp up the degree of cure (DoC), and hence, the resin viscosity, to a controlled level but prior to vitrification. Based on prior resin characterization the gel point was identified at a conversion rate of 40-50%. The forming trials were carried out after taking the resin in stabilized areas to a conversion rate of 10% (70°C for 2 minutes) and 30% (70°C for 4 minutes).

3.2.2. Bulk Patching Forming Trials

Two initial patch configurations were explored, which are termed ‘bulk batching’ and ‘line patching’ going forwards. Bulk patches are defined as large approximately square patches covering a significant portion of fabric, line patches are narrower rectangular patches covering a smaller area.

Placing bulk patches is based on understanding of critical locations where shear deformations may be high and shear bands narrow. Increased material resistance in selected regions is expected to delocalize fabric deformation, redistribute the shear angle over a larger area, minimise the magnitude of shearing in the regions of interest, and hence reduce the probability of defect occurrence. Especially in instances when geometry is complex and contains multiple critical regions, choosing the positioning of the stabilising elements correctly is difficult. Stabilising material in one location may lead to a defect in a different location. Line patches are considered later based on the reasoning that they may help to limit shearing without impacting on bending properties of the patched area.

In the initial design stage, four major zones were selected as candidates for stabilisation, the dashed lines in Figure 3.2 mark the perimeter of the patches. Zones 1 and 3 were the areas of potentially highest shear concentration in concave and convex corners, whereas zones 2 and 4 bridge them. This gave 16 possible combinations ranging from no zones stabilised (reference case) to all zones stabilised. The patch dimensions were set at 16 mm × 20 mm.

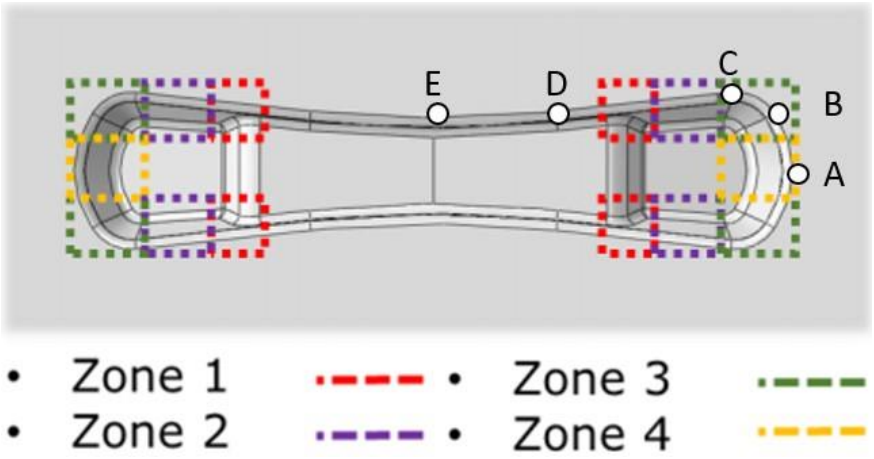

Figure 3.2: Definition of zones for introducing stabilising elements, the inner corners are zone 1, the mid-section are zone 2, the outer corners are zone 3 and the ends are zone 4

Both bulk patching and line patching were implemented in a series of experiments:

A. Reference trial where no liquid resin was applied.
B. Spray binder over the whole surface of the fabric.
C. Three trials where resin patches were brought to DoCs of 0%, 10% and 30% prior to forming.

Problems were anticipated in ensuring that the reference sample retained its deformation once the male mould was removed, hence the second spray binder sample was considered to prevent this spring back effect. After forming, the fabric was left on the female mould and examined optically.

Figure 3.3 shows the shear map of the formed fabric. In the spray binder case significant wrinkling of the fabric occurred, the injected but untreated fabric and low degree of cure fabric also showed problems with wrinkling. The highest degree of cure resin caused the most significant change in the shear pattern appearing to reduce wrinkle occurrence though instead causing a major fold to appear. The cause of folding was traced back to the increased bending stiffness at the stabilized zones due to the patch-wise applied resin. The experimental trials showed that a modified stabilization approach was needed that would maintain the local resistance to shearing without causing an excessive rise in bending stiffness.

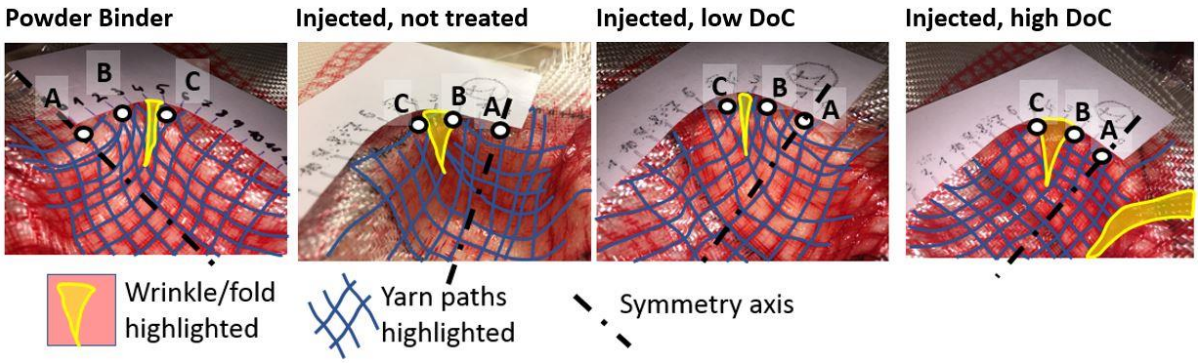

Figure 3.3: Shear map of the bulk patch injected fabrics; far left: shape formed with powder binder sample; middle left: shape formed with uncured patch sample; middle right: shape formed with low degree of cure patch sample; far right: shape formed with high degree of cure patch sample

3.2.3. Line Patching Forming Trials and Model Validation

Off-axis line injection patches were considered as an alternative to bulk patching. The work is presented as a series of separate case studies with issues and improvements outlined at each stage.

Initial trials A-C above highlighted two significant problems. Firstly, spray binder was found to be unsuitable as a reference case due to the high shear stiffness this imposed (see Figure 3.4). Binder made it both hard to maintain the deformed shape after removal from the mould and very resistant to shearing, it was therefore decided to remove the spray binder case from the trial.

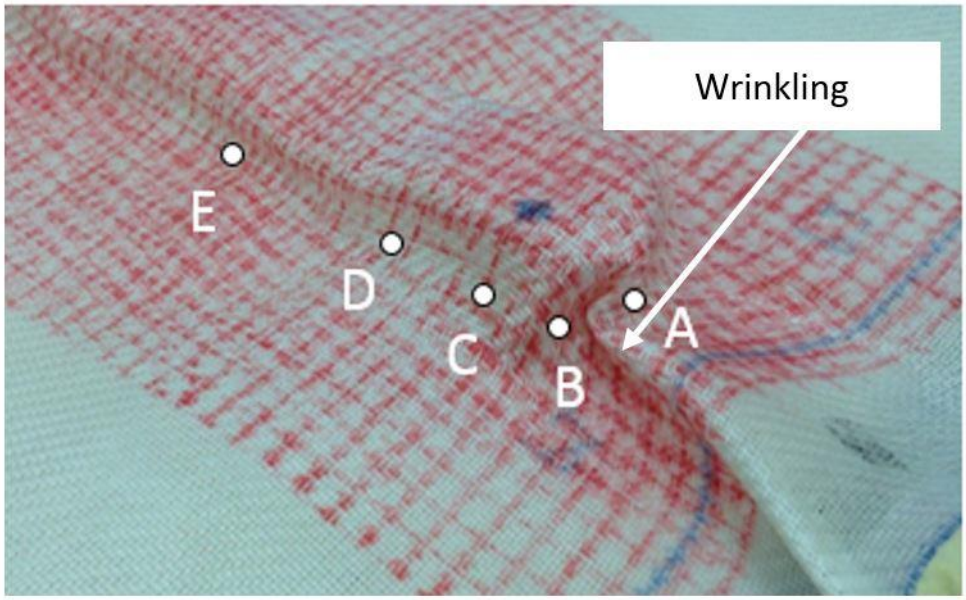

Figure 3.4: Spray binder reference sample showing a large fold/wrinkle with the various relevant locations 'A'-'E' labelled and the stamped square pattern to aid in shear measurement visible

Secondly, as anticipated, the dry reference sample lost much of its deformation pattern upon removal of the male mould due to spring back and therefore this data is unreliable as a reference case. In order to obtain a full closure deformation pattern for the reference unstiffened case, a sample was created identically to case A, except that the fabric had been soaked briefly in water beforehand. The results of this experiment are shown in Figure 3.5 with both moulds now removed.

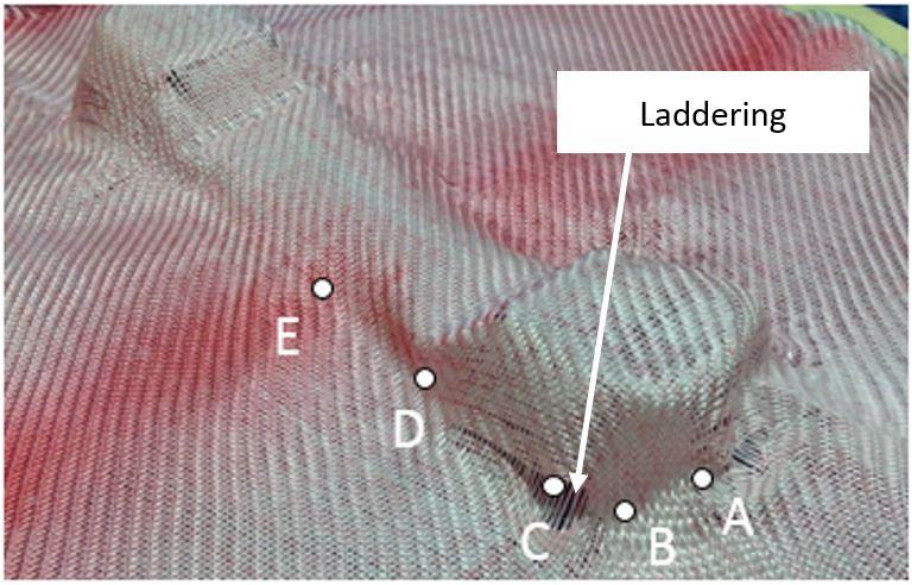

Figure 3.5: Wet fabric reference sample (unstiffened) with the various relevant locations 'A'-'E' labelled; note that the dyed pattern has been lost due to the presence of water which leads to the red coloration that is visible

This modification had the slightly unintended result of significantly increasing friction with the mould, which in effect introduced tensioning to the forming trial. This resulted in a sample with much reduced wrinkling and excellent adherence to the mould once the male mould was removed. However, as the purpose of this experiment was to create a suitable reference case this improved formability was not appropriate for comparison purposes, nor was it suitable for applying across the board due to the risk of these effects outweighing any observable impact of patch placement.

Therefore, due to the unsuitability of soaking the whole fabric, a small amount of water was instead applied to the troughs in the female mould before closure. This created two shallow wells, thereby taking advantage of the surface tension and extra weight (once capillary action had wetted the wider area of fabric) to avoid losing the deformation pattern once the male mould was removed. The water was placed in such a way as to only come into contact with the fabric very near to full mould closure so as to avoid any influence on the results. This procedure was also carried out for the samples with resin patches (as well as for the reference sample) for consistency.

With these amendments implemented trials A and C above were carried out and the observed forming results are shown in Figure 3.6. Once demoulded the samples were sprayed thoroughly with spray binder to maintain the deformation.

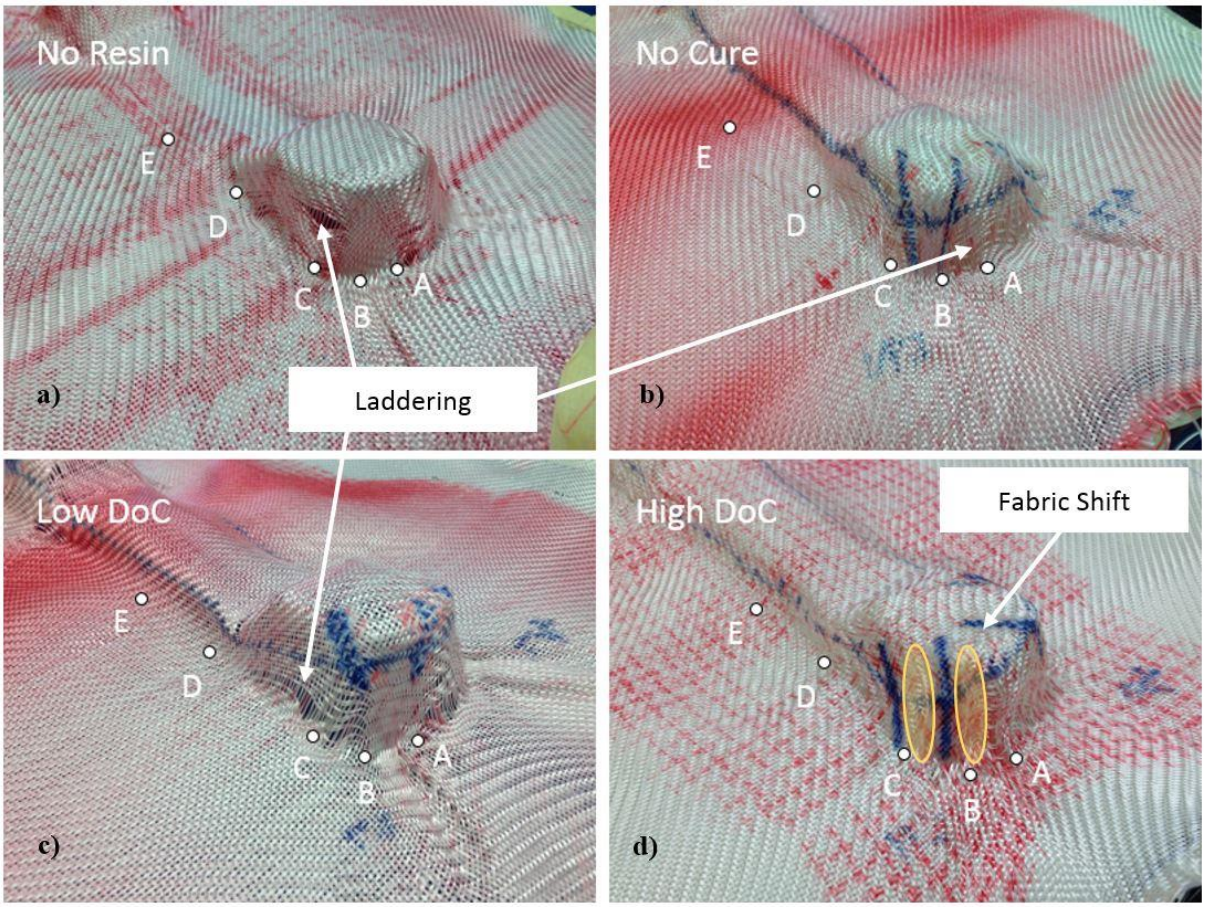

Figure 3.6: Forming images from case study 1 a) unstiffened fabric b) stiffened with uncured resin c) low degree of cure d) high degree of cure; the laddering locations are labelled along with the wrinkle location from the high degree of cure sample; all samples have been sprayed with powder binder after the top mould is removed to preserve the deformation shape

It can be seen that in this trial all samples successfully avoid significant wrinkling with the exception of the high DOC patching case where two wrinkles span the height of the corner either side of one resin patch (highlighted in yellow). In this case there is a shift in the centrality of the fabric leading to the patches being off centre. However, it was also observed in this trial that 'laddering' was occurring (see Figure 3.6) where parallel tows are dragged away from each other leading to distortions and openings in the fabric. This was predominantly due to localised friction forces arising during mould closure. This laddering is detrimental for composite performance, and although the previous discussions were mostly focused on wrinkling, this defect needs to be eliminated in manufacturing practice as well. Differences in forming behaviour at different patch stiffnesses is roughly in line with the numerically observed effects, see Figure 6.6a (non-stabilised) and Figure 6.7 (line patch

stabilised) specifically it shows correct description of locations with maximum shear intensity, correct indication of positions of major wrinkles or folds and correct description of the fabric contours, however full comparison cannot be made due to fibre distortions.

The no cure and low degree of cure scenarios are difficult to distinguish between in terms of successfulness, this distinction is further complicated by the various defects shown. The low DoC scenario has therefore been chosen to carry forward into the next case study along with the dry fabric baseline due to ease of handling when compared to no cure and greater contrast in patch properties when compared to dry fabric. Figure 3.7 shows the shear map of the low degree of cure formed fabric from Figure 3.6 illustrating the shear angles along path A-B-C-D-E for each of the four corners. It can be seen that the shear map varies significantly depending on which corner is examined and the forming result is non symmetrical despite a symmetrical mould. This behaviour was also observed in the simulations. Due to this lack of symmetry it is difficult to quantify a comparison between the simulation results (see Chapter 6) and manufacturing trials based on measured shear angle, instead the equivalent images will be visually compared.

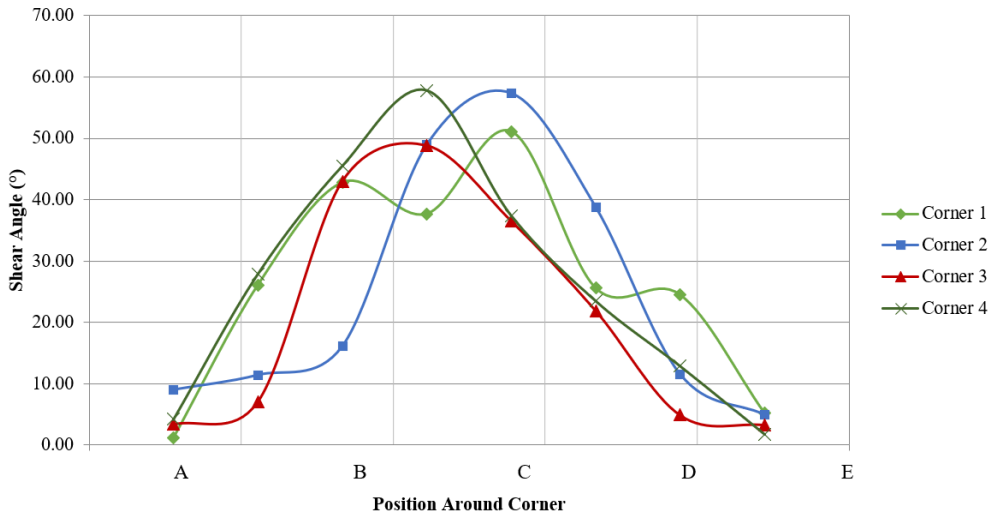

Figure 3.7: Shear map of the line patch injected fabrics (low DoC), the graph is split into shear angle measurements at each corner to avoid any bias in the results and to account for the level non-symmetry

In order to address the problem of laddering, a very thin sheet of release film was placed between the mould and the fabric on both sides which significantly reduced friction. The low thickness of the film material ensured that it had negligible resistance and consequently no effect on the formability other than to reduce friction. The unstiffened case and the low degree of cure case from the first case study were then repeated with this amendment to the setup. The results of this case study are shown in Figure 3.8 and Figure 3.9.

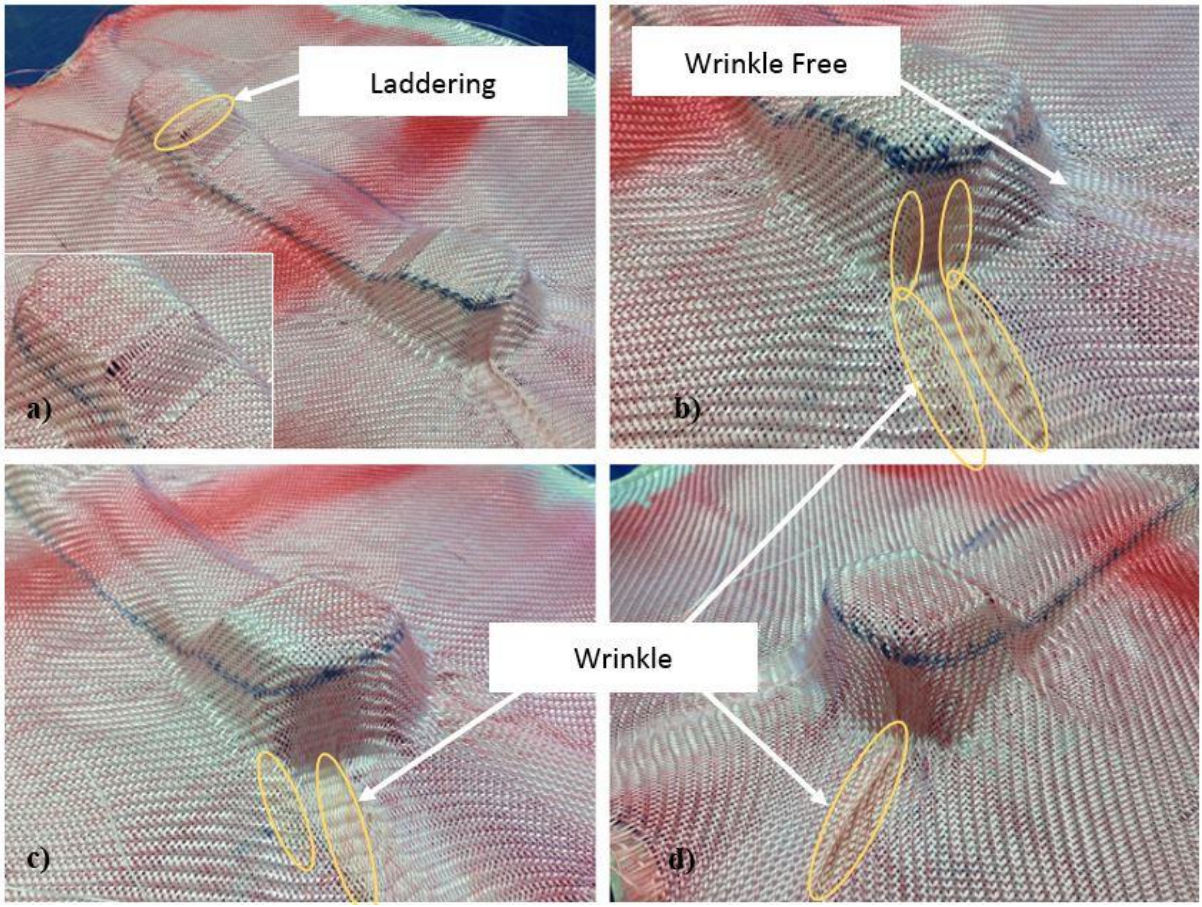

Figure 3.8: Forming images from case study 2 for unstiffened fabric a) full view b) corner 1 c) corner 3 d) corner 4 (rotating sample clockwise); the laddering locations are labelled along with the wrinkle locations; the sample has been sprayed with powder binder after the top mould is removed to preserve the deformation shape

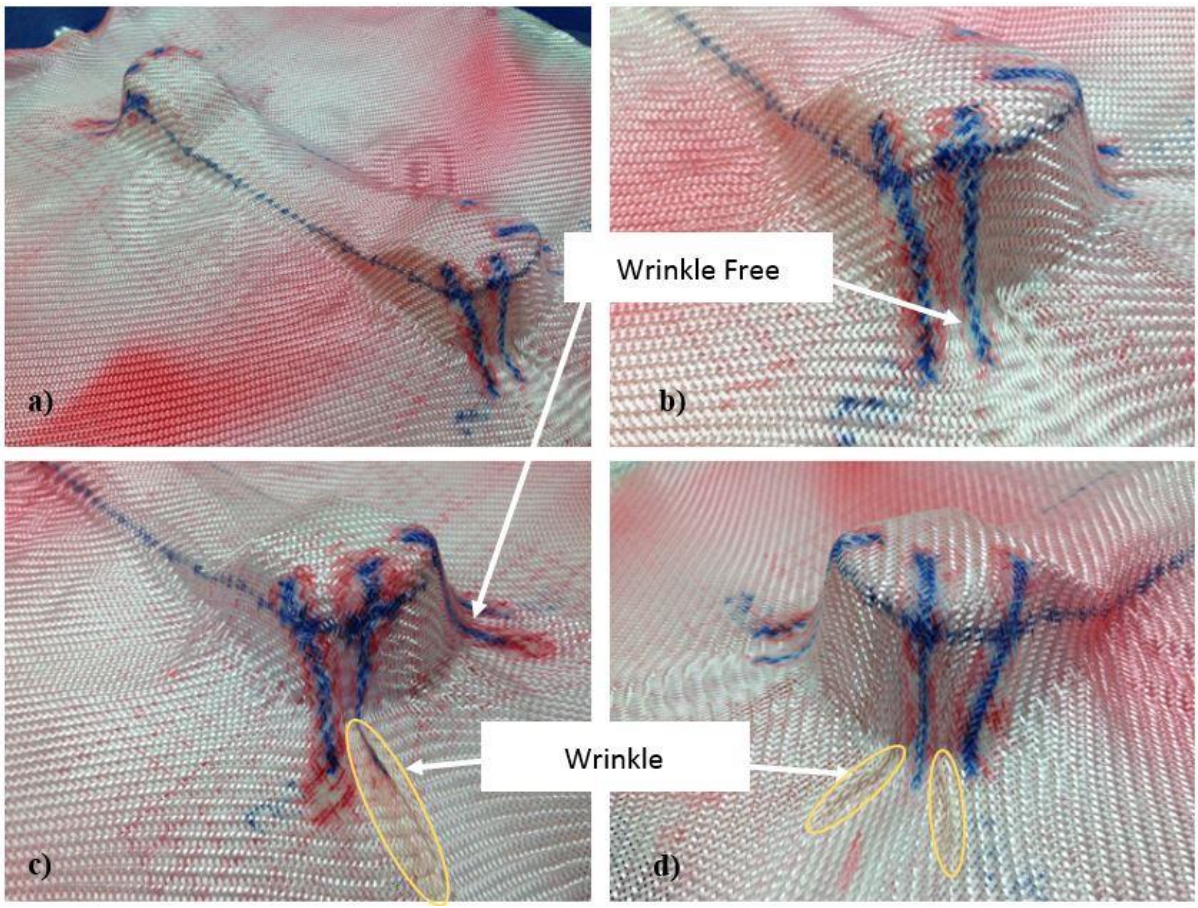

Figure 3.9: Forming images from case study 2 for low degree of cure a) full view b) corner 1 c) corner 3 d) corner 4 (rotating sample clockwise); the wrinkle locations are labelled and the patch locations at each corner shown in blue pen; the sample has been sprayed with powder binder after the top mould is removed to preserve the deformation shape

3.2.4. Discussion

It is apparent that this setup produces a significantly higher quality component than previous attempts. Both in the stiffened and unstiffened manufacturing trials wrinkles were largely suppressed. The dry fabric has minor wrinkles in three of the four corners whereas the low degree of cure sample has minor wrinkles in just two. Generally these wrinkles are occurring just outside the perimeter of the actual component with just one notable case for the unstiffened fabric where these wrinkles make major inroads into the component itself. However, a near defect free component was achieved only for the stabilized materials. In dry fabric laddering occurs on the top region of the shape, whereas this has been avoided entirely in the stiffened sample. Therefore, on the basis of this experiment it has been possible to achieve a higher quality component through the placement of resin patches.

3.3. Requirements for Fully Automated Dispensers for Forming

The most successful preform modifications over the course of this thesis were achieved through the use of an epoxy film, or deposited by hand using a pipette and needle, however due to the desire to automate the process as much as possible various attempts at printing resin onto the fabric were made.

A 3-Axis Robot was used in conjunction with a TH-2004AB two components meter-mix dispenser both manufactured by Cixi Tian Hao Electric Technic Co Ltd to work as a resin printer which has the capacity to mix resin and hardener and inject this through a nozzle or needle along a pre-programmed path. However, various issues were encountered with this technique which limited its effectiveness. Generally, the resin barriers or patches created with this technique were of poor resolution and had imprecise geometry and corners. This was due to a range of problems including poor mixing of resin and hardener, unsuitable viscosity levels, difficult to control flow rate and excessive spreading due to capillary forces.

The issue of determining viscosity was especially problematic as the resin printer required a relatively low viscosity such as that typical of liquid resins, whereas for the patches or barriers to consolidate well without excessive spreading considerably higher viscosity was required. The process of creating patches or barriers involves firstly the deposition of resin onto the fabric followed by a heating and pressing process to consolidate the patch into the fabric. When liquid resin was used as opposed to epoxy film this led to an uncontrollable and usually excessive spreading of the deposited resin as shown in Figure 3.10. It is therefore desirable for the deposited resin to be as viscous as possible and also for it to be deposited in a very narrow strip. Attempts were made to use low viscosity resin with a fine needle and then to partially cure the resin before any pressure was applied. This resulted in considerably less spreading, however this also caused uncontrollable thickness variations in the regions where the resin had been deposited.

The requirements for a successful bespoke resin printer are therefore as follows. The printer must have the capacity to accurately control flow rate, there must be no lag between actuation and flow at the nozzle, as well as an abrupt stop in resin flow after actuation has ended to prevent any more deposition due to the effects of gravity. The dispenser must thoroughly mix resin and hardener before deposition whilst keeping these constituents separate initially to enable continuous production. A needle can be used to help control resin flow, however fine needles may not be compatible with highly viscous resin, especially when additives have been introduced to raise the viscosity. Three degrees of freedom are required to allow for through thickness deposition for multi-ply preforms.

Various attempts to create neat barriers and patches are shown in Figure 3.10. Ultimately these were not successful and demonstrate what happens when the bespoke requirements outlined above are not met. The decision to revert back to manual deposition was favoured. It should be noted that the resin

mixing issues could have been resolved by using a more basic resin printer where the resin is pre mixed and injected from one single chamber as was used in [78], however it was not anticipated that this would resolve the issues of capillary forces causing excessive spreading as the geometry printed in [78] had simpler requirements.

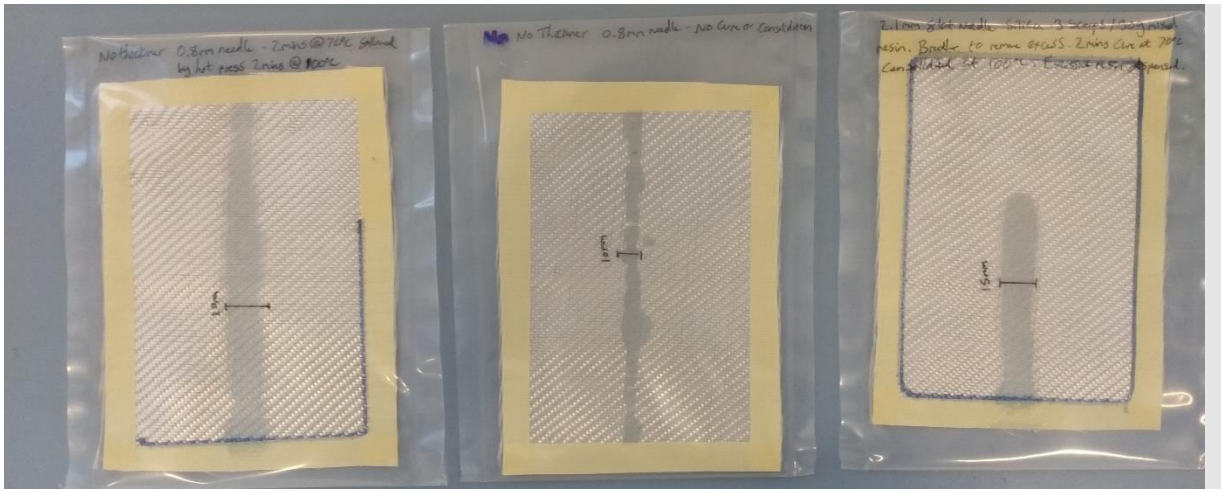

Figure 3.10: Various resin printing attempts (left: no thicknener, 0.8mm needle partially pre-cured; middle: no thickener, 0.8mm needle no pre-cure; right: 2.1mm needle, thickened with silica, partially pre-cured)

An alternative technique would be the approach of printing resin onto the surface with a LaserJet type printer as this allows for much more precise application and ultraviolet curing. This technique is in development with Joesbury [94].

Primarily the issues encountered in this project are considered to be related to the equipment available and a more appropriate and precise resin printer should allow for the accurate deposition of resin to form patches or barriers on a dry fabric without any significant issues. This therefore presents a potential opportunity for improved automation of the process allowing for a scaling up of technology readiness level and applications in mass production.

4. Numerical Techniques for Defect Detection

The previous chapter demonstrated the possibility of formability enhancement with local modification of preform properties. The position of stiffening elements, such as tufts/stitches/patches, is fundamentally important in changing the forming pattern. The design space with regards to placing the patches is vast – patches can be of various dimensions, shapes and introduced anywhere on the preform. The consequences of placing the patches can often be difficult to predict in advance as too many factors are at play and the material properties are highly non-linear. The most important factor to consider is forming defects, particularly wrinkling of the fabric. To establish the relationship between the location of patches and intensity/probability of wrinkles, the numerical framework needs to be established.

This chapter explores the concept of using an automated algorithm to identify defects within a simulated formability trial. An important part of this algorithm is an automatic assessment of defect likelihood/intensity and a built-in approach about driving the algorithm to an optimum scenario of patch placement. The study in this chapter examines various criteria for assessing defect likelihood and attempts to build a foundation for fully parametric optimisation. Removing subjective visual assessment of wrinkling is an important step in that direction. A detailed step by step algorithm is presented along with a demonstration of the algorithm which can identify the location of wrinkles within a simulation without requiring human input. The application of the algorithm to a test case study is then examined. The further work required to turn this into a fully autonomous patch-design program is detailed. Possibilities for run time optimisation are considered to enable more effective use of the tool.

4.1. Model Formulation / Description

To design patch placement, a continuous 2D surface representation of the fabric was adopted. Following the approach suggested by Khan et al [27] it uses a hypo-elastic model implemented into a VUMAT user material subroutine for Abaqus explicit. The model defines shear stress-strain response in the coordinate system associated with the orientation of warp/weft yarns and tracks the fibre reorientation to ensure correct stress computation for material undergoing large deformations. A hypoelastic model is ideal for tracking the large scale deformations found in composite preforms where accurate stress computation relies heavily on tracking the fibre orientation. An important further development suggested by Thompson et al [33], [48], includes the superposition of shell and membrane elements to realistically represent both the high in-plane tensile stiffness and low out of plane bending stiffness, an important characteristic of fibrous and woven materials. Thus, the model correctly captures the dominant features of fabric behaviour: fibre rotation, shear stiffening, uncoupled bending and tension responses. In addition, the continuous formulation makes it more

computationally efficient and numerically stable than the discrete model [53]. All these features make it an appropriate and rational choice for the purposes of patch placement optimisation.

Driven primarily by the needs of patch position design, the shear stiffness of the fabric is considered to be non-linear and increasing exponentially with shear angle, with the unpatched fabric used here having a lower initial stiffness and higher locking angle than the patched fabric used in later chapters. The shear behaviour is described by the polynomial expression in (5) which gives the shear stiffness, G_{12}, as a function of the inter-fibre shear angle, γ. This characteristic behaviour of woven fabric was adapted from the study of Thompson [48], exhibiting exponential stiffening typical for many engineering fabrics including carbon and glass woven preforms

$$G_{12}(\gamma) = 193.8\gamma^5 - 253.3\gamma^4 + 121.9\gamma^3 - 21.53\gamma^2 + 0.9932\gamma + 0.05827 \quad (5)$$

The slight non-monotonic variations in shear stiffness at low shear angles is a widely observed behaviour introduced by the boundary conditions of the picture frame shear test and can be seen in a number of studies [95], [96]. Compared to the large shear deformations observed in forming over the studied shape these variations are negligible and do not affect the solution.

For the membrane elements (M3D4R) a Young's modulus of 35,000 MPa was assigned to the fibre directions whereas the shell elements (S4R) were assigned a modulus of 50 MPa equivalent to a bending rigidity of 0.52 Nmm^2 for an element thickness of 0.5mm, to represent the low bending stiffness (obtained from [48]). The shell elements were given five integration points. Both element types were assigned a thickness of 0.5mm. It is important to note that the model parameters are not being matched to the specific fabric considered in the manufacturing trials of Chapter 3, this is given further consideration in Chapter 5, however the focus in this chapter is on post-processing of the model output.

To examine the application of the model to defect detection, a case study with single diaphragm forming over the tool considered in the previous chapter is considered. At present, there is no established methodology for patch property identification, this is explored later in Chapter 5. In the simulation presented below the focus is on contrast between the properties of the patches and the fabric, whereas the exact properties of the preform are less important. Hence, the generic properties of a characteristic fabric have been used as the input for the material model [48]. The fundamental features of the solution, such as the defect location/orientation and trends in shear angle distribution, are likely to be preserved when exact properties are tuned. Overall, numerical trials with variation of these properties and experimental trials presented in section 3.2 confirm this assumption.

The mould included a flat area outside the component contour of 250×250 mm in-plane dimensions. The meshed fabric was created to be slightly larger than the mould in-plane (see Figure 6.1) and was meshed with quadrilateral elements. It is possible that fabric size will influence the resulting wrinkle pattern, consequently these dimensions were chosen to be similar in size to the experiments of section 3.2. The choice of preform dimensions in the experiments on the other hand was chosen by the motivation to minimise the influence of edge effects. A Coulomb friction model with a penalty algorithm was used to model contact between the fabric and the mould. A small coefficient of friction (10^{-6}) was added to stabilize the numerical solution. The mesh size was set at a seed spacing of 2 mm for both the fabric and the mould, with an analysis time of 10 seconds. The mould is simulated as un-deformable rigid body shell elements (S3R, S4R). A PC with the following specifications has been used for the simulations: 3.4GHz, 4 Cores, 8 Logical Processors, 16GB RAM.

A mesh sensitivity study was carried out to ensure that the model outputs were not overly influenced by mesh size. It was found that mesh sizes with characteristic linear dimensions larger than 3 mm generally caused the run to crash due to excessive distortion of the mesh. On the other hand, mesh sizes lower than 1 mm caused excessive run time. A significant change in shear angle resulted from the reduction in mesh size from 3 mm to 2 mm, this then levelled out and no significant change was found in reducing further to 1 mm. It was also found that to reliably achieve full mould closure with a range of patch combinations whilst avoiding premature failure of the run a characteristic linear element size of 1mm was needed, however 2mm was generally adequate for achieving partial closure (60% or better). The reason for this premature failure was due to the mesh size being too coarse prohibiting the mesh from closely following the contours of the component, which combined with the assumption of incompressibility in the through thickness direction blocks full closure. A comparison of the deformation patterns between the 2mm mesh and 1mm mesh is shown in Figure 4.1. The wrinkle occurrence sites, severity and shear angle are all consistent across both arrangements. On this basis the 2 mm mesh size was chosen as a good balance of accuracy and achievable run time. A few exceptions to this were made, and these are noted where they occur later in the thesis.

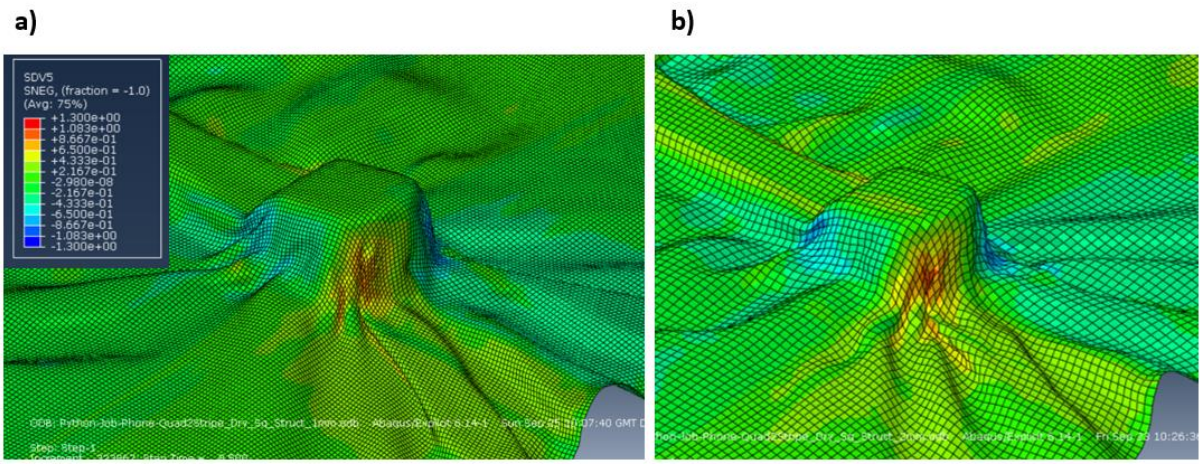

Figure 4.1: Comparison of deformation pattern with a) 1mm mesh and b) 2mm mesh with colour plot overlay of shear angle.

4.2.Defect Detection Algorithm

There can be different criteria for characterizing success of forming simulations or the risk of wrinkling. Inherited from kinematic modelling, shear angle is often considered as the most indicative metric of wrinkle occurrence [15], [16], [22], [53], [44]. This refers to the concept of the locking angle at which the yarns in fabric come into lateral contact and no further shearing is possible. Hence, the shear angle is the simplest geometrical approach that can flag a risk of wrinkles. In this concept, the defects would be predicted in regions where shear is highest. This criterion has a series of drawbacks and did not seem plausible in practically relevant situations [54]. A high shear angle does not guarantee the presence of a wrinkle nor does reducing the shear angle guarantee less defects. Shear angle is a good indicator of the most likely locations for a wrinkle to occur but depending on other constraints such as tensioning a wrinkle may or may not appear in reality. For instance, the type of forming operation can dictate what the critical locking angle is [15], [16]. Early buckling, on the other hand, prevents the development of high shearing. It is therefore desirable to further the process of automating the detection of wrinkle formation with a more complex measure which takes advantage of the high fidelity model available.

Of particular interest is the development of a numerical tool to identify wrinkle formation without the need to rely on shear angle. This would need to compare distortion of the preform to the 'ideal' distortion of a hypothetical perfect adherence to the tool face. This would then allow for identification of defects predicted by a forming model which would be ideal for the development of iterative optimisation models. Taking advantage of high-fidelity simulations, other criteria for buckling can be deduced – e.g. wrinkling can be directly informed by the rotation and folding of material. On the other hand, the numerical simulations at this stage are time consuming and often are not stable. Earlier indications of wrinkling may be needed particularly in the context of the parametric optimisation. One

such indicator could be the compressive stresses acting along the fibre direction, as suggested by Matveev et al [97]. In the current research, various indicators have been examined and assessed.

Acknowledging that the physical wrinkle is an out-of plane buckling phenomena, the algorithm compares the angular rotations of the nodes within the fabric with respect to the corresponding surface of the mould once the simulations have been completed. It works on the basis that in a hypothetical 'perfect' forming scenario the fabric would always comply with the geometry of the mould. For example if the tool surface is planar then the fabric adhering to it would also be flat. Wherever a defect occurred it is reasonable to say that there would be a noticeable discrepancy in the plane of the fabric and that of the mould in the local area.

This algorithm has been implemented in Python as follows:

- Each point on a 3D surface, evaluated at the nodal locations of the mould mesh, is characterised by the normal vector to the mould surface and equivalently by the tangential plane (plane A).
- Likewise, the normal to the preform surface and the correspondent tangential planes (plane B) are calculated for each node of the preform and tracked throughout the forming operation.
- The coordinates of the node in the mesh are compared to the coordinates of the nodes in the mould. The node on the mould nearest to that on the fabric is chosen for the comparison and the node couples in the mould-preform surfaces are identified.
- The angles between the normals of the mould-preform nodes couples (or, equivalently between planes A and B) as well as the distances between the nodes are calculated. This angle is used as a measure of the discrepancy of the preform adherence to the mould.

Indeed, the rotation of the preform plane, characteristic for wrinkles and folds, would be visible by the examining the normal at the locations where the preform complies to the tool shape. A flowchart of this process is also shown in Figure 4.2.

At this point the process can already give an indication of problematic areas, however it is important to (a) filter out numerical noise and distinguish sporadic shape fluctuation from the wrinkle, (b) join separate indications of non-adherent elements into the integral representation of wrinkle. The dimensions of a wrinkle, as well as its orientation, is an important parameter of defect intensity and can serve as a measure of success or failure in forming operations. This is done by identifying chains of adjacent non-adhering nodes whereas isolated rotations on single nodes are deemed to be associated with mesh issues and discarded. This process is carried out as follows (note that a downselect of 300 is chosen for demonstration purposes only):

- Nodes from the previous stage are down selected by disregarding all but the top 300 nodes based on the angle discrepancy.
- These nodes are considered one at a time. For each node an adjacency check is carried out to see if this node is adjacent to any of the other nodes in the top 300.
- Where a chain of two or more nodes is established each node added to the chain also undergoes an adjacency check and the chain is lengthened until all adjacent nodes are exhausted.
- This process is repeated for all nodes in the top 300, resulting in the assessment of the number of chains, their length and orientation. These parameters are then used to establish the severity of the wrinkling.
- The visualisation is then applied to highlight the problematic areas on the deformed shape.

The criteria for the downselect threshold of 300 is somewhat subjective and may need to be justified for each preform and/or NDT capability separately and/or defect severity requirements. For the purposes of this example all chains of two or more nodes (which corresponds to the characteristic size of 2mm) are plotted so that they can be validated by a visual inspection and the accuracy of the wrinkle determination algorithm can be assessed, as shown in Figure 4.3. A more detailed description of the computational steps within Python is provided in Appendix A.

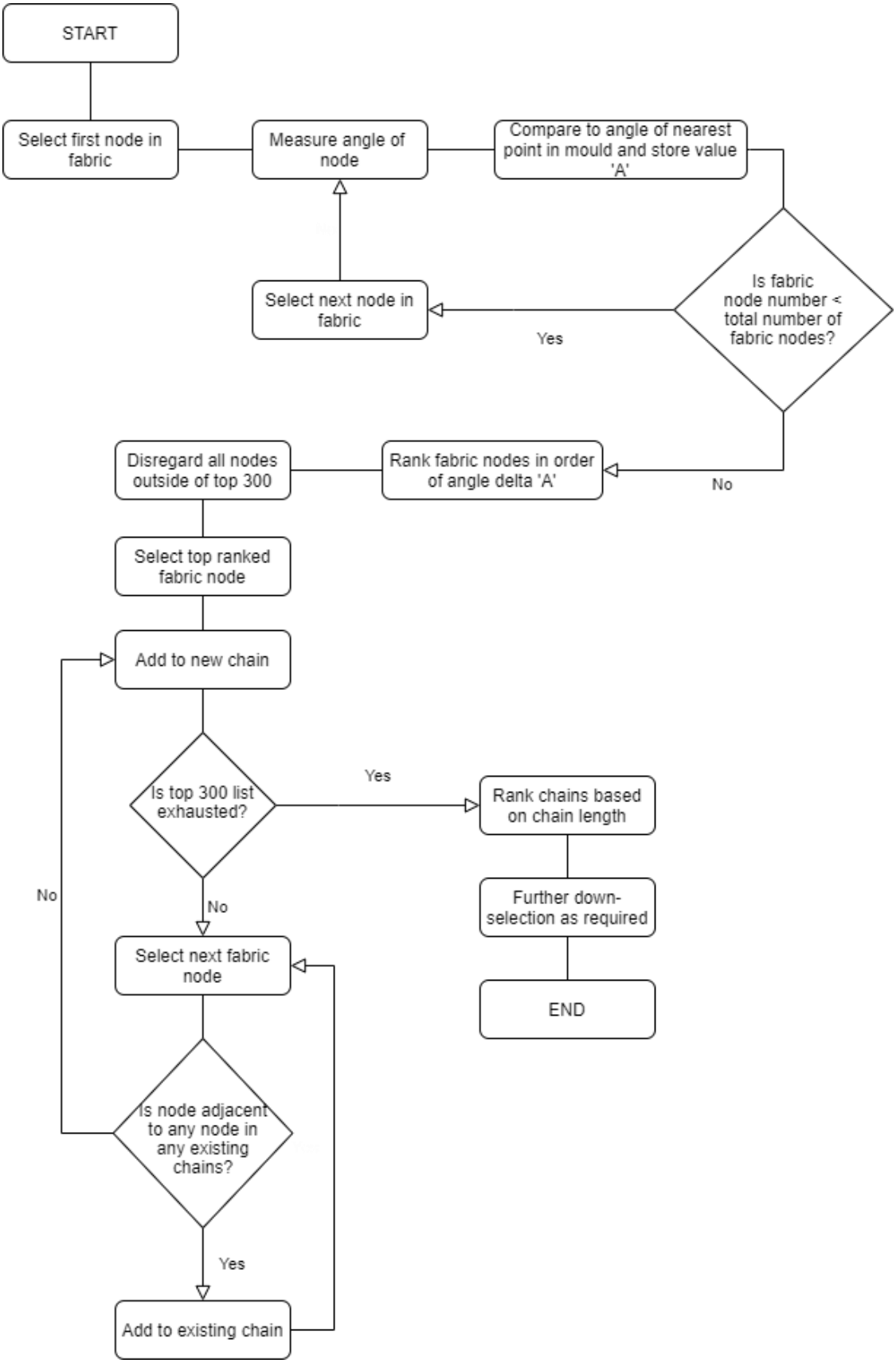

Figure 4.2: Flowchart showing the steps of the wrinkle detection algorithm. Actions are denoted as squares and decisions are denoted as diamonds.

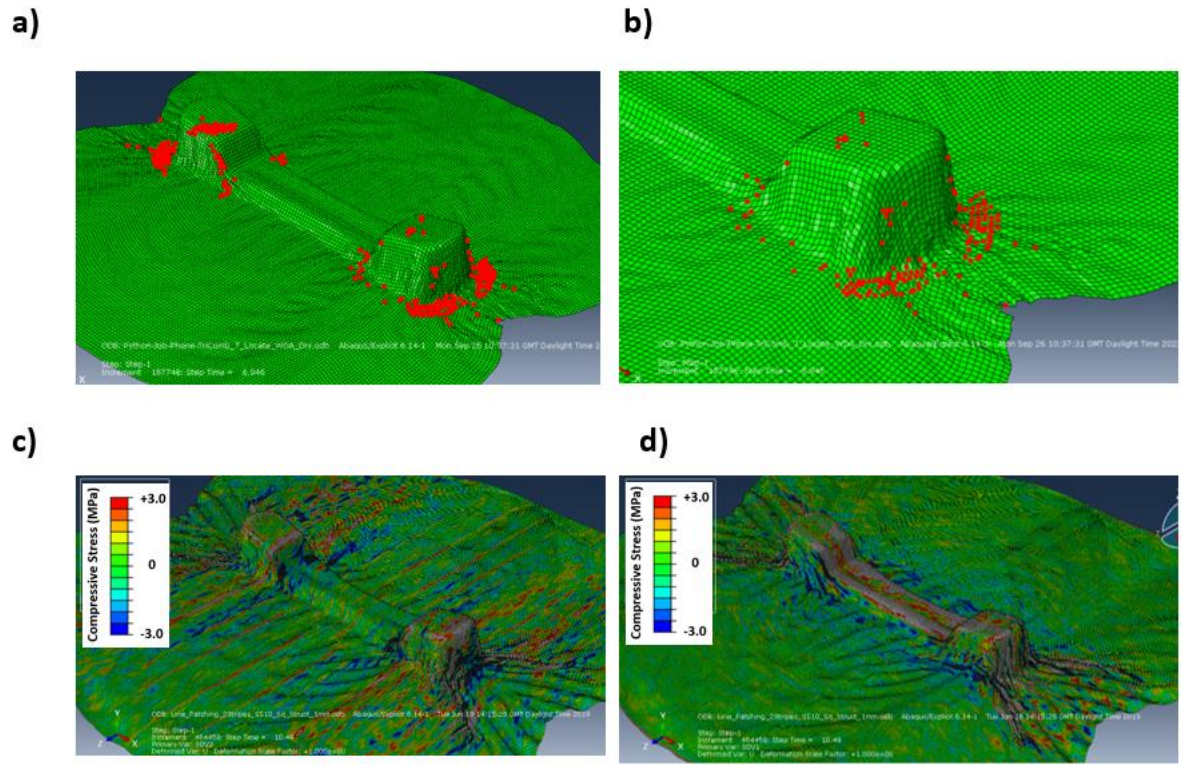

Figure 4.3: a) Down selected chains highlighted in red over deformation pattern, they can be seen to be largely clustered around visible wrinkles; note that nodes hidden behind the mould are shown through as if the mould were transparent b) close up view c) compressive stresses in x-axis d) compressive stresses in z-axis

From Figure 4.3 it can be seen that the tool effectively identifies the visible wrinkles around the difficult to form regions of the mould. It can be seen that some visible wrinkles are not highlighted and for some only a part of the wrinkle is covered. This is due to the exact placement of the threshold and a higher threshold would allow for more wrinkles to be identified. However, this is not necessarily beneficial as it may start to highlight irrelevant features, such as fabric waviness associated with not having full closure of the moulds. Wrinkles near the corner of the component are identified, however many of these are merged together with no clear wrinkle direction identifiable, this is likely due to multiple wrinkles fanning out from the corner overlapping each other and so being treated as one by the tool. Wrinkles are not detected as they propagate further from the component due to dropping below the threshold. As expected the effectiveness of the tool is determined in large part by the down-select criterion applied as well as some influence of the mesh size.

This algorithm now allows for the automated placement of patching to mitigate these defects and creates a framework for the fully automated process where wrinkles could be detected and resolved automatically through an iterative process of patch placement.

It is envisaged that this tool for wrinkle detection is helpful for more than just informing patch placement. It is generally acknowledged that shear angle is not the ideal method for identifying potential wrinkles and that better measures are needed. This tool has great potential for any scenario where multiple formability trials are to be carried out and compared. Another significant limitation of identifying wrinkles 'by eye' or using shear angle as the measure is that it is difficult to rank and compare the severity and number of wrinkles if the simulation results are visually similar.

This tool provides as an output a set of node chains of varying length, with the length roughly representing the severity of a wrinkle. It is necessary to devise a method of quantifying the overall severity of wrinkling for the whole component in order to quantify whether a set of formability parameters has resulted in a desirable outcome. Comparable measures utilising shear angle would be either the maximum shear angle occurring in the region of concern or the average shear angle. The equivalent of these measures using this wrinkle detection algorithm are either the length of the most severe wrinkle (in number of nodes) or the total number of wrinkles occurring in the area of concern. Neither of these measures are perfect, especially as the tool is still in the development stage and the exact definition of a wrinkle is ambiguous (do all the nodes have to be in a line, for example? Are two small wrinkles worse than one large?). Therefore a hybrid measure is considered to be most appropriate as follows:

1. All wrinkles (node chains) not in the region of interest are discarded (i.e. beyond the contours of the final component).
2. The minimum critical length of a wrinkle is considered to be 6mm, as finer wrinkles are believed to be suppressed in the subsequent consolidation process.
3. The total number of remaining nodes in all remaining wrinkles are counted.

The exact threshold for step 2 depends to some extent on the meshsize, for the case of this thesis six is considered suitable with a meshsize used of either 1.5mm or 1mm throughout, therefore a wrinkle would need to be at least 6mm long to be considered which is comparable to preform thickness and can be considered to be indetectable with current NDT capabilities. This quantification method allows for the 'weight' of wrinkles occuring in the area of concern to be compared across simulations. This tool is used in Chapter 6 as a key tool for assessing wrinkle severity in addition to shear angle, where it is trialled and its merits and disadvantages compared to shear angle are discussed.

4.3. Discussion

For the successful use of this wrinkle detection algorithm it is very important to have a highly accurate model. Search algorithms such as this are only possible due to recent developments in fabric formability modelling which have allowed for sufficiently accurate models to show the individual

shapes of wrinkles. To identify a wrinkle automatically it is essential to first have an accurate representation of where wrinkles should occur followed by an effective algorithm to identify that wrinkle. On top of this requirement to have accurate modelling is the requirement to consider the impact of simulation parameters on the wrinkle locations. It is well known that mesh size and mesh uniformity can bias a model towards wrinkles in certain locations, it is therefore essential that before this algorithm is applied the underlying model must first be validated and demonstrated to work in practical formability experiments. Once the effectiveness of simulations is established it is hoped that this detection algorithm can be used in conjunction with the optimization procedure presented in Chapter 6 to allow for a fully automated optimization process, ultimately aimed at reducing experimental time and designing a streamlined system for effective and efficient use of patch placement to optimise formability.

An important part of this algorithm is its ability to specifically detect wrinkles (as opposed to other types of defect), presently chains of nodes are identified simply based on their relative rotation with respect to the mould and therefore a fold is indistinguishable from a wrinkle, except for the fact that a fold may well have a more gentle curvature making it more likely to fall below the threshold. From the point of view of optimization however it is not currently necessary to distinguish between the two as this can equally be targeted by patch placement for wrinkle mitigation. However, in order to identify wrinkling other modes of defect formation had to be eliminated, foremost among these was the elimination of swirl which in modelling terms equates to in plane rotation. As the primary identifier of wrinkling is out of plane rotation, all in plain rotation had to be dismissed to avoid excessive complication of the algorithm. this does lead to the potential scenario whereby major defects are not identified by the algorithm simply due to them not strictly being a wrinkle. Another excellent example of this is bridging which, as it forms a gentle slope with only minor deviation from the angle of the mould, is unlikely to appear above the threshold. This is not a significant problem but does need to be considered and will require a check by a human to ensure sensible results are obtained and major defects are not overlooked. It would be beneficial to run a series of experiments in conjunction with simulations and automated wrinkle detection to identify firstly how well significant wrinkles can be detected and secondly how well the algorithm distinguishes between major defects and minor defects. As a result of this it would then be possible to update the threshold and downselect criteria to better tailor the model to identifying defects which are of greatest concern and avoid flagging up defects which are either minor or do not actually appear in experiments. It should be a learning process which will effectively teach the algorithm how severe a discrepancy is required in a simulation in order to be identifiable in experiments.

Further validation of the algorithm to identify its robustness in various geometric situations would be beneficial to ensure that equally sized wrinkles are equally likely to be identified, regardless of where they appear in the component geometry. For example it would be beneficial to confirm that wrinkles

occurring at the flat plane outside of the area of interest are equally likely to be identified as those occurring near a corner or inclined surface. Finally a very important consideration for this algorithm is how effectively it works when used on different types of model, for example in this thesis it is only trialled on two geometries. An important further step in establishing it as a useful approach would be to see how it works with alternate mesh shapes and modelling approaches. The range of models to choose from for this validation is limited as it must be a model that is able to physically predict wrinkles as they are formed rather than just identify areas of significant distortion or shear.

The run time for this tool is significant, requiring approximately 3 hours to process a model with 60,000 elements contained within the fabric with 4CPU. There are potential optimisations available which can be used to improve run time. The model currently attempts to match every node in the fabric with every node in the mould to identify which is it nearest node to compare rotations with. This is highly inefficient and could benefit significantly from partitioning the model into quadrants or potentially even smaller. Due to the lines of symmetry of the simulation shown this would allow each node in the fabric and each node in the mould to be assigned a quadrant allowing the number of nodes to be searched when finding the nearest partner to be cut by a factor of 4. This step currently accounts for the biggest delay in the algorithm run and therefore it is anticipated this could reduce runtime by at least half allowing for the tool to be more practically used when optimising formability. Ideally for an optimization run the detection algorithm may be used up to 5 or 10 times in a row for the automated placement of patches as discussed in Chapter 6. This is in conjunction with the runtime of the simulation itself and it is therefore essential for good optimization to keep these times as low as possible. The efficiency of the algorithm is also important as it allows for a finer mesh and therefore more accurate identification of wrinkles.

5. Characterisation of Enhanced Preforms

This chapter follows the demonstration of wrinkle detection techniques in Chapter 4, the topic of how to characterise localised enhancements is explored. This chapter focuses specifically on attempts to characterise how resin patches behave in shear to allow for more accurate formability modelling. It is demonstrated how a bias extension test can be adapted to identify patch shear behaviour to a good level of accuracy, allowing for the proposed technique to be put forward as a method of material characterization. The approach of partially covering the bias test in patch material is shown and the effectiveness of differing levels of coverage reviewed. Two models are explored, one for viscous materials such as stage cured resin or resin film and a second for high stiffness non-viscous materials. These simulations are shown initially to demonstrate the theoretical possibility of the technique before experiments are carried out to assess whether the models were realistic and whether the experiments are able to provide accurate stiffness or viscosity values.

The success of the forming operation described in Chapter 3 depends on the balance of properties between dry and patched materials. At present, there is no clearly established methodology for the characterisation of these formability enhancements. Patches are local and an isolated coupon often cannot be extracted from a hosting fabric. This chapter discusses the feasibility of adapting the conventional bias extension test to extract the shear properties of locally enhanced material. The obtained properties are critical for modelling tools that can inform the optimum patch location and orientation. The suggested approach is practical, simple to implement and proven able to provide properties to a reasonable degree of accuracy for non-linear elastic and visco-elastic patch behaviours.

This study seeks to investigate the feasibility of a new experimental procedure where the properties of patches, which can be highly non-linear and time-dependent, are extracted by testing a larger volume of the material. This testing will also give a deeper insight on how localised enhancements affects the macroscale behaviour. The experimental procedure is based on several elements: (a) reference testing of blank fabric, (b) detailed deformation analysis using optical methods, (c) concurrent numerical modelling. The process is first analysed in a virtual environment where input (hypothetical) properties of the patch need to correspond to deduced properties from the test. The methodology for the derivation of shear behaviour using an experimental setup needs to be practical, repeatable and reliable.

For validation of the testing procedure, this chapter explores two different characteristic material behaviours; (a) approximating patches with increased localised stiffness response through the use of PLA (poly lactic acid) (non-linear elastic) and (b) increased localised viscosity through the use of epoxy resin film (viscoelastic). Elastic response is implemented using a non-linear hypoelastic model, and time-dependent response of impregnated fabric is modelled using a hypo-viscoelastic model

where the exponential stiffening behaviour of fabric is superimposed with a dash element connected in parallel. In the case of elastic response the validation is deemed satisfactory if the emulated experiment succeeds in reproducing the input shear stress-strain curve assigned to a patch. In the case of visco-elastic response, this also includes successful derivation of the viscosity of the dash element. Once the numerical procedure has confirmed the methodology is suitable, the approach can be attempted experimentally.

This chapter begins by exploring how the bias extension test could be adapted to derive the properties of a patch with non-linear elastic properties. These properties are characteristic for thermoplastic printed elements. In a virtual testing procedure the properties are derived from independent "measurements" and checked against the input properties. This procedure is then expanded to viscoelastic patches which may be close in behaviour to the case of epoxy resin film. Based on the outcome of these two modelling approaches experiments are conducted to deduce the actual properties of PLA and epoxy resin film.

5.1.Methodology

This chapter explores the possibility of modifying the sample by depositing patches on the bias extension sample and deducing the stress-strain relationship within the patch based on local optical measurements and scaling of load along with crosshead load and displacement. The main motivation for choosing the partial coverage test configuration is that the method needs to be robust for various modification/patch types such as tufting [20], [98] or fast curing resin [71], where full coverage is clearly not an option. It is important to distinguish wrinkling seen in the test on bias experiments and wrinkles that can be expected during forming. Patches play different roles in these two cases. It is anticipated that restraining the fabric will help in different circumstances, such as creating additional tensile stresses in critical locations or mitigating against excessive shearing beyond the locking angle. The discussion of this has been initiated in the papers of Turk et al [71] as well as on the papers with stitched/tufted patches [20], [98]. The purpose of this layout is solely the derivation of patch properties and not formability enhancement.

From forming and testing perspectives, various configurations of patch placement were considered. For brevity only the two that were deemed more plausible are discussed. The main factors of patch placement are the following:

1. **Orientation of the patch**. Chapter 3 demonstrated that the most promising configuration was the placement of narrow line patches at 45° to the fibre direction and enveloping a critical location. This orientation modifies shear resistance of the fabric without having a major impact on local bending properties of the fabric (NB: aligning the patch along the fibre

direction does not change the stiffness but may affect bending stiffness and lead to folds). Placing patches along the direction of the bias test is the logical choice as it maximises the contribution to the measured force response.

2. **Length of the patches.** The main choice here is between placing patches only in the central zone of pure shear or to make them span continuously through the length of the sample. The latter option was deemed preferable because it results in a more homogenous sample overall. See Figure 5.1. With this arrangement each individual region of the BET sample has the same percentage coverage and therefore the same average stress-strain response.
3. **Spacing and number of patches**. These parameters are assessed through numerical simulations and, as will be shown later, may be different for various patches depending on their properties and contrast in stiffness with the hosting fabric.

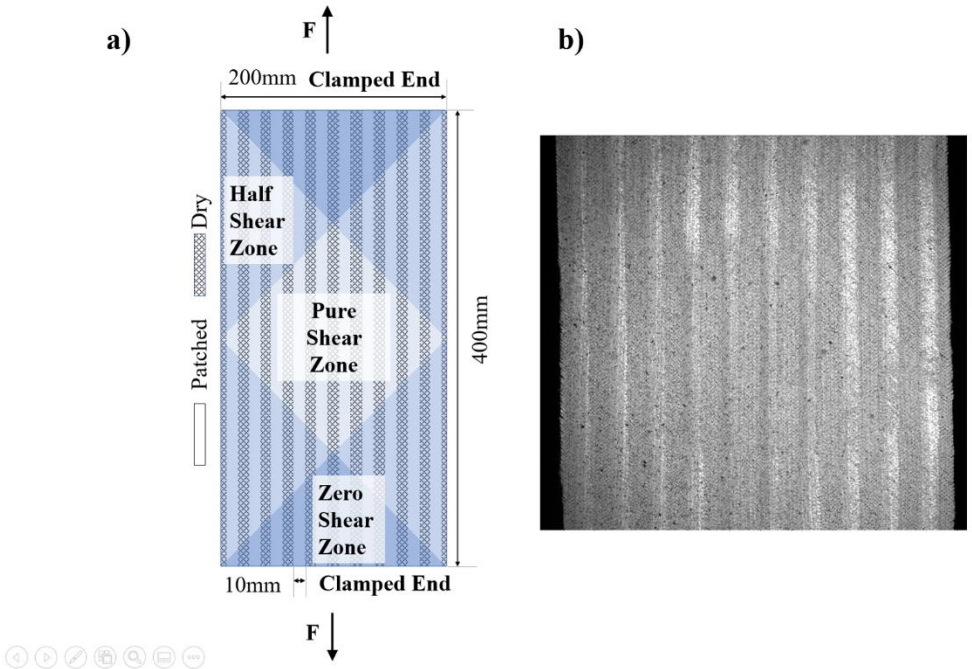

Figure 5.1: Bias extension test with modified sample geometry a) schematic diagram of patch distribution; b) actual geometry of the sample with 50% coverage of PLA patches (painted).

The procedure suggested for patched samples relies on several key assumptions. The primary assumption is that the total reaction force of the sample can simply be summed up from the contributions of the dry area and average response of the patches. It also assumes that the stress field within the patches is relatively uniform. In reality, the addition of patches inevitably violates the

homogeneity of the deformation even in the central zone of the sample, adding to the intrinsic non-uniformity of the deformation field in the BET test. Hence, the virtual experiment needs to assess the precision with which the properties can be extracted.

The proposed procedure for extracting patch shear behaviour can be condensed to the following key elements:

1. The fabric is partially covered in striped patches placed at a regular spacing and spanning throughout the length of the entire specimen – Figure 5.1
2. The BET test, instrumented with optical measurements of local deformations, is conducted both for patch-treated fabric and, separately, untreated preform. The behaviour of untreated preform is then used to subtract the contribution of dry areas to sample deformation.

Shear stress vs shear strain plots are generated for both types of specimen using equations 1 and 2. Equation 1 allows the calculation of shear angle as a function of crosshead displacement, based on the geometry of the sample. Equation 2 allows for the calculation of shear stress in the central pure shear zone as a function of shear angle, though it should be noted that this equation is iterative and therefore can only be solved incrementally. These two equations are used to first calculate the shear angle in the pure shear zone and second to calculate the shear stress allowing this to be plotted.

A scaling of the load needs to be applied to calculate how much of the load fraction can be attributed to patch deformations. The dry fabric shear stress value is subtracted from the patched sample value for a given shear strain and the resulting graph scaled up based on the percentage patch coverage (3).

$$\tau_{scaled} = (\tau_{Average} - \tau_{Fabric})/w_p \quad (3)$$

Where w_p is the relative area fraction of the patches with respect to the total surface area of the sample, and $\tau_{Average}$ is the average shear stress over the central region (zone C). This equation in effect subtracts the known shear stress contribution of the dry fabric from the shear stress of the patched sample, leaving an approximation of the stress contribution of the patched regions only, this is then scaled by the percentage coverage to allow meaningful comparison.

Another important aspect that needs to be explored through virtual testing is susceptibility of the chosen sample configuration to undesired deformation modes such as buckling. As will be shown the patch coverage may play a significant role in this.

Due to the evolution of the proposed methodology presented across this chapter in light of both simulated and physical experimental results, more detailed methodologies are presented within each sub section as the approach develops.

5.2.Non-linear Elastic Patches

In this section the feasibility of deducing non-linear elastic properties of patches from the bias extension test is explored. These properties are likely to be exhibited by patches with fully cured resin or patches created by dry sub-reinforcement, *i.e.* tufting and stitching. Various patch arrangements are trialled and the accuracy of the technique is assessed by comparing model output (replicating how data is acquired in actual test) to input, defined by the hypo-elastic model.

5.2.1. Model Description

In the model of the bias extension test the fabric was modelled in a continuous shell formulation. In line with a common modelling approach [71], the hypo-elastic modelling framework that was used to model both the dry fabric and modified patches, specifies that the materials exhibit nonlinear, but reversible behaviour. This is not strictly accurate of dry fabrics as upon unloading and reloading they exhibit a different loading trajectory, however for the purpose of active loading where each sample is only loaded once this approach is deemed satisfactory. Following the formulation, initially suggested by Khan et al [27], the fabric is modelled using a hypo-elastic VUMAT user material subroutine in Abaqus explicit. The model allows for the tracking of fibre reorientation and enables the correct calculation of shear angles at large deformations. The shear stress and shear strain behaviour are defined in the coordinate system associated with the orientation of yarns. The main issue with the shell formulation is coupling of tensile and bending behaviour which is not characteristic for preform behaviour. As demonstrated by Thompson et al [33] and similarly to Haanappel et al [55], the superposition of shell and membrane elements allows for the realistic modelling of both the high in-plane tensile stiffness and low out of plane bending stiffness. This enables the realistic representation of the main features of woven fabric behaviour: fibre rotation, shear stiffening, uncoupled bending and tension responses.

The simulated bias extension test is conducted on a sample of dimensions 100 mm by 200 mm with a crosshead displacement of 30 mm. A mesh size of 1mm was used, bearing in mind that the patch width used is 5mm resulting in each strip being approximately 5 elements wide. Rectangular elements were used, oriented at 45° to the loading direction. It has been well-documented that shear-locking of elements can lead to spurious wrinkles when simulating forming processes [99], [100], [101], these non-physical deformations are a product of shear locking of the elements. While using reduced integration elements can minimise this phenomenon, it was been shown in [99] that this does not

eliminate the occurrence of shear locking for all orientations of the mesh in respect to the fibre orientations. To avoid shear locking, the mesh has therefore been aligned with the fibre direction when simulating the bias extension test. The solver used is Abaqus explicit.

5.2.2. Simulation Input

The simulated test is run with various different patch coverage levels, in this case 25%, 50%, 75%, and 100% (see Figure 5.2). Using this range of coverages it is possible to get a clearer idea of how much patch material must be present on the surface of the fabric to obtain sufficient material data for property extraction. The 100% coverage scenario is not practical to replicate experimentally but is included here for the purpose of verification of the patch property extraction procedure.

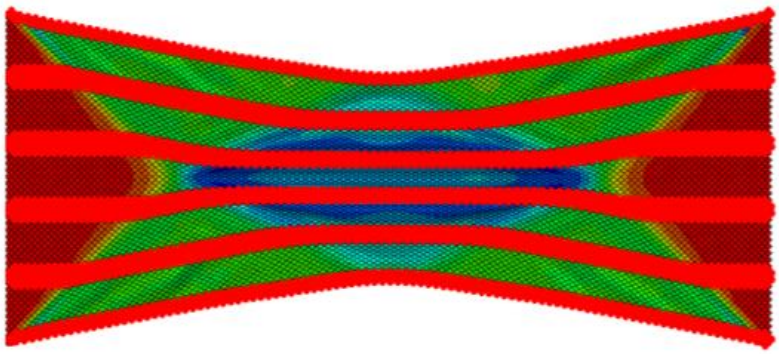

Figure 5.2: Bias extension simulation with striped patches at 25% coverage

The characteristic input properties for the dry fabric are provided as an empirical dependency of shear tangent rigidity vs shear angle. Driven by simplicity of implementation, this dependency is defined as a fifth order polynomial.

The plot of shear stress vs shear angle is shown in Figure 5.3. The chosen patch behaviour is not intended to be representative of a specific material at this stage but rather to examine features that may be observed in practice and show sufficiently contrasting properties. The patched regions are modelled as having a shear stiffness of approximately one order of magnitude higher than that of the dry fabric. There is also a significantly differing early stiffness response at lower shear angles. The early stiffening is chosen to reflect the initial resistance of the patches, which for some material forms may be more similar to composite-like behaviour than dry fabric. As the sample approaches the locking angle the influence of the dry fabric begins to contribute significantly to the overall loading response.

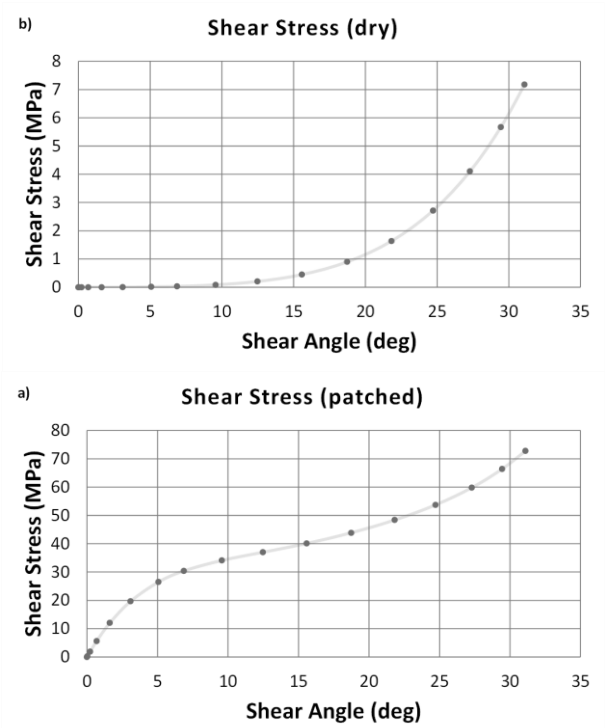

Figure 5.3: a) Shear stress input for dry regions b) shear stress input for patched regions (note: differing y-axis scale)

The underlying polynomial equations for dry and patches fabrics behind the graphs of Figure 5.3 are shown below:

$$\frac{d\tau}{d\gamma} = \sum_{i=1}^{5} a_i \gamma^t \tag{4}$$

The dry and patched fabric input polynomial coefficients are shown in Table 5.1. (obtained from [48]), where α is a coefficient, τ is shear stress and t = 6-i.

Table 5.1: Polynomial coefficients for dry and patched fabric as used in simulations

	a_1	a_2	a_3	a_4	a_5	a_6
Dry fabric	193.8	-253.3	121.9	-21.53	-0.99	0.058
Patches	-45449	107100	-88940	-35115	-6529	511

Note that these polynomials define the shear rigidity not shear stress and therefore define the gradient of the graphs of Figure 5.3.

The shear stiffness is of an order of magnitude higher in the patched regions when compared to the dry fabric behaviour, This relatively low contrast is chosen to allow the simulations to cover a wide range of potential future patch properties. In practice it is anticipated that the contrast in material properties between the two would be considerably larger than this for PLA patches. It is expected that a larger difference in behaviour will lead to a more accurate identification of the patch properties. The

modelling exercise is set to establish the protocol for the property extraction ahead of the experimentation and hence, the specific behaviour of the fabric does not affect the outcome of the exercise (processing of data obtained from the test). The characteristic behaviour of woven fabric was adapted from the study of Thompson [48], exhibiting exponential stiffening typical for many engineering fabrics including carbon and glass woven preforms.

5.2.3. Result Post-Processing

The post-processing of the patched sample is done in several steps. First, the effective response of the sample is assessed using the conventional methodology for BET using the crosshead load and displacement data (1)-(2). Second, the shear angle used in the calculation, is revised and instead averaged over the diamond shaped pure shear zone in the centre of the sample (zone C) based on local strain measurements rather than derived from (1). The resultant shear stress vs shear angle curves can be compared to the input shear properties of the patch. Particular attention is paid to the onset of lateral out-of-plane buckling and what impact this has on the validity of the shear angle calculations. The shear stress vs shear angle derived patch results for the range of coverages are shown in Figure 5.4a with the input curve overlaid. Both graphs are scaled based on percentage coverage as per equation (3).

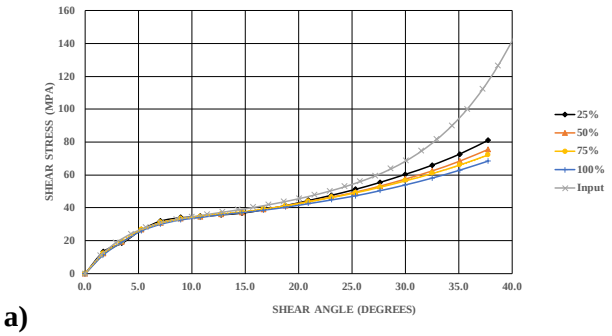

a)

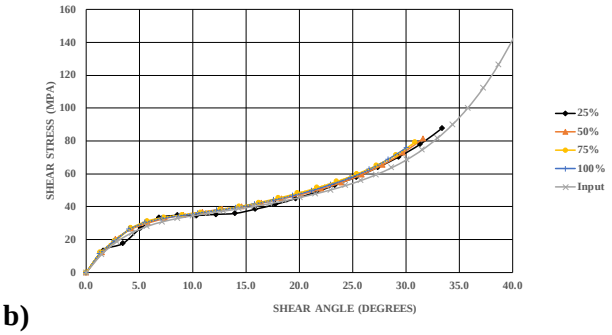

b)

Figure 5.4: a) Derived patch shear stress outputs compared with patch property input a) output crosshead derived b) output based on average local strain measurements

It can be seen in Figure 5.4a that because of the dominance of patch properties the dry fabric does not contribute to the apparent behaviour of the sample for shear angles up to approximately 20 degrees, with relatively little impact of percentage coverage on the result. At 20 degrees the largest error of recovered properties is 6.8% and, somewhat surprisingly, observed for the 100% coverage sample. Above 20 degrees the derived shear stress begins to fall below the actual patch response. Based on the significantly better correlation shown in Figure 5.4b this can be attributed almost entirely to the overestimation of shear angle by (1) due to the onset of out of plane buckling, which begins almost immediately and gradually worsens over the course of the simulation (see Figure 5.5). Any significant out of plane buckling leads to lower shear than equation (1) predicts due to the material finding another degree of freedom to accommodate the deformation. These results show that with a patch material of sufficiently higher shear stiffness than that of the dry fabric, the shear response of the patch regions dominates allowing for extraction of patch properties. For reference the height of the out of plane buckling visible in Figure 5.5b is 3mm from peak to trough compared to a patch width of 5mm.

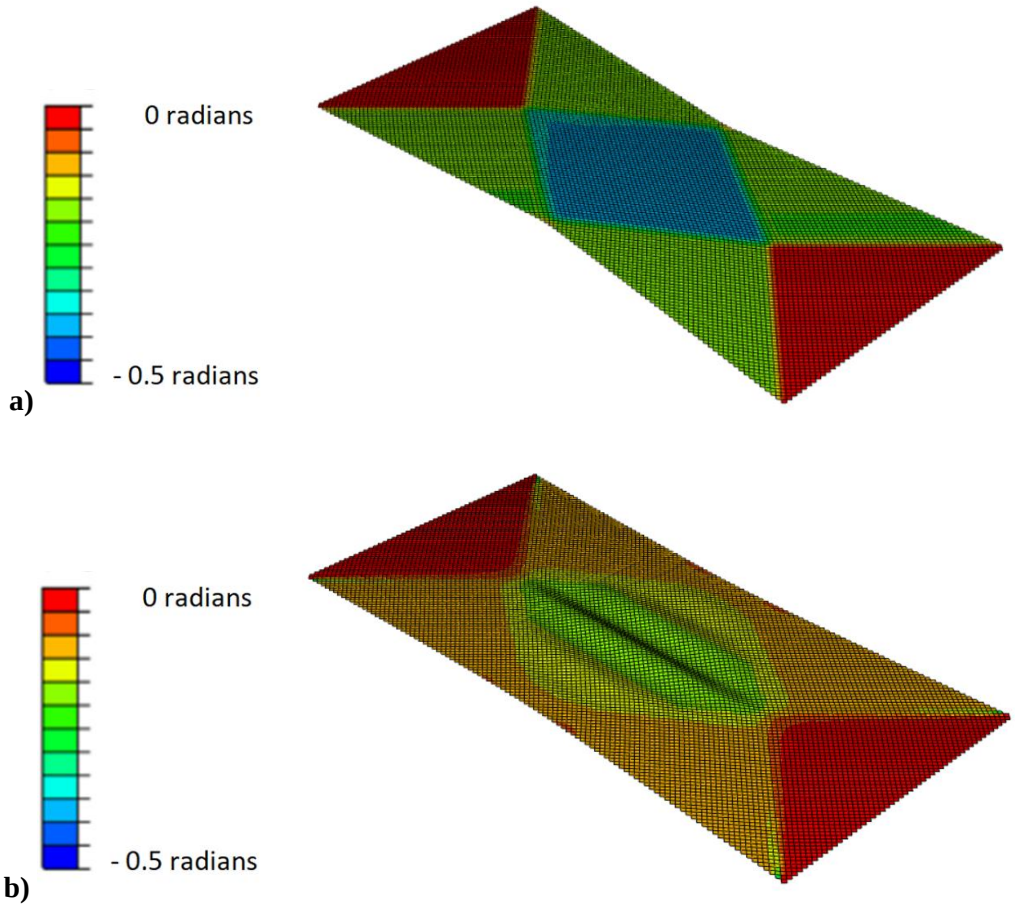

Figure 5.5: Comparison of deformation pattern for a) dry fabric and b) 50% coverage at 16.5mm crosshead displacement (theoretical equivalent of 20 degrees shear angle in the pure shear zone).

The limit of accuracy at 20 degrees is concerning as when using patches with relatively low shear stiffness this threshold could well be exceeded [71]. To improve the accuracy of property extraction, the shear strain within the patches could be directly measured rather than calculated from the cross-head displacement. This would rely on the assumption that the kinematics of the test would not be changed when incorporating the patches. These measurements could be realized by optical methods, such as digital image correlation (DIC). The shear diagrams extracted from the direct strain measurements based on averaging over the whole of zone C are presented in Figure 5.4b, these have been scaled based on percentage coverage as per (3). The results show that kinematics of the test and stress balance are now accurately captured to higher shear deformation despite the progressive lateral buckling of the samples. Note that the initial instability is caused by the iterative calculation of shear stress using (2) which is extremely sensitive to minor initial fluctuations in load.

5.3. Viscoelastic Patches

Section 5.2 explored the derivation of patch properties with a hypoelastic model for the scenario where there is a strong contrast in shear stiffness between patched fabric and dry fabric. This section considers the scenario where the desired patch property may be much less pronounced. This could be representative of the case of uncured or partially cured epoxy resin film deposited on the preform. Thermal conditioning of the deposited resin prior to forming allows the obtainment of various viscosities and hence, allows the user to flexibly tailor material performance to the requirements of the process.

5.3.1. Model Description

In the virtual testing experiment, the resin patch is modelled as a combination of a fully viscous element, representing the behaviour of resin film, and a non-linear elastic element, representing the behaviour of impregnated fabric. The elements are connected in parallel assuming that the deformation of the viscous and elastic elements are the same:

$$\tau = G\gamma + \eta\dot{\gamma} \tag{6}$$

Where τ is shear stress, γ is shear strain, $\dot{\gamma}$ is shear strain rate, G is the shear stiffness of the fabric and η is the Newtonian viscosity representing rate-dependent behaviour of the impregnated fabric.

This model is implemented through a user material subroutine based on a simplification of the work of Wang et al [102] using the Kelvin-Voigt model (Figure 5.6) [103], the overall stress being the sum of the contributions from the two elements. Significant work has been carried out previously in this field [104], [105], [106], [107].

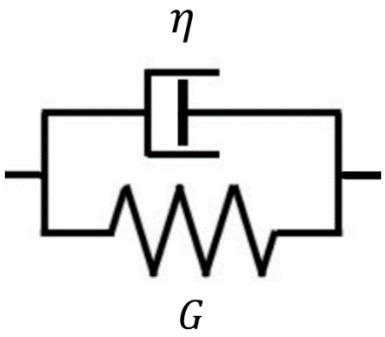

Figure 5.6: Kelvin-Voigt model

This relation is obviously a significant simplification of the actual behaviour of the impregnated fabric, which is known to be more complicated for materials such as prepregs [102], [108], [109],

[110]. However, this exercise investigates conceptual feasibility of extracting viscous patch properties from a BET. For a start, the behaviour of the elastic elements G(γ) is assumed to be the same as the behaviour of the dry fabric (4) and the virtual trial is focusing on deriving the viscosity of the liquid (damping) element from the BET. In practice, the lubrication is likely to affect the behaviour of the fabric. The possibility for generalization of the methodology will be discussed upon review of actual experimental results in later sections.

5.3.2. Result Post-Processing

The viscosity is explored in the wide range of 0.15-1500 MPa·s which covers a wide range of values that could be observed in practice from thermally-conditioned liquid resin intended for liquid moulding, to rigid PLA patches. The experimental procedure is adapted for the visco-elastic behaviour of the patches by conducting a series of tests at different strain rates. It is important to note that the constant strain-rate of the cross-head does not guarantee constant strain-rate within the patch, on the contrary strain rate will gradually increase as the shear angle increases. To deduce the viscosity, the results of the tests are mapped in the 3D space of shear stress / shear strain rate / shear strain. The viscosity is then obtained by regression of the data points with equation (4).

The total time of the test for the given displacement of the viscoelastic simulations varies from 10 seconds to 100 seconds to give a range of strain rates. Only the 50% coverage scenario is implemented in the experimental trials to keep the number of experiments manageable.

The crosshead load, represented in the model by the reaction force is converted to shear force using (2) and normalised by the nominal cross-sectional area to obtain shear stress - plotted on the Y-axis of Figure 5.7. Due to the accuracy errors previously found when using equation (1) in section 5.2, results are presented from both crosshead derived and directly acquired shear angles. Directly acquired shear angle is extracted from the quad elements within the model and averaged over zone C, this mimics optical measurement techniques. Shear strain rate is calculated by measuring the increment of shear deformation at each step of the run and dividing this by the duration of the step. A surface fit is calculated using MATLAB for the discrete data points. The surface fit is organized such that across every shear stress-shear strain cross-section the curve is described by 5th order polynomial in agreement with the dry fabric elastic response (4) and across every shear stress shear strain-rate cross-section is fitted by 1st order polynomial in agreement with a Newtonian flow model. Thus, the fit presents as a curve extruded in the shear strain rate space. This surface fit based on data from the five different strain rates is shown in Figure 5.7a (note that for brevity only the directly acquired ‘optical’ derived results are plotted). The fit was implemented using built-in MatLab polynomial regression with its quality characterised by R-square value of 0.97.

A 5th order polynomial was chosen as this matches the input polynomial prescribed for the fabric shear behaviour in equation 5. It is of sufficiently high order to capture the rapid initial elastic stiffening of the material followed by a levelling out dominated by viscous forces and also the later exponential stiffening dominated by fabric shear forces.

The gradient of the surface fit in the z (shear strain rate) – y (shear stress) plane corresponds to the viscosity value, this is evident from equation 6 where the only term which contains strain rate is a linear relationship with viscosity ($\eta\dot{\gamma}$). However this gradient fit varies with x (shear angle), therefore it is necessary obtain the gradient at a given shear angle x = 0.288 in order to get one fixed gradient value. The detailed reasons for selecting 0.288 radians as the shear angle are justified based on the later experiments shown in section 5.4, this is sufficiently far through the simulation to avoid initial fluctuations but well before the onset of exponential stiffening, therefore being the ideal point to obtain the most accurate viscosity reading.

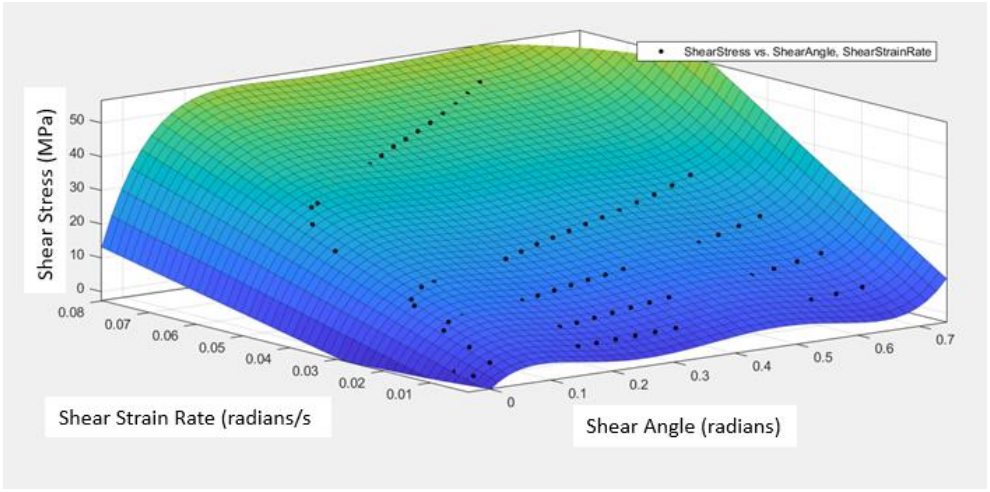

a)

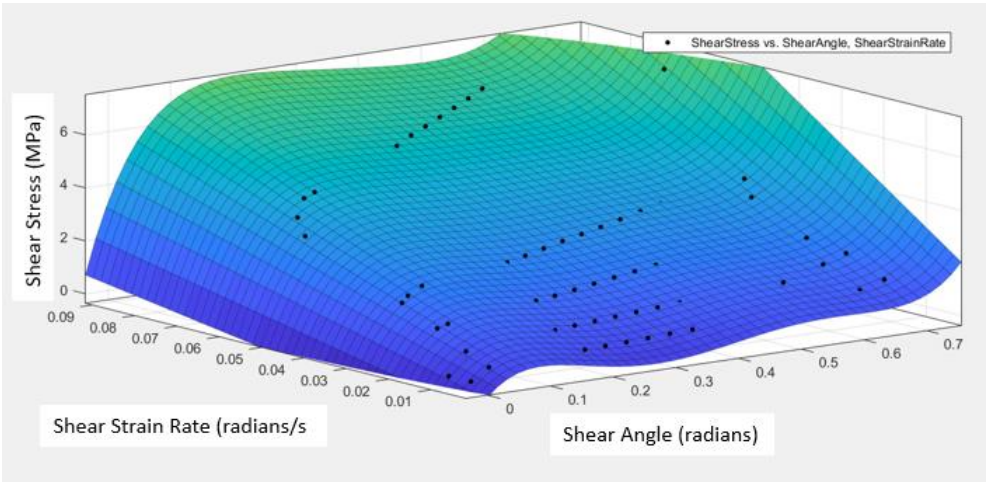

b)

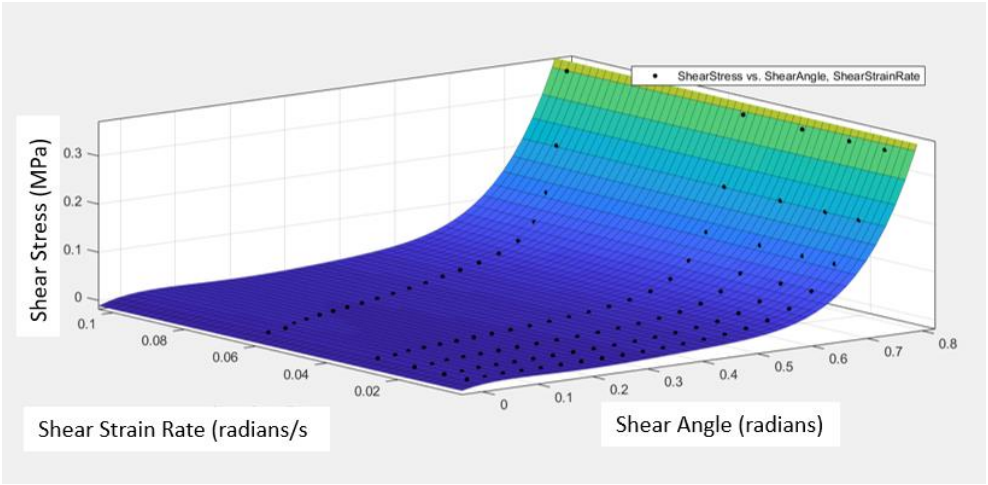

c)

Figure 5.7: Surface fit of shear stress response at various strain rates a) 50% coverage b) 5% coverage c) dry fabric

Derived viscosity values are shown in Table 5.2. The viscosity value is the gradient scaled by the percentage coverage. The viscosity value derived using the crosshead displacement has an error of 28% when compared to the input viscosity of 1500 MPa.s, this is a significant level of error, by

contrast the results based on local strain assessment is considerably better at 6.9%. This shows that due to the buckling and non-uniformity of the deformations, equation (1) does not represent the actual intensity of shear in the central zone. It is also observed that due to the relatively high coverage of patches out of plane buckling occurs very early on in the run.

Method	Coverage (%)	Target (input) viscosity MPa·s	Derived Viscosity (MPa.s)	Percentage Error
Crosshead Derived	50	1500	1075.2	28.3%
Based on local shear angle (Averaged over central zone C)	50	1500	1397.2	6.9%
Crosshead Derived	5	1500	1476.0	1.6%
Directly Acquired	5	1500	1632.0	8.8%
Crosshead Derived	50	0.15	0.098	34.7%
Directly Acquired	50	0.15	0.102	32.0%

Table 5.2: Calculated viscosity at both 50% coverage and 5% coverage firstly derived using equation 1 based on crosshead displacement and then secondly derived by averaging the pure shear zone C taking values directly from the model

On the basis of these issues it is decided to reconfigure the experiment in the hope of improving the accuracy when calculating shear angle based on crosshead displacement. A dry fabric sample with identical dimensions as before is treated with just one central stiffened strip 5mm wide, as shown in Figure 5.8, this reduces coverage significantly and avoids multiple patches alternating with unpatched regions across the sample.

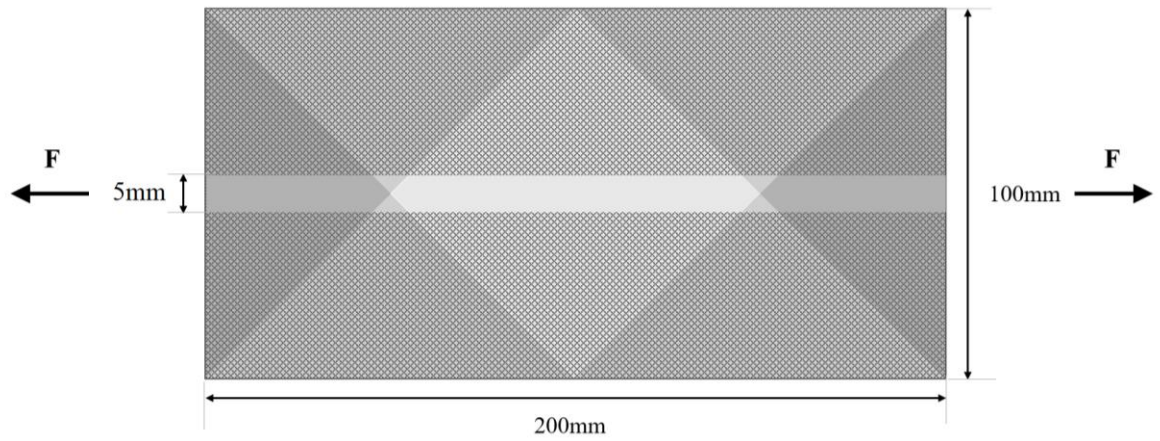

Figure 5.8: Bias extension test with one central stiffened strip

The simulated deformation pattern is compared with the previous setup in Figure 5.9, demonstrating that this new approach does indeed significantly reduce out of plane bucking. The comparison between 50% coverage and 5% coverage is shown at the midway point of 0.277 rad/15.9° shear angle.

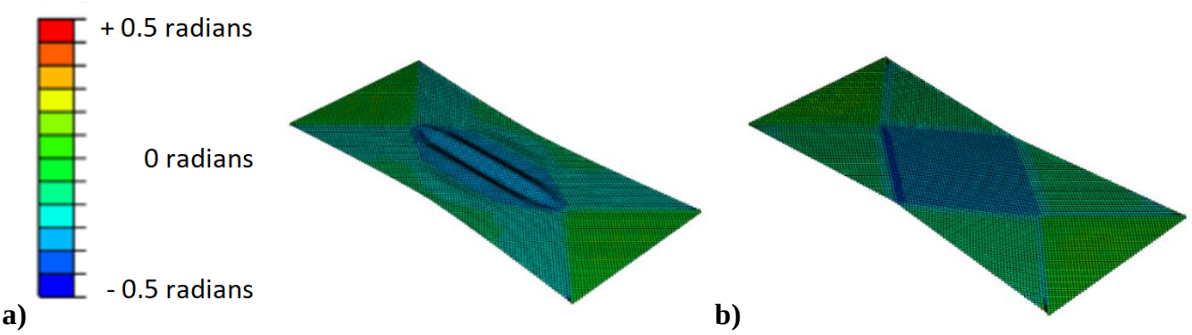

Figure 5.9: Comparison of out of plane buckling at midway point a) 50% coverage b) central stripe at the average shear of 0.277 radians

The 3D cure fit for the data from these experiments are shown in Figure 5.7b with the derived viscosity shown in Table 5.2. Again, for brevity, only locally derived shear results are plotted. As before the gradient is taken at 0.288 radians.

It can be seen that the derived viscosity values from this second method show a significant improvement in accuracy for the crosshead derived results, with the error reduced from 28.3% to 1.6%. This comes directly from eliminating earlier buckling. By contrast the directly acquired error increased from 6.9% to 8.8% due to difficulties associated with the stress resolution as the single central patch provides smaller relative contribution to the reaction load compared to heavier patching. It can be surmised that the close proximity of multiple patches to each other overly constrains the dry fabric between, meaning that its effect on the load displacement curve can no longer be considered negligible. In agreement with observations of elastic patching the viscosity can be extracted even beyond buckling onset if local deformations in the central zones are tracked directly.

The previously considered cases proves the fundamental feasibility of the viscosity extraction but examine a rather extreme value of viscosity (1500 MPa.s). To further explore the applicability of the method the viscosity is significantly reduced for further trials and matched to the characteristic value of thermally-conditioned liquid resin deposited in liquid form (0.15 MPa.s). The 3D cure fit for the data from these experiments are shown in Figure 5.7c with the derived viscosity shown in Table 5.2.

It can be seen that at lower viscosity values, the algorithm loses its accuracy though still correctly identifies the scale of viscosity values. This happens due to the fact that stress resolution is reduced. Lower viscosity means that the stress in the patched region is considerably lower than in previous cases and the test resolution does not succeed in capturing the exact contribution of patched region.

Based on Table 5.2 and observations of the deformation in the simulations, the out of plane buckling has been fully avoided, leading to an excellent match between crosshead derived and ‘optical’ (directly acquired) measurements. However, this has not led to an improvement in overall accuracy. This appears to be due to the lack in contrast between the patched fabric behaviour and dry fabric

behaviour compared to higher viscosity. The exact viscosity of low-viscocity patches present less practical interest as it does not necessarily contribute significantly to the behaviour of the fabric and hence their application for defect mitigation may be limited. In either case the characteristic values were extracted with the precision satisfactory for the optimisation of forming using modelling tools.

5.4.BET Tests on Treated Fabric

The simulations have shown the theoretical feasibility of the two approaches proposed in sections 5.2 and 5.3. This section aims to validate the feasibility of property extraction experimentally and explore the behaviour of heterogenous samples . To validate the procedure the following steps are carried out. Firstly, striped patches are applied to the fabric and a bias extension test is carried out. Data from this test is post processed and from this patch shear behaviour is calculated (either non-linear elastic or viscosity depending on the assumed material behaviour). The experiments are conducted with varying patch coverage to (a) verify the role of buckling predicted by the model, (b) validate the robustness of experimental procedure. The validation tests are compared with the results of numerical simulations deploying properties extracted at different patch coverages.

There are several key characteristics of the BET which are worth bearing in mind with these experiments. The calculation of shear stress (2) and shear strain (1) in BET begin to break down at large shear angles (e.g. above 40°, [35]) due to intra-ply slippage becoming a significant deformation mechanism [35], [20]. . The BET also requires at least one end of each yarn to be free on order to prevent any significant tension within the yarns, a condition which can easily be undermined by the presence of localised stiffening. Finally, the conventional result processing is assumed to be valid until the onset of out-of-plane buckling. In the previous paragraph it was shown that the deployment of local strain measurement can lift some of these limitations and successfully extract properties beyond the conventional constrain with the help of optical tracking of fibre reorientation, using DIC or other optical systems [35], [72], [111], to ensure that shear angle readings are accurate even at higher shear angles.

A final significant consideration is the effect of pre-shearing of the sample due to gravity. This is noticeable primarily for the dry fabric samples, where patches were present this shearing due to gravity was significantly reduced. There is no obvious way to avoid this problem except by experimenting with a smaller sample. The mitigation used here was to ensure the top and bottom grips were exactly spaced apart by the as cut length of the sample when the experiment began ensuring the sample dimensions were maintained and that crosshead displacement was therefore comparable between experiments, even if this led to some sagging (slack) in the middle of the sample. The samples with patches of either PLA or resin film were considerably less prone to this problem.

5.4.1. BET on Preform with Deposited PLA Patches

BET tests were carried out by applying PLA patches integrated to dry glass fabric to assess the procedure for extraction of non-linear elastic properties and to establish whether experimental results support the hypothesis presented in section 5.2 with a reasonable correspondence.

PLA is chosen as it is easy to handle, simple to shape and press into the fabric and exhibits a shear response of significant contrast to that of the dry fabric.

Experiments were conducted with samples of 280g 2x2 twill woven glass cloth (Easy Composites LTD GF-22-280-100). The fabric was cut to a size of 440mm x 200mm including an extra 20mm each end for clamps. The fabric yarns were aligned at 45° to the loading direction. A sample prepared for the bias extension test is shown in Figure 5.1.

The 8-mm in width PLA strips were prepared using Ultimaker 2+ 3D printers and were hot pressed into the fabric from one side at 160°C and 0.4 MPa for 2 minutes to ensure impregnation of the fabric without excessive spreading of the polymer within the fabric. It is observed that the strips printed at 8mm initially spread to approximately 10mm after the hot press has been used. The PLA thickness was selected to approximately match that of the fabric, though this was not considered critical for demonstrating the concept, providing there is consistency of sample dimensions.

PLA coverage was set at 25%, 50% and 75% giving a total of 3 samples. Three PLA-free samples were also tested to be used as a baseline for establishing the properties of untreated fabric. These tests revealed, that in line with the hypothesis discussed in section 5.2, there is minimal impact of strain rate on the results . The sample was clamped into custom made grips across the full width top and bottom (see Figure 5.1). The total displacement of the upper grips constituted 60mm which roughly corresponds to 73° theoretical shear. The PLA samples were assumed to be rate-independent and tested at only one crosshead displacement rate of 1.2mm/s with the total time of experiment being 50 seconds.

Through the trialling of various methods the most effective way to ensure 45º yarns and zero pre-shearing when cutting the samples was through the use of a weighted stencil matching the dimensions of the bias test. This allowed for accurate dimensions and manual alignment of the yarns against the stencil edges to ensure no yarns were dropped and no shearing occurred during cutting. To ensure the required yarn orientation at the start of the test, the grips were kept horizontal by aligning the top of the grip to the load cell clamps using a solid metal flange built into the grip.

A full 3D DIC system (LaVision) was set up to examine both the shear deformation and susceptibility of the samples to out-of plane buckling. For the samples with PLA patches the samples were painted with a white background and black speckles of approximately 1mm diameter. Two 5MP cameras

were used at a frame rate of 2fps, these were focused on the central portion of the test with the window size measuring 250mm x 250mm. Prior to the test the cameras were calibrated according to the procedure recommended by the manufacturer of the system (using calibration plates) to ensure spatial correlation. A subset size of 31 pixels was used with a step size of 8 pixels. The shear angle was calculated by averaging a horizontal rectangular strip across the centre of zone C (see Figure 2.1).

The added paint is expected to impact the fabric behaviour. However, this did not affect the extracted properties. The patch behaviour is not influenced by the presence of the paint as they are too stiff compared to the fabric. The shear stresses resulting from the underlying fabric behaviour and the paint in the dry samples were found to be negligible compared to the patched samples. The behaviour of painted fabric itself, on the other hand, was accounted for by the testing painted patch-free fabric.

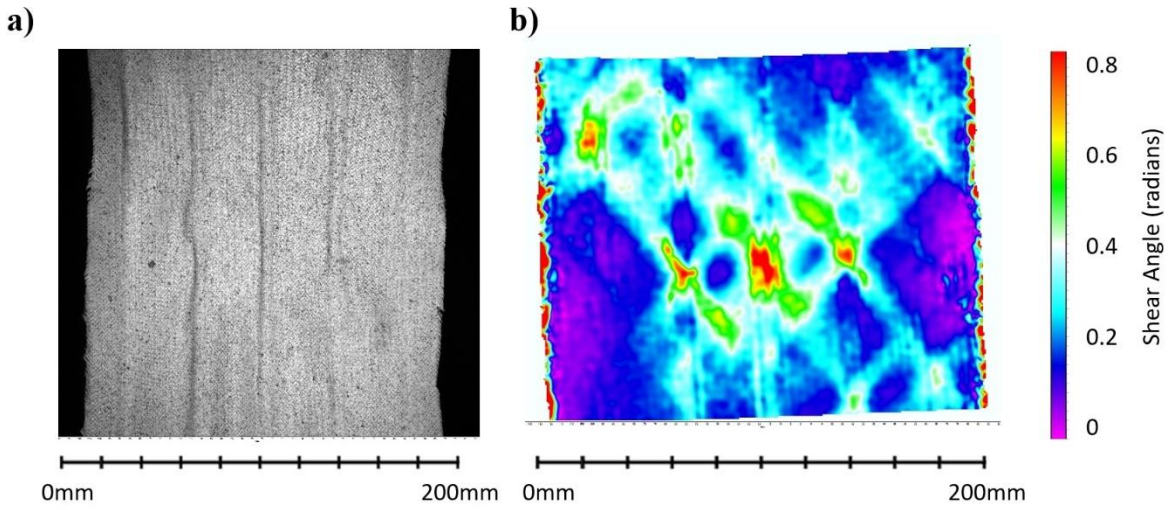

Figure 5.10: a) Image taken by DIC camera and b) shear map generated for 25% coverage of PLA (at 16.8 mm crosshead displacement out of 60mm)

A typical shear map taken by the DIC cameras is shown in Figure 5.10, this image corresponds to a crosshead displacement of 16.8mm out of 60mm total resulting in an average shear angle in the central zone of 6.5°. The non-uniformity induced by the PLA patches is clear in the central zone where the three middle stripes have considerably higher shear interspersed with non-patched regions with lower shear due to distorting out of plane instead [41].

The crosshead load and optically measured shear angle data is first processed in line with the methodology shown in section 2.3 (1), (2). This derived shear stress vs shear angle dependencies were compared at different coverage levels. Following the data extraction procedure established by the simulations in Chapter 3, the baseline dry fabric behaviour has been deducted and the results scaled up based on coverage level. The results are presented in Figure 5.11.

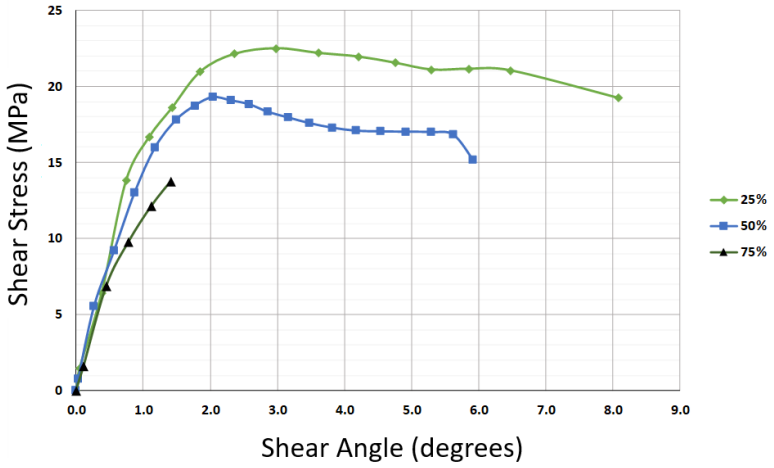

Figure 5.11: PLA shear stress response at various coverage levels

The most important observation from Figure 5.11 is that all three sample configuration show patch rupture at very low shear angles – between 6° and 9°. In the case of the 75% coverage, the load capacity of the tensile machine (1KN) was reached before patch failure and the test was stopped.. At lower coverage, the experiment is aborted due to the fabric beginning to tear (for clarity data points after the onset of tearing are not plotted). The tearing occurs well before the characteristic deformation at which exponential fabric stiffening occurs. These patches behave more like composites than like a stiff fabric as was modelled in the previous section. The measurement of bending properties, though possibly critical, goes beyond the scope of the current paper. Numerical simulations are important to understand the implications of those factors and their influence on mechanical behaviour in the context of forming simulations.

In general, the patch behaviour exhibited at various coverage is in sensible agreement, at 5° shear angle the deviation between 25 % and 50% coverage is 20%. This is reasonable in the context of the characteristic scatter for the dry fabric testing and discussed in the next section. The testing confirms the hypothesis of property extraction procedure.

5.4.2. Experiments on Visco-Elastic Patches

For the verification of the procedure for viscoelastic property extraction presented in section 5.3, BET tests were carried out on dry glass fabric preforms with imprinted XPREG XA120 Epoxy Resin Film. The selection of this resin offered a reasonable balance between wide range of viscosities that can be achieved through thermal conditioning and stable behaviour for the time scales of the test.

The resin film was hot pressed into the fabric at 70°C and 0.4MPa for 30 seconds. These parameters ensure that the resin propagates through the thickness of the fabric without excessive spreading due to capillary forces. Tests were carried out with either 5 strips evenly spaced resulting in a coverage of

50% or 100% coverage of resin film conducted as a validation test. Some initial experiments were carried out with 5% coverage in one central strip as suggested by the simulations in section 5.3, however these resulted in too low a registered crosshead load and accurate results could not be obtained, this is discussed further in section 5.5.

Dry fabric was tested once more to be used as a baseline, this time without paint. A few amendments were made as detailed below. The displacement range was unchanged however the total time of the experiment was now varied depending on the strain rate required. Runs at each coverage level were carried out (Dry, 50% and 100%) at three strain rates, with the dry fabric and 50% samples each repeated 3 times, and the 100% coverage samples only conducted once. This gave a total of 21 experiments. The crosshead displacement rates were 1.2mm/s, 3mm/s and 12mm/s.

The properties of infused thermosetting patches are comparable with the properties of the fabric. Hence, the application of paint may significantly affect the deformation of the samples. Therefore, shear deformations were tracked manually on the images since the warp and weft yarns were clearly visible in in the patched regions. Two sample images at 16.5° shear angle (as measured in pure shear zone C) are shown in Figure 5.12. Even with a thinner paint, a noticeable impact on the shear properties is still expected. Paint remains a viable option where there is a strong contrast between patch and host fabric properties. For patches produced by liquid resin, a direct observation of fabric shearing was considered to be a more reliable method for determining the local shear.

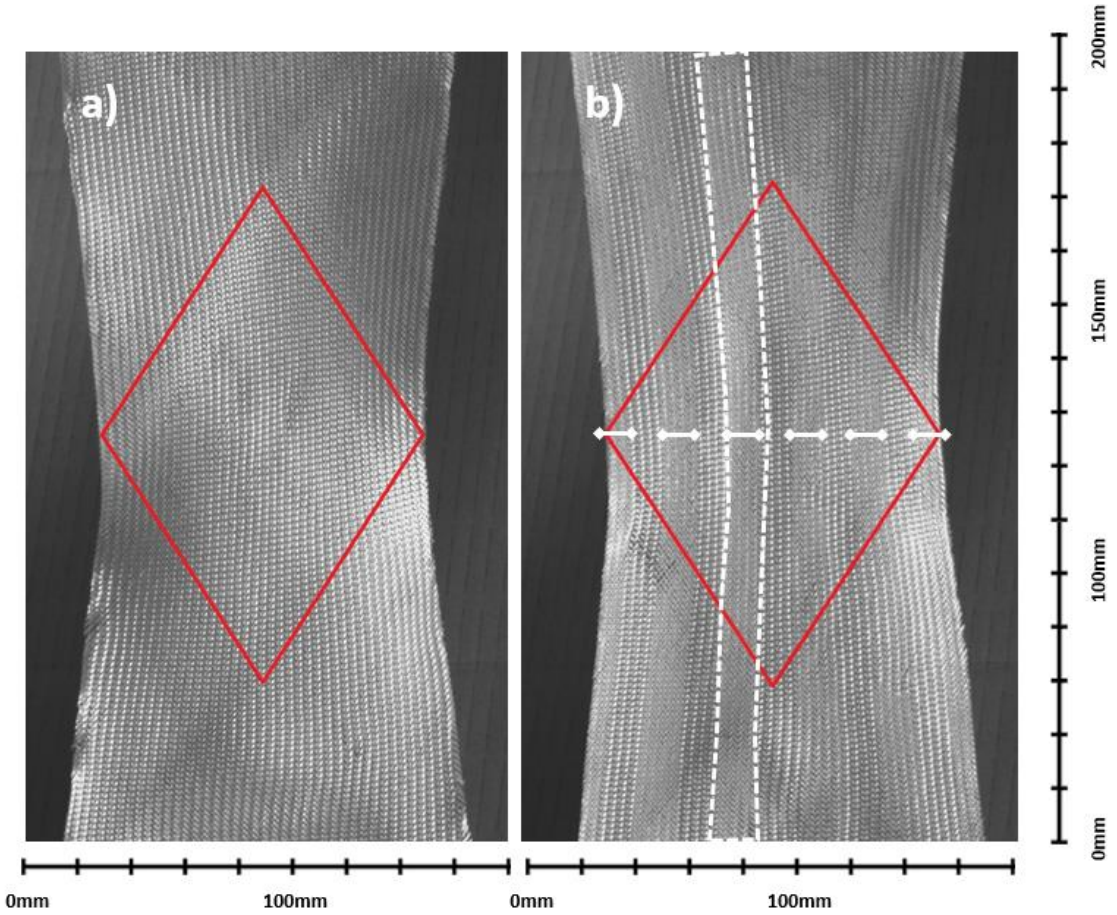

Figure 5.12: a) Image taken by videogauge at 0% coverage b) Image taken by videogauge at 50% coverage. The red diamond outlines the approximate edges of the theoretical pure shear zone. The patch locations are indicated in white with one patch outlined

The extraction of patch viscosity is conducted as described in section 5.3 (i.e. plotting the results in 3D space, surface fitting and taking the viscosity measurement from the gradient of the material response surface). However, it is first necessary to narrow down the range of shear angles where the viscosity can be extracted with better confidence. When observing the central ("pure shear") zone C it is observed that the onset of out of plane buckling occurs at shear angle of approximately 26° for the 50% coverage samples, with exponential stiffening beginning to dominate from approximately 21° upwards. Hence, this level of deformation represents the upper limit for the identification of viscosity. It is also observed that a clear deformation pattern with central shear zone is not fully developed before the angle of approximately 12° shear angle. This therefore provides a narrow window for determining viscosity with 16.5° identified as a suitable mid-way point (this corresponds so a shear angle of 0.288 radians).

Manual calculation of the shear angle based on images is estimated to give an error of approximately ±2°. Given that the shear level chosen was just 16.5° as stated above it was decided that using

crosshead displacement in conjunction with (1) would actually lead to more accurate results, however the shear angles calculated are later verified against the corresponding images to confirm their accuracy. Note that Figure 5.4a demonstrated an error of at worst 6.8% for (4) up to 20°, with the subsequent loss of accuracy attributable to out of plane buckling occurring beyond this shear level.

The shear angle values for three of the runs are compared in Table 5.3 against the shear angles measured on the images to assess any discrepancy. To reduce the manual error as much as possible four readings were taken at the four corners of the diamond shaped central shear zone and the average and range calculated. The three experiments selected for this verification were the first run of each coverage level at the highest shear crosshead displacement rate (12mm/s). According to (1) the identified shear angle of 16.5° occurs at a crosshead displacement of 20mm, therefore the videogauge frame corresponding to this displacement was analysed and the shear angle measured from the image. The results are shown in Table 5.3.

Coverage (%)	Local Average Shear Angle 'A'	Crosshead Derived Shear Angle 'B'	Range of Manual Shear Angle Measurements	Delta (A-B)
0 (dry)	16.65°	16.5°	10.90°	+0.15°
50	17.30°	16.5°	5.10°	+0.80°
100	15.35°	16.5°	4.00°	-1.15°

Table 5.3: Shear Angle Measurements by Coverage Level as Measured from Videogauge Frame

Based on the very low delta values of Table 5.3 these results were concluded to give sufficient confidence to proceed using shear angle measurements derived from the crosshead displacement. The significant range in manually measured shear angle is notable and reduces confidence in the delta values given, however this gives further weight to the usage of crosshead derived shear angle as the measure as this is not vulnerable to local fluctuations in the pure shear zone.

To assess the uniformity of the pure shear zone shear angle measurements were taken from an image of a 50% coverage sample, again at 16.5°, show in Figure 5.13. This coverage level was deemed to be the most likely to have a non-homogeneous shear zone due to the contrasting material properties. It can be seen that the shear angle does vary across the sample but this appears to mostly be random scatter with no clear pattern in terms of location or if patched/unpatched. This therefore can be attributed to a combination of minor variations in fabric properties and inaccuracy of the measurement itself.

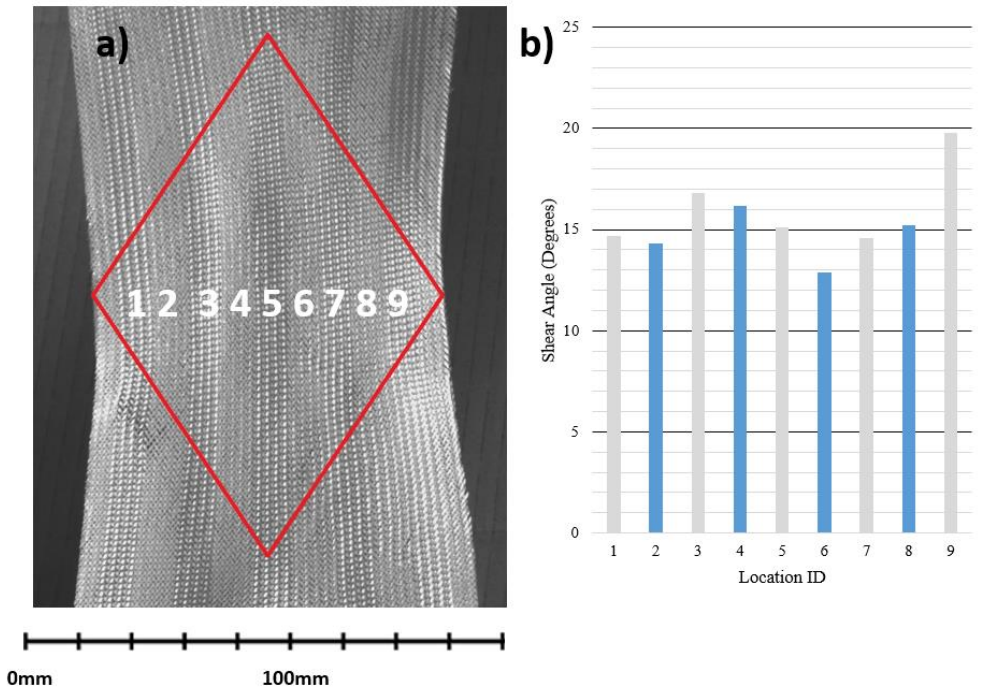

Figure 5.13: Shear angle measurements reading horizontally across the sample a) labels the locations measured b) charts the shear angle with grey denoting dry fabric and blue denoting patched locations.

The results from the 50% coverage scenario at the three different strain rates were plotted in 3D space and the results mapped to a surface in keeping with (4) and the earlier simulated results. As the 50% coverage scenario was repeated three times each for each of the strain rates the shear stress values were first averaged reducing 9 data sets to 3. This data fit is shown in Figure 5.14. This averaging was required to allow for a clear graph due to significant variations between repeat experiments (see Figure) which is discussed further in Section 5.5. Such variations are not uncommon, see for example [95].

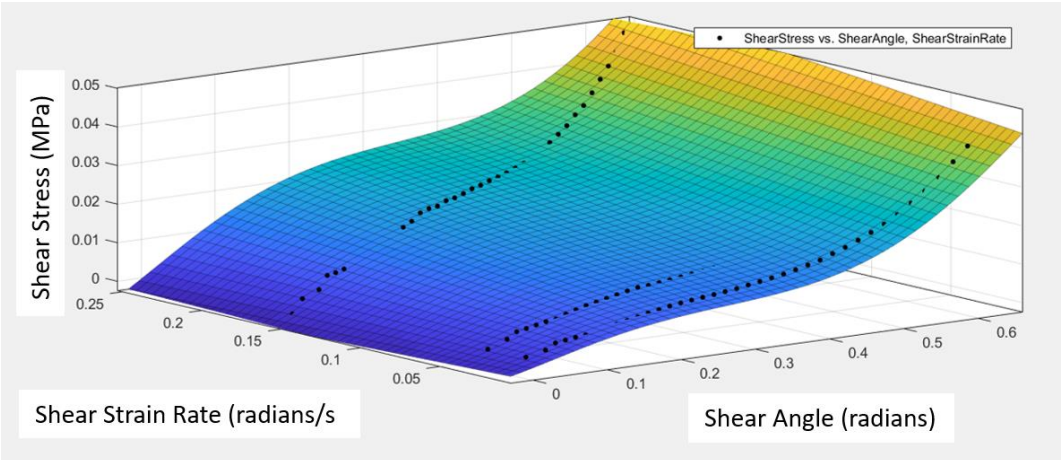

Figure 5.14: Surface fit of shear stress response at 50% coverage

The R-value for this surface fit is 0.94. Solving the polynomial equation generated for the fit with x = 0.288 results in a gradient of 0.0565 MPa.s and hence a viscosity value of 0.113 MPa.s, in accordance with the methodology of Table 5.2.

The results from the 100% coverage samples are plotted in the same way and the gradient again derived, this is shown in Figure 5.15a. For brevity the polynomial is not shown here, however with this coverage a viscosity of 0.167 MPa.s was derived. This value is 47% higher than that derived from 50% coverage. It is noted that the experiment at the highest strain rate has a small initial peak in the stress-strain diagram, followed by a trough, this is due to the initial frictional resistance of the fabric being overcome and levelling out which is more pronounced at higher coverage levels and strain rates. The R-value for this surface fit is 0.99.

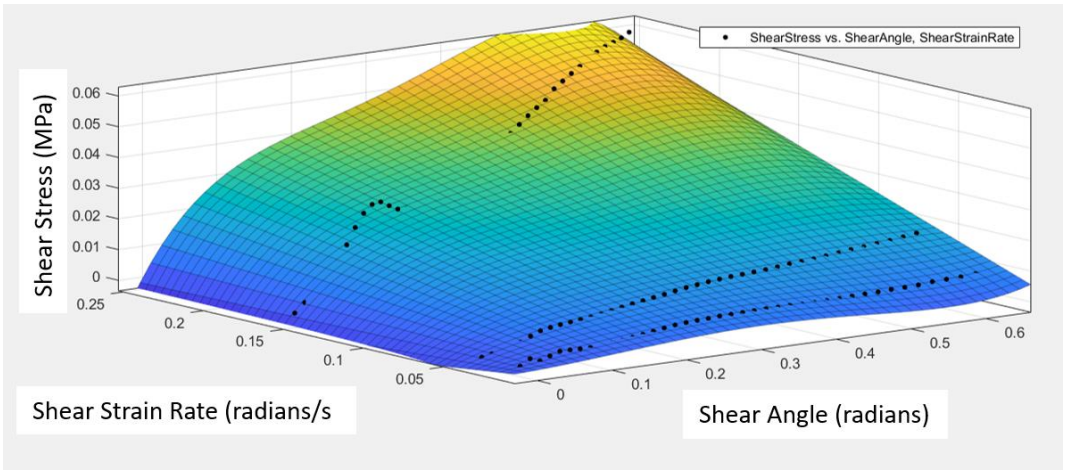

a)

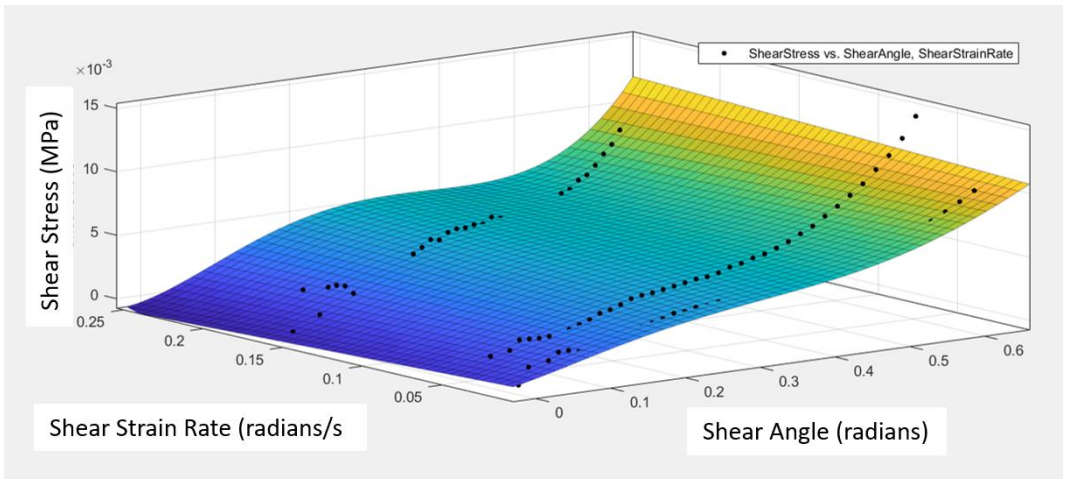

b)

Figure 5.15: Surface fit of shear stress response at a) 100% coverage b) 0% coverage

Before concluding that the viscous behaviour shown is due to the applied resin it is also necessary to establish whether the dry fabric itself displays any viscous behaviour. The same graph is therefore plotted following identical steps as for the 50% and 100% scenarios above. The results are shown in Figure 5.15b, the R-value for this surface fit is 0.97.

This results in a gradient and hence viscosity value of 0.002 at a shear angle of 0.288. This is over 50 times lower than the viscosity obtained for the 50% coverage sample and is negligible, therefore it can be concluded that the dry fabric alone is not behaving in a viscous manner.

In order to quantify the accuracy of the viscosity value of 0.113 MPa.s derived from the 50% coverage scenario, the value is used as the input for a simulated run of both the 50% and 100% coverage samples, and subsequently compared to experimental results. As discussed in section 5.3 the two required inputs are the shear behaviour of the underlying fabric defined as the shear modulus in the form of a fifth order polynomial, and the viscosity already obtained. The input polynomial is taken as the derivative of the average of the experiments plotted in Figure 5.15b. Similarly to the 50% coverage samples the simulated and experimental results are post processed in order to plot shear stress against shear angle. As the viscosity is this time treated as an input value (as it is derived from the experiments), the results are not plotted in 3D and instead a of comparison between experimental results and simulated results are produced for the highest strain rate trialled (12mm/s) at both 50% and 100% coverage. This strain rate is chosen because it leads to the highest stresses and hence errors are more noticeable and easier to distinguish from noise. The results are shown in Figure 5.16.

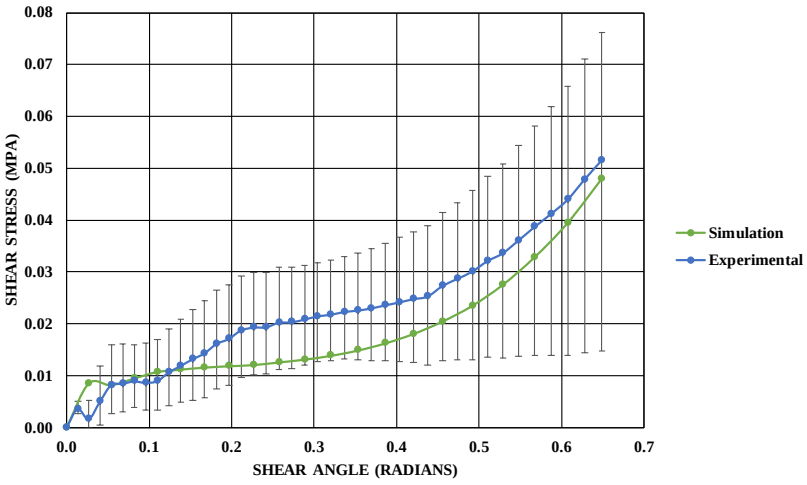

a)

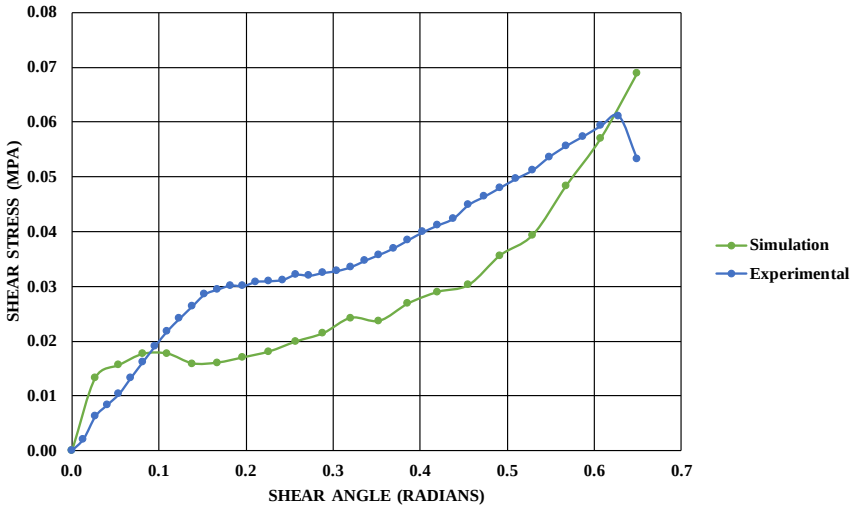

b)

Figure 5.16: Comparison of experimental and simulated results for a) 50% and b) 100% coverage at 12mm/s

The simulated and experimental results for 50% coverage shown in Figure 5.16a show reasonable correlation, however, it can be seen that the simulated results give a 59% lower shear stress compared to the experiments in the critical central region of interest at 0.288 rad shear angle. For the 100% coverage sample shown in Figure 5.16b the simulated results give a 41% lower shear stress compared to the experiments at this same shear angle. It remains noteworthy that the experimentally derived results for the 100% coverage sample gave a higher viscosity value than at 50% coverage suggesting the discrepancy is a combination of both the method and the modelling approach. It is also noted that the discrepancy between the 50% and 100% coverage results is within the experimental scatter of the experiments.

The noise noticeable from the simulated results is primarily due to the use of the iterative equation (2) which is very sensitive to fluctuations introduced when there is a large initial step up in load as we have here. It is good practice to have a gradual ramp up in displacement when using an explicit time stepping scheme in order to minimise dynamic fluctuations, however this was not possible here due to the need to have a fixed crosshead strain rate.

5.5.Results and Discussions

5.5.1. Experimental Set-up

There are various practical aspects of the bias extension test vital to obtaining accurate results which are often underreported and are especially problematic when working with dry fabric rather than pre-preg or binder. Most critical is the proper orientation of the fibres within the sample and the exact alignment of the sample itself. Creating a rectangular sample with yarns running at exactly 45º to the loading direction is challenging when bearing in mind that the fabric must be kept at zero shear across

the full surface of the sample to achieve this. It was found in preliminary experiments that the dropping of even a single yarn led to noticeable skewing of the pure shear zone. Through the trialling of various methods the most effective way to ensure 45º yarns and zero pre-shearing was through the used of a weighted stencil matching the dimensions of the bias test. This allowed for accurate dimensions and manual alignment of the yarns against the stencil edges to ensure no yarns were dropped and no shearing occurred during cutting.

To ensure the required yarn orientation at the start of the test, the grips were kept horizontal by aligning the top of the grip to the load cell clamps using a solid metal flange built into the grip. Vertical alignment of the grips was ensured by hanging a vertical plumb line from the top grip and aligning the lengthwise edge of the sample to this plumbline.

Despite all the considerations mentioned and with considerable care being taken in their implementation it still proved difficult to ensure a perfect pure shear zone occurred across all samples. The main issue being the pure shear zone occurring at a slight angle deviation away from vertical when comparing the upper and lower tips of the diamond. All the issues mentioned are considerably more problematic for dry fabric samples than for pre-preg. It is concluded both that the bias test when conducted on dry fabric is extremely sensitive to sample misalignment and also that minor inherent variations between the weave of each sample contribute to a notable level of variation between even 'identical' runs. This was mitigated in this chapter through up to 3 repeats of each scenario to give a clear idea of experimental discrepancy.

5.5.2. Hypo-Elastic Model and PLA Experiments

It was shown in section 5.2 that the accuracy of the simulated results for high stiffness non-viscous materials was heavily dependant on extracting shear angle measurements directly from the sample rather than deriving from crosshead displacement using (1). This was concluded to be due to early onset of out of plane buckling at very low shear angles (<20°) whenever a significant proportion of the sample is covered by high stiffness patches. The planned approach to tackle this experimentally was to track shear angles optically through the use of DIC tracking a speckled paint pattern painted on top of the fabric and patches, thus allowing useful material data to still be collected even after the onset of buckling. This tracking was successful in measuring shear angle for the PLA samples.

A key limitation in the experiments is the low cohesion of the yarns at the edge of the specimens, when under deformation the yarns slip relative to one another causing large relative displacements to occur between individual yarns and ultimately 'unweaving' of the material. This leads to disintegration/tearing of the speckled pattern and hence the DIC is no longer able to track the deformations. This occurred at the edges of the patched samples which led all samples to fail at less than 10º. It is therefore concluded that excessive stiffening of the fabric architecture with such

materials as PLA leads to impractically high loads on the fabric leading to sample failure rather than shearing. A less stiff material or a considerably lower percentage coverage may lead to more useful results. This technique remains promising but 50% coverage of such a stiff material as PLA is clearly pushing the boundaries of this technique.

The results obtained are still useful for giving an approximate idea of the shear stiffness of PLA patches in simulations as the following exponential stiffening behaviour can be inferred from the dry fabric behaviour with the two experiments combined to give an approximate hybrid curve. Despite the relatively low shear angle at which the experiment had to be stopped, useful data has been obtained within the region 0° to 6°. Given the very high stresses shown here compared to those involved in dry fabric only testing, patches with such high shear stiffness as PLA would be expected to have very minimal shearing in a formability experiment. Were a lower stiffness material used or a lower percentage coverage more data at higher shear angles could be obtained effectively.

Should the approach to be extended to idealize the impact on shear behaviour of stitching or tufting consideration would again need to be given to keeping the percentage coverage as low as practically possible.

5.5.3. Visco-Elastic Model and Resin Film Experiments

In the visco-elastic simulations similar issues with out of plane bucking leading to the inaccuracy of (1) were found as for the hypoelastic model. As before these were partially resolved through directly obtaining the shear angle from the simulated mesh itself. A second approach was also trialled for the visco-elastic simulations of using only 5% coverage in one central strip. This approach seem promising is the simulations but when it was trailed experimentally these resulted in too low a registered crosshead load and accurate results could not be obtained. The load obtained at such a low coverage was only slightly higher than that of dry fabric and was very hard to distinguish from the inherent error of the method. It was also discovered early on in the experiments that the influence of the paint required for the DIC shear tracking was heavily influencing the results as the paint itself was viscous and has notable thickness. Therefore the decision was made to run the experiments without DIC and instead take images with a video gauge to be analysed manually using the visible warp and weft to calculate shear angle rather than requiring paint. Though as mentioned in section 5.4.2, due to the low shear angle for extracting the viscosity value, the crosshead derived shear angle was ultimately considered the most accurate at low shear and this was verified in Table 5.3.

A viscosity value was successfully obtained from samples at both 50% coverage and 100% coverage. The value obtained at 100% coverage was 47% higher than that obtained from 50% coverage. The primary aim of identifying a reasonably accurate viscosity value to assist formability simulations is

therefore fulfilled. However it is unclear why this variation in apparent viscosity between coverage levels. The three most feasible options are:

1. The dash-pot model [102] is not fully applicable. This is a very rough approximation as it treats the patches as a fully viscous material and does not consider the patch to have any resistance at infinitesimally small strain rates. This is far from sufficient and needs more data to derive an adequate model. This study gives it a first go and proves the fundamental possibility for finding an appropriate form of a model.
2. Experimental variation between samples accounts for the discrepancy. Significant variation was found between experiments of up to 100% of the total load (i.e. results from two or more 'identical' experiments could have the highest result recording as much as twice the load as the lowest sample for a given shear angle). In literature such variations are not uncommon [95].
3. The error is inherent to the method, i.e. the higher the coverage the higher the apparent viscosity (even after scaling so that results are comparable).

The only clear way to distinguish the cause between these two options would be to run considerably more bias extension tests to establish more accurate average responses in order to quantify and eliminate the impact of variation between samples.

It is important to emphasise here the difference between the viscous properties of the resin and the viscous properties of the resin impregnated fabric. The viscosity value obtained here is the viscous behaviour of resin infused fabric not the viscosity of the standalone resin. The two components superimposed in the modelling work are the underlying fabric behaviour and the viscous behaviour of patched fabric, rather than the underlying fabric and the viscous behaviour of the resin alone. This means that a direct comparison between the values obtained and the manufacturer data for both PLA and the imprinted resin is not directly applicable and is therefore beyond the scope of this paper.

5.5.4. Discussion

The numerical experiments tested the applicability of the suggested approach for various material types and property ranges. It was found that both non-linear elastic and viscous properties of the patches can be deduced when there is a sufficient contrast between the properties of the patch and the hosting fabric. When these properties are comparable, the procedure becomes less robust. However, in the case of low contrast, a very accurate estimate of the patch properties becomes less practically

relevant. The precision of property determination is well within the scatter observed when testing common engineering preforms [95].

The technique shown in this study is a promising approach for characterising the properties of preform enhancements. It is currently demanding both in experimental and simulation time but nonetheless the viscous model allows for a good level of accuracy when attempting to model patched fabric shear behaviour. It remains to be explored how well the technique can be carried across to other material combinations. The overarching conclusion is that the required coverage of patch material needs to be carefully tailored depending on the stiffness/viscosity of the patch material. It is clear that for high stiffness patching materials a very low percentage coverage is required (~5%) in order to obtain results at higher shear angles, in the experiments presented here only the initial behaviour for the shearing of PLA was successfully obtained, with the experiment failing at approximately 10° due to excessive load on the sample as a result of the high shear stiffness. For low stiffness/viscosity patching materials such as the resin film used, the opposite is true – high percentage coverage is required (50-100%) to ensure significantly higher crosshead loads are registered compared to the reference unpatched sample, allowing the influence of the patched material to be distinguished from the noise and sensitivity levels of the load cell. Obtaining the viscous behaviour of resin film was successful with the simulations matching well to the experimental results and a viscosity value in the range of 0.11-0.17MPa.s was obtained, further work is needed to investigate an accurate value for experimental variability.

6. Numerical Tool for Patch Placement

Following on from the successful experimental trials shown in Chapter 3, this chapter examines the feasibility of developing a design tool for placing local patches for optimisation of forming. This forming tool is based on the hypo-elastic model presented in Chapter 4, which is capable of simulating both the shear and bending behaviour, whereas the experimental data for such a tool can be derived using the methodology described in Chapter 5. The ability to capture correctly both the shear deformations and bending-induced wrinkling gives a basis for studying the implications of placing patches in various locations, in different patterns, and of arbitrary configurations. This is necessary to reduce the design space and find the most efficient solutions prior to manufacturing trials.

To create the design tool, the model needs to be complemented with the criterion of wrinkle occurrence, an automatic assessment of wrinkle severity, and an iterative algorithm for improving the patch placement based on the results of previous forming runs. The demonstrations of the tool are studies both in application to the geometry of a curved spar and the shape explored in previous manufacturing trials. Both vacuum bag and rigid tool forming are examined in these two cases. Various scenarios of patch placement are explored with this tool. The placement can be motivated by the objective to decrease shear intensity in the critical region, redistribute shear over a larger area, reduce wrinkle severity, reduce magnitude of compressive stresses, etc. Each of these options can be examined and give a basis for an objective function for fully autonomous optimisation.

The computational efficiency of the model is discussed as this has a significant impact of the practical applications for the simulations. The impact of patch properties on wrinkle likelihood first considered in Chapter 3 are revisited in light of the modelling work presented. Finally, trials on an alternate geometry are shown to consider how effectively the model works for alternative shapes and to establish if the same patch placement optimisation techniques can be transferred over.

The chapter begins with a discussion of the general optimisation strategy for patch placements followed by implementation with the model correspondent to the rigid tooling manufacturing study of Chapter 3, this is then followed in section 6.4 with a flexible tooling (diaphragm) formability simulation tackling a new geometry. It will be explored how effective the attempted enhancement approached are across the two simulated geometries and what impact the order/sequence of surface contacts have on the results.

6.1. Optimisation Strategy

Optimisation of patch position and patch properties can be a difficult task. The parametric space is vast, while every simulation is computationally demanding. Traditional optimisation procedures cannot therefore be applied here, particularly when the purpose of the simulations is a process design rather than sophisticated analysis of all the aspects of forming. In this study, a pragmatic optimisation strategy is taken. While this approach is not universal it can be easily adapted to other geometries.

The optimisation criteria, in agreement with conventionally used criteria [15], [16], [22], [53], [44], is maximum shear angle. Whilst not necessarily the best criterion for indication of wrinkle occurrence, at this stage it provides a good understanding of the intensity of shear deformations. This is based on the assumption that once the fabric exceeds its locking angle, out of plane deformation is unavoidable. This is an effective method for assessing formability at a first approximation, but it has limitations. A high shear angle does not guarantee the presence of a wrinkle. In fact, wrinkles often manifest a situation when more favourable out-of-plane loss of stability occurs at lower shear angles or at zero shear. It does however give some ideas about whether localised modifications can work for redistributing potential problems to outside of the area of concern. An alternative approach to wrinkle identification based on buckling behaviour rather than shear angle has been assessed by Matveev et al [97].

For the purpose of computational efficiency, particularly when considering contact-intensive rigid mould closure, the simulations are not run to completion but stopped at sufficient closure depth (approximately 60%). The latest stages of simulations require excessive run time. Hence, at this level of closure a likely wrinkle may not yet necessarily have formed, but an indication of what may then happen is provided. The output of these simulation are used then to assess critical areas where the patches need to be positioned. This strategy is only required for rigid tool simulations.

The process optimisation is divided onto two steps. At the first stage, called ‘rough optimisation’, an approximate location of patches is explored out of a limited number of possible candidates, defined based on specific features of geometry. The purpose of the first step is to narrow down the optimisation space. The patches considered in the first step cover relatively large areas compared to feature sizes. The results of the simulations at this stage are indicative only.

At the second stage; a) patch geometry is refined: instead of bulk patches narrower zones are used, which as discussed further appear to be more suitable, and b) precise patch position in the targeted region is defined in ‘line patch’ simulations. The success of the patch positioning at the second stage is evaluated by direct examination of wrinkle intensity predicted by the forming simulations rather than by shear magnitude.

6.2.Rigid tool forming

The rigid tooling simulation has a solid top and bottom mould as in Chapter 3. The bottom mould is held still and the top mould lowered. This leads to first contact occurring between the base of the top (female) mould and the fabric, followed by contact between the top of the male mould and the fabric. There is therefore minimal tension in the fabric until a significant way through the mould closure. By contrast the later diaphragm forming simulation of section 6.4 pressurises the space between the diaphragms leading to tension throughout and first contact is between the top of the male mould and the lower diaphragm. The forming implications of these differences are discussed later.

In the following simulations the shear stiffness of resin patch regions were artificially increased by 10 MPa whereas the shear stiffness in the bulk material defaults to a near negligible value, both patched and bulk material subsequently increase non-linearly with shear angle. The bending resistance of the patch regions was kept the same as that of the bulk material, which is justified by the off-axis orientation of the patch as discussed in section 3.2.3. The male mould is simulated as slightly smaller than the female by 1.6 mm allowing space for the fabric once closed, which is characteristic of the actual mould gap used in the experiments of section 3.2 and also essential for model convergence. A geometrical pre-processor for the forming simulations was created in Python to assign the position, size (height/width), orientation and the number of rectangular patches parametrically. The mould layout is shown in Figure 6.1.

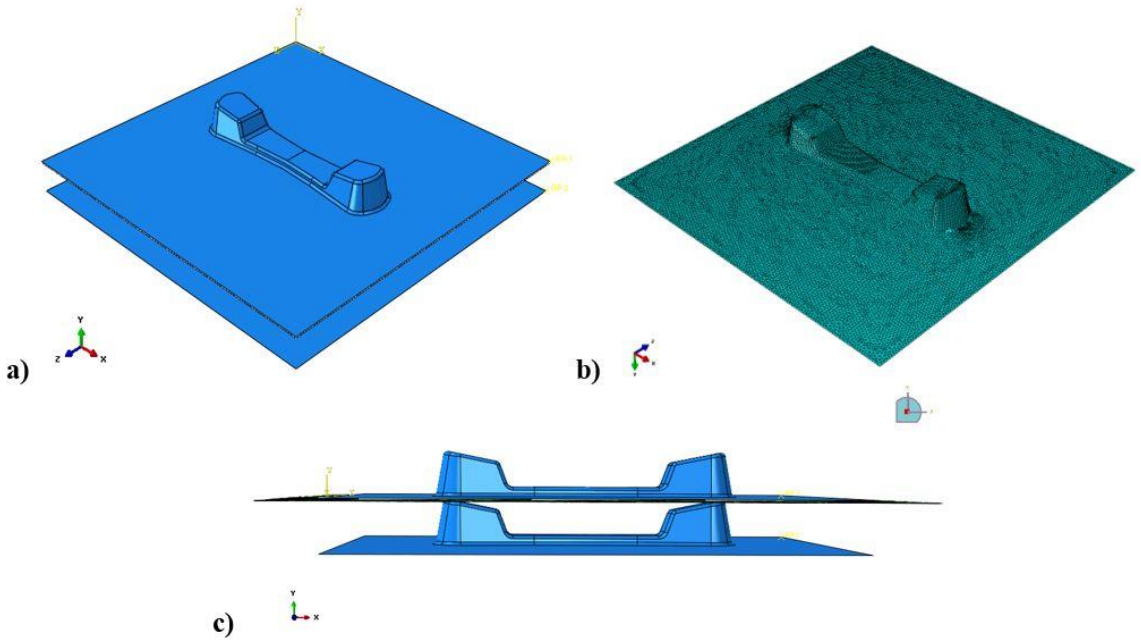

Figure 6.1: a) Matching moulds b) top view of meshed male mould c) moulds with fabric shown between

6.2.1. Forming of Non-Stabilised Material

The finite element model was applied to explore forming of non-stabilised material over the tool geometry. The results of these simulations are shown in Figure 6.2. In this case the linear mesh size was chosen to be 2 mm on the basis that this is refined enough to capture the onset of wrinkles and still be indicative of where patches should ideally be placed, while not excessively computationally demanding. Bringing the mould to full closure required a mesh size of approximately 1 mm rather than 2 mm to avoid premature termination of the run, this became prohibitive when attempting to run 16 different combinations (15 hours per run rather than 3 hours, with 4CPU). However this mesh size reduction from 2mm to 1mm had very little impact on the simulation in terms of changing the shear distribution and wrinkle pattern and so results are considered to be mesh independent in the 1mm to 2mm mesh size range.

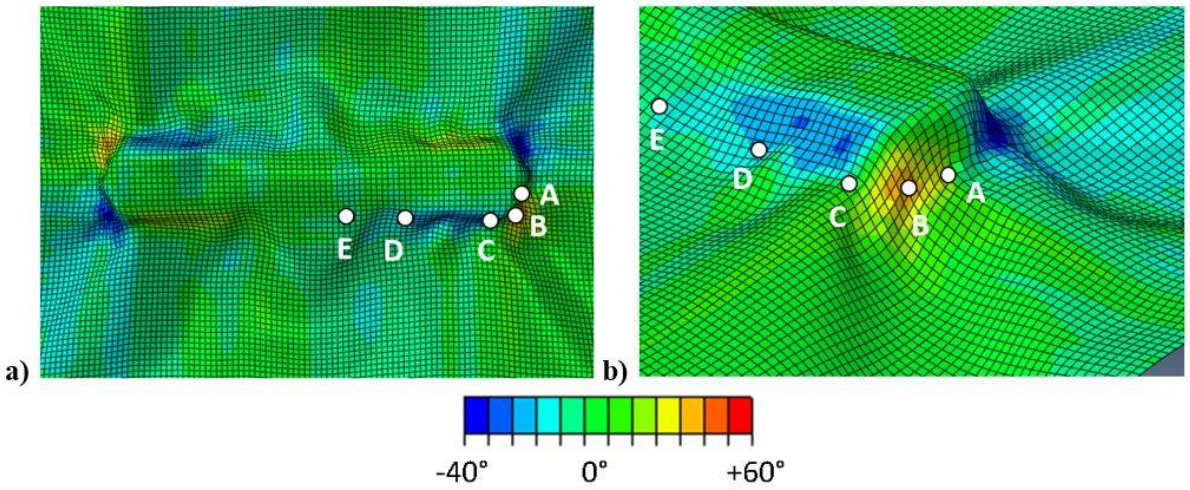

Figure 6.2: Shear angle distribution in forming simulation without stabilising patches (female mould hidden): a) top view, b) side view on critical region B-B′-C′-C, note that the mould is not at full closure as mentioned in the text

Even at incomplete closure the wrinkle pattern is revealed well. It can be seen that one large fold occurs in the preform at each corner in the region BC with the fold tip propagating towards B'C'. The position of this wrinkle is consistent with the locations of highest shear angle. At this stage shear angle is used as the main indicator of where damage/wrinkling may occur. The primary challenge of patch placement is therefore to eliminate the major wrinkles or to drive them away from the contours of the component shape. Due to the fact that the position of the wrinkles in this instance correlates with high shearing it seems intuitively correct to start with changing the shear response in those regions. The other possible approach is utilising patches for the reduction of compressive stresses which are plotted in Figure 6.3, this would focus more on the side of introducing tensioning to the

fabric, which is a well known technique commonly used with blank holders for example and is explored later.

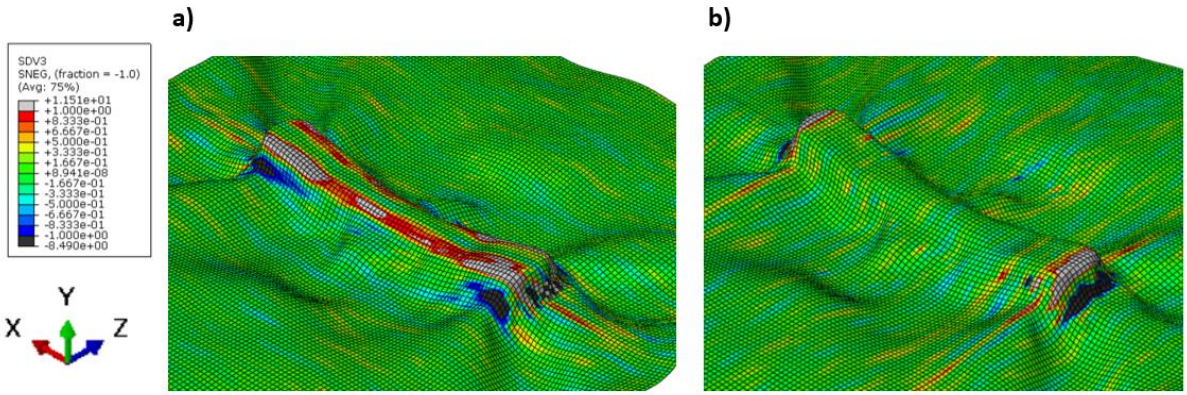

Figure 6.3: Plot of In-plane stresses for rigid mould simulation (at 60% closure) a) no patches, x-direction (warp), b) no patches z-direction (weft)

It is worth noting that the experimentally observed wrinkles (shown in Figure 3.9) occur at the intersection of the compressive bands in warp and weft shown here, this may be an effective way of identifying likely wrinkle sites at an early stage of the simulation well before the tool based on material rotation demonstrated in section 4.2 can be used.

6.2.2. Rough Forming Optimisation using Bulk Patching

The patch dimensions were set at 16 mm × 20 mm. In these preliminary trials a simplified behaviour of patches is chosen with the contrast between patch properties deemed important, therefore the patch shear stiffness is artificially increased by 10 MPa. The same 16 arrangements were trialled as in the experiments in section 3.2.2, zones 1 and 3 were the areas of potentially highest shear concentration in concave and convex corners, whereas zones 2 and 4 bridge them (see Figure 6.4). Not all the simulations out of 16 could be brought to successful completion and some of the simulations were aborted before the moulds were in full contact. Hence, for fair comparison, all the forming simulations were stopped at 15 mm upper mould displacement out of 25 mm required for complete closure, at this deformation the results for all the runs could be successfully derived. At this stage, the most successful combination was deemed to be the one where maximum shear angle within the shape of the component is minimal.

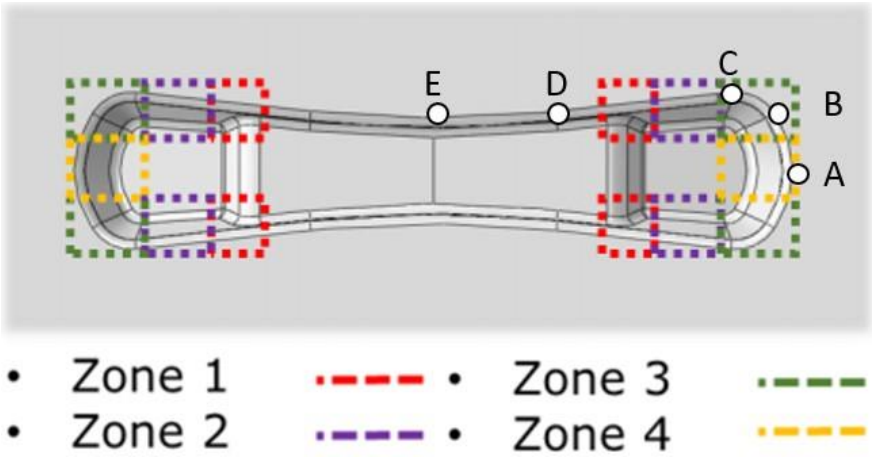

Figure 6.4: Definition of zones for introducing stabilising elements, the inner corners are zone 1, the mid-section are zone 2, the outer corners are zone 3 and the ends are zone 4

The simulations showed that bulk patching generally results in a noticeably worse outcome than the unpatched reference run when observed visually and in terms of maximum shear angle, with a few exceptions where the configuration was of comparable effectiveness. The most promising patch configuration at 60% closure, with the exception of the reference case, was to place stiffer material in zone 3 (see Figure 6.4 and Figure 6.5 for reference). Stabilisation slightly increased the maximum intensity of the shear from 42° to 43°. This also led to a shift in the location of maximum shearing inwards towards the lengthwise symmetry line. However, as well as slightly increasing the overall shear angle the rough stabilisation introduced more areas of instability with larger folds appearing. Instead of localized wrinkles, one or more large folds tend to appear – Figure 6.6. Variation of the bending rigidity of the patched regions for the zone 3 configuration in the range of 0.01 Nmm^2 to 100 Nmm^2 resulted in fluctuation of maximum shear in the 40°-50° window. The worst configuration was found to be stabilising zones 1, 2, 3 and 4 resulting in a maximum shear angle at 60% closure of 54°, it is unsurprising that such excessive stiffening of the fabric should give the worst result. It is apparent at this stage that bulk patching is not producing a better result than the unstiffened configuration, however it does provide useful information to inform patch placement.

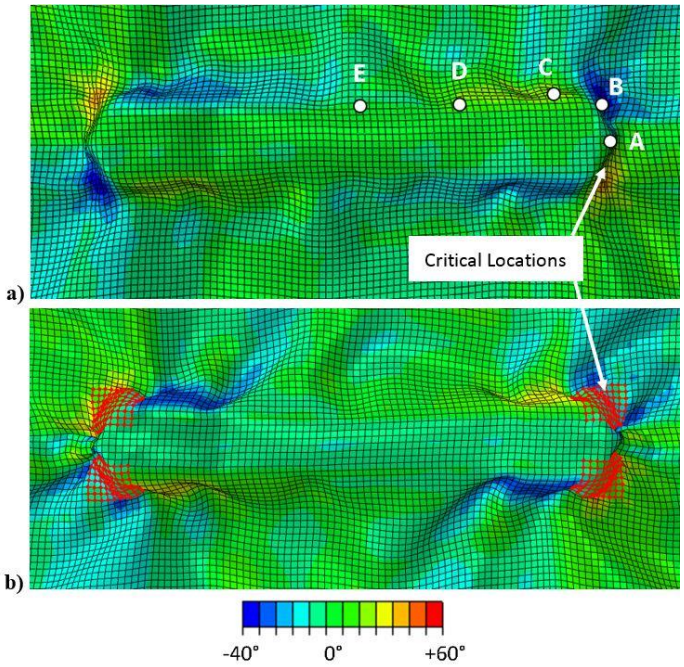

Figure 6.5: Comparison of shear maps in a) reference (non-stabilised) and b) stabilised configurations (zone 3) at 60% closure, the critical locations are labelled and the patch locations highlighted in red

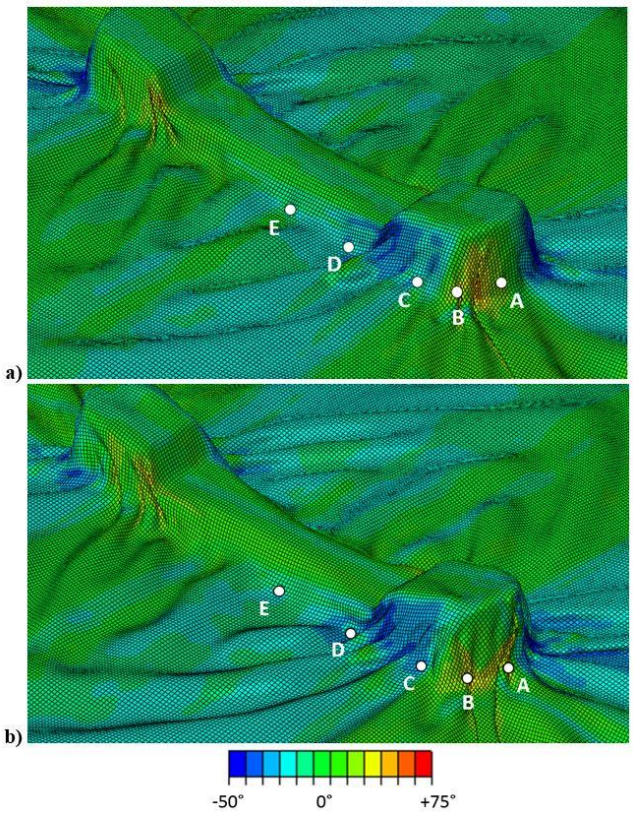

Figure 6.6: Comparison of shear maps in a) reference (non-stabilised) and b) bulk stabilised configurations (zone 3) at full mould closure; with the various relevant locations 'A'-'E' labelled and the top mould hidden

Once the bulk patching configuration with the lowest shear angle was established, this configuration was successfully brought to full closure by reducing the mesh size from 2mm to 1 mm giving a final maximum shear angle of 65° with zone 3 stiffened. Full closure for the unstiffened configuration gave the slightly higher maximum shear angle of 67° by contrast. Though as discussed in section 4.2 minimal shear does not necessarily correspond to an optimal solution. A comparison of the shear maps of these two runs is shown in Figure 6.6.

Comparing Figure 6.5 to Figure 6.6 the contrast in fabric behaviour can be clearly seen at 60% closure as well as an indication of the number of winkles or folds. In the non-stabilised sample a wrinkle occurs primarily at point B whereas for the bulk-stabilised sample a larger fold occurs at A with a smaller wrinkle also occurring at point B. Full closure is nonetheless needed to have clarity on the severity of wrinkles and their final location.

6.2.3. Line Patch Placement - Sequential Placement

The sequence of bulk patching simulations helps to rule out the options where the interference with material properties lead to a worse wrinkling situation. Based on the well-documented trials on the role of bending-stiffness/shear resistance ratio [44], it could be hypothesized that to avoid large folds associated with contrasting properties, it is desirable to maintain resistance to shear but at the same time to avoid ramping up the bending stiffness.

To achieve this, the addition of diagonal (with respect to yarn direction) line patching is proposed in the region of interest rather than bulk patching. Patches introduced at an angle to the fibre direction can help to decouple bending response of the patches from high tensile stiffness of yarns.

The new stabilisation approach where narrow patches of 25 mm in length and 5mm in width were placed in the regions B-B' and C-C' (see Figure 3.1) was trialled and the simulation results are shown in Figure 6.7. Note that in this run full mould closure was achieved by using a mesh size of 1mm.

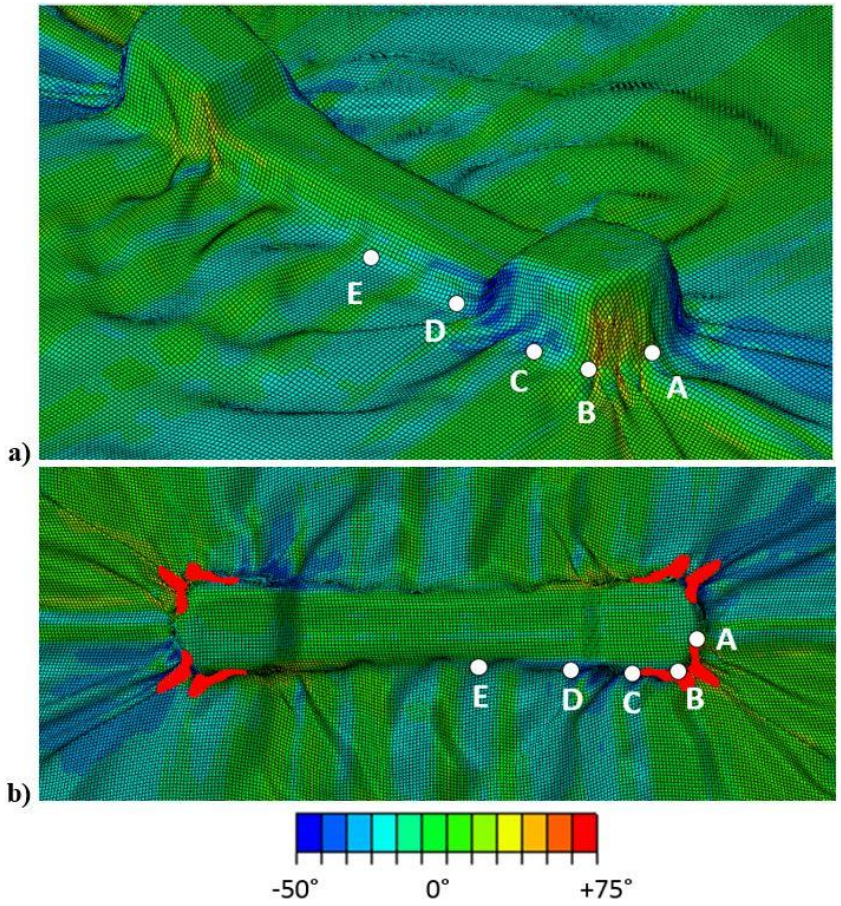

Figure 6.7: a) Shear angle distribution resulting from forming simulations with stabilising line patches (patch locations hidden) b) top view with patch locations shown in red; with the various relevant locations 'A'-'E' labelled and the top mould hidden

Figure 6.7b shows the line patch locations. The model predicted a maximum shear angle of 70° which is a slight increase compared to 67° for the unstiffened scenario (see Figure 6.6a). The model demonstrates the redistribution of wrinkles in the critical location and the formation of two large folds outside the shape of the component (contrasted to one large fold in the unstiffened case). It is key to note that the line patching did not result in the additional cost of substantial instability elsewhere as is observed for the bulk patching (Figure 6.6b). This gives an indication that by using line patching it is possible to flexibly tailor a fine balance between bending and shear resistance and potentially reduce wrinkling instabilities in the preform. However, in contrast to experimental trials, the elimination of the wrinkle has not been achieved. One hypothesis is that the forming simulations are sensitive to the actual balance between the shear and bending properties. At present the shear and bending behaviour are estimated and are not matched to experimentally derived results. The next section explores how varying the shear stiffness of the patches impacts on the forming behaviour. The bending behaviour is kept constant.

6.2.4. The Effect of Patch Properties on Wrinkle Likelihood

One of the advantages of patching with liquid thermosetting resin is that by thermal treatment, particularly if it is a snap-curing system, a wide range of viscosities and hence, patch properties can be achieved. To better understand the sensitivity of the model to patch properties the initial shear stiffness of the bulk patches was varied for the zone 3 only configuration (see Figure 3.2) whilst all other parameters remained the same. As discussed previously, the highest shear angle over the entire domain is chosen as the measure of model sensitivity and the mould is closed only to 60% closure. Results are also compared to the baseline configuration (no patching). Note that the patch behaviour remains non-linear, the values quoted here are the initial constant values.

Results are plotted in Figure 6.8. It can be seen that the model is sensitive to variations in shear stiffness and shear angle can vary by up to 10° over a relatively narrow distribution of shear stiffness. It can also be seen that the trends are non-monotonic and can hardly be intuitively predicted. From this plot the model suggests an optimal initial patch shear stiffness of approximately 50 MPa for this arrangement of patch locations, it is important to bear in mind however that this is not a representative value as the model parameters have not been matched to actual material properties. It can be seen that the effect of the shear stiffness on maximum shear angle is not linear but precise tuning of the patch properties can have an effect, albeit minimal. The shear angle is not measured from the same location in each run, rather it is the highest shear angle appearing anywhere in the modelled fabric. Given that the variations in shear angle are not greater than 10° it is possible that these deviations are primarily due to scatter rather than any observable effect. The higher shear angles at higher shear stiffness can be explained as the much stiffer patches lock up regions of the fabric making it harder for the remaining material to conform to the mould geometry, leading to wrinkling. An observation of the contrast between the wrinkle patterns for the best scenario (50 MPa shear stiffness) and the worst scenario (100 MPa shear stiffness) reveals minimal difference in the deformation pattern.

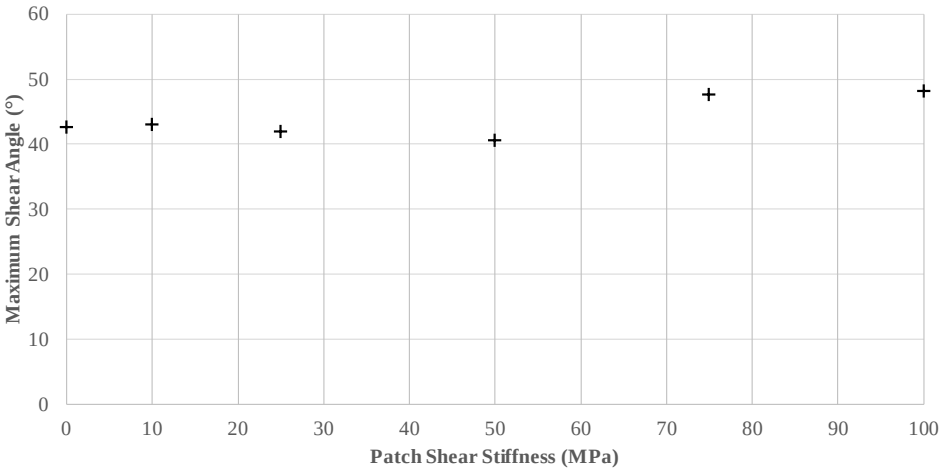

Figure 6.8: Plot showing the variation of maximum shear angle as shear stiffness is increased (at 60% mould closure)

There is a clear discrepancy between the successful formability improvement achieved in the experimental trials of section 3.2 and the lack of corresponding formability improvement demonstrated by the simulations for the same arrangement. This indicates that in some way the model is not fully capturing the true behaviour of the fabric. Critically the model does not entirely capture the sequence at which the tool comes into contact with the material. In reality gravity shapes the fabric drape first and then material is pushed towards the centre, whereas in the simulation the fabric is fully flat at first. This can lead to the entrapment of some fibre length that prevents the patching from showing any significant difference. The flexible tooling case which follows exaggerates some of these features on the one hand, and one the other hand makes a move towards taking the sequence of steps in account.

6.3.Rigid Tool Forming with Experimentally Derived Properties

In order to better understand the discrepancy between the formability improvement demonstrated in Chapter 3 and the lack of corresponding improvement demonstrated in the simulations thus far in this chapter, the rigid tool forming of section 6.2.3 is repeated now with the shear properties of dry fabric and patched fabric behaviour being based on the experimentally acquired values in Chapter 5. This should allow the fabric deformation in dry and patched regions to reflect reality more accurately and to better understand why the simulations do not fully reflect the experiments.

The shear behaviour is again described by a polynomial expression (7) which gives the shear stiffness, G_{12}, as a function of the inter-fibre shear angle, γ, these values are derived from the dry fabric behaviour of section 5.4.

$$G_{12}(\gamma) = -0.006\gamma^5 - 0.8985\gamma^4 + 1.8052\gamma^3 - 0.8439\gamma^2 + 0.0984\gamma + 0.0125 \quad (7)$$

The viscosity value used is 0.14MPa.s as this is the midway point in the range of 0.11-0.17MPa.s established previously in section 5.5.4. It should be noted that this is the approximate viscosity of the resin film infused fabric used in Chapter 5 not the low DoC resin infused fabric used in Chapter 3 and therefore are not an exact match, however they are considered to be comparable and sufficient for the purposes of this study.

This configuration was simulated for two runs, firstly with unpatched fabric to act as a new baseline and second with two line patches in each corner in accordance with the established ideal configuration from section 3.2.3 (experimental) and section 6.2.3 (simulated), see Figure 6.7 for details. The shear plots of these two runs are shown in Figure 6.9.

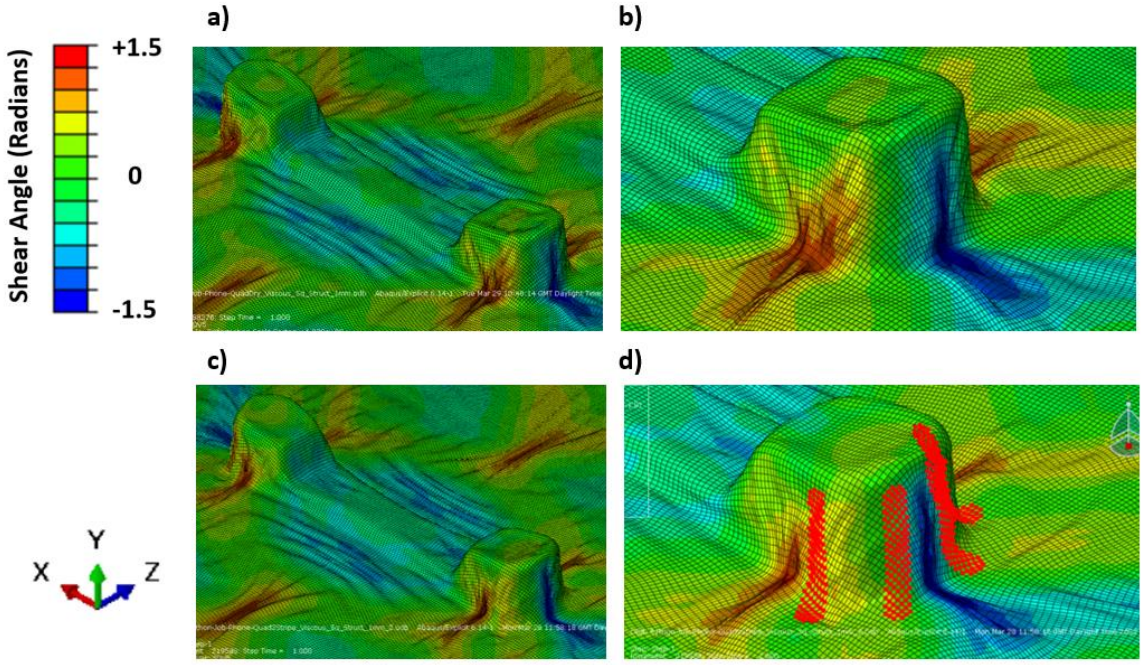

Figure 6.9: Shear angle distribution resulting from forming simulations with experimentally derived material shear behaviour with a) unpatched fabric b) closer view of a c) stabilizing line patches (patch locations hidden) d) closer view of c with patch locations shown

It can be seen from Figure 6.9a that the shear bands have moved from the corners to the midsection of the flange for the dry fabric sample, there is also significant out of plane buckling occurring rather than shearing in regions where high shearing was previously shown in Figure 3.7 and Figure 6.7. This same pattern is observed in the patched fabric sample shown in Figure 6.9b with some notable impact of the patches redistributing shear also evident. Comparing the experimentally measured shear stiffness of the dry fabric to the generic properties used in Section 6.3 the shear stiffness is

approximately an order of magnitude lower despite being measured for very similar textiles, whereas the other material properties are unchanged. This has altered the ratio of shear stiffness to the rest of the material properties of the model more significantly than expected, leading to a visibly different shear pattern. This discrepancy is due in large part to the shear behaviour being measured with a bias extension test rather than the picture frame shear test which was used for the original generic properties, a contrast which is well known to result in significantly differing results. In order to better reflect reality, loose forming of material on the mould due to gravity prior to mould closure, was later added to the model, however this did not have a significant impact on the forming pattern and does not account for the notable change in shear distribution from the model with the generic material properties.

It is interesting to note that this shear pattern eliminates the major wrinkle observed in the corners and favours shearing in the areas away from the direct vicinity of major curvatures. It could be argued that this mode of deformation is preferable unless it establishes other problematic domains. The presence of visco-elastic patches does not change the position or the intensity of the shear bands but makes them more localised and somewhat eliminates instabilities around the shear bands in the unpatched configurations.

Therefore it is concluded that further material characteristics need to be incorporated such as bending stiffness and friction to confirm that the model is getting closer to an accurate result than further away. Bending behaviour is essential to accurately model the fabric deformation and a further methodology to that proposed in Chapter 5 is required in order to capture this for both patched and unpatched regions. Friction between the mould and the fabric is also an important factor that influences the amount of tensioning in the fabric and hence, directly affects the forming patterns.

Obtaining the bending behaviour of the dry fabric is straightforward for example using the ASTM cantilever bend test [42]. However, the methodology for establishing the local properties of the patches is far less straightforward. At this stage of the development, it could be suggested that bending properties of the patches need to be derived in a parametric calibration procedure. In addition to the unknown bending properties, friction is also not known. This uncertainty leads to difficulties in establishing a direct match between experiments and simulations.

6.4. Flexible tool forming

So far the idea of resin patch stabilisation has been trialled only on the initial geometry of Figure 6.1a. It is important to gain a wider understanding of how effective the technique is for alternative geometries and how difficult or easy the optimisation process is for a different manufacturing process, such as double diaphragm forming or consolidation of fabric using flexible tooling. In order to give a better idea of general applicability this section investigates its effectiveness; a new case study is

considered – a curved spar component, see Figure 6.10. In addition to the characteristic features of the previous geometry it also includes the macro curvature of the entire component, and a flat segment suitable for accommodation of functionalised patches that makes it relevant for other aspects of this study, such as the creation of multi-matrix components discussed in Chapter 7. The production of this component is simulated for liquid moulding with a vacuum bag. In this case the material is first deposited on the mould, possibly thermoformed if the preform contains binder, then bagged and infused.

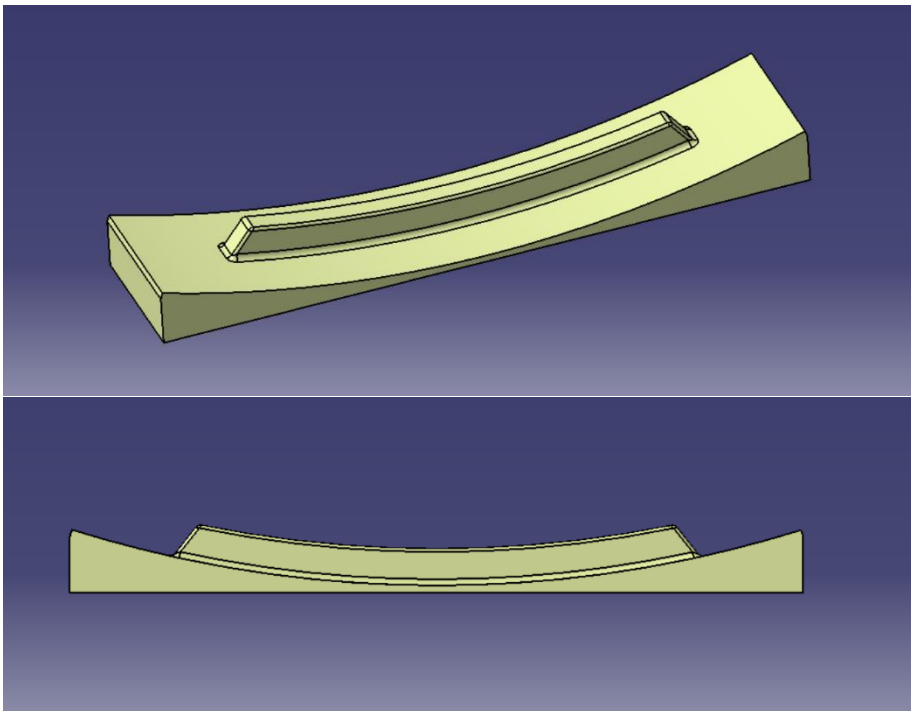

Figure 6.10: Curved spar mould with a flat base but a curved plane for forming, all radii are chamfered to allow for smooth sliding of the fabric over the mould

Compared to the rigid tool case, this geometry retains a balance between being drapable but not easily formable. The steepness of the ramp at each end was carefully chosen to ensure that wrinkling occurs when formed with dry fabric whilst not being so severe as to be impossible to mitigate. This was done by running several simulations with varying steepness to partial completion to identify the precise angle. A curved spa is a common component for various applications such as an aeroplane fuselage, the underside of a boat, or support structures within a car. It is therefore more common as a structural member than the rigid tool case study previously trialled. The shape also provides the potential for structural testing to establish whether patching has a negative effect on structural integrity.

The simulation is cut down to a quarter size to reduce run duration with symmetry in the X and Y axes. The symmetry conditions allow vertical displacement along the lines of symmetry and transverse displacement but not direct displacement. The basic set up of the model is retained from

section 6.2 with the addition of symmetry constraints, diaphragm forming and the change in geometry. The trial is simulated in two versions, one diaphragm forming and one consolidation with a vacuum bag / thermoforming. The former is simulated with upper and lower diaphragms which are pressurised to clamp the fabric before the pressure on the upper diaphragm is increased, leading to lowering of the fabric onto the mould. The latter is simulated in the same way except with the addition of an initial stage where the fabric and diaphragms are lowered onto the mould under gravity before any clamping pressure between the diaphragms are applied. This appears similar but in fact changes the nature of the initial contact with the mould allowing an assessment of the extent to which wrinkles can be 'trapped in' to the simulation due to excess length of fabric. The initial diaphragm formability simulation carried out with dry fabric only suggest that one large wrinkle will form in each corner of the mould as shown in Figure 6.11a. The corresponding vacuum bag simulation with the initial gravity only phase shows significantly improved formability in Figure 6.11b.

It is observed that two pronounced shear bands spread in the directions perpendicular and parallel to the orientation of the ramp with estimated magnitude based on geometry of 56.3° for the wider shear band and 40.8° for the narrow shear band. This rough estimate of the shear intensity is made based on considering the length of fibres in the base and ramp regions, the fibres passing over the spar section follow a longer path and therefore drive a draw in at the perimeter corresponding to this extra length. By contrast to the simple geometrical estimates the simulations predict a range of angles from 61.5° to 59.1° for the wider shear band.

a)

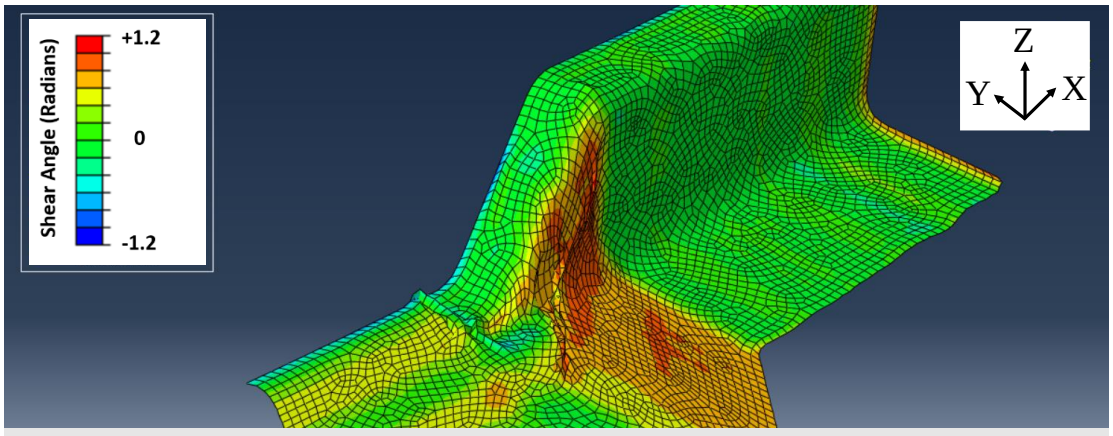

b)

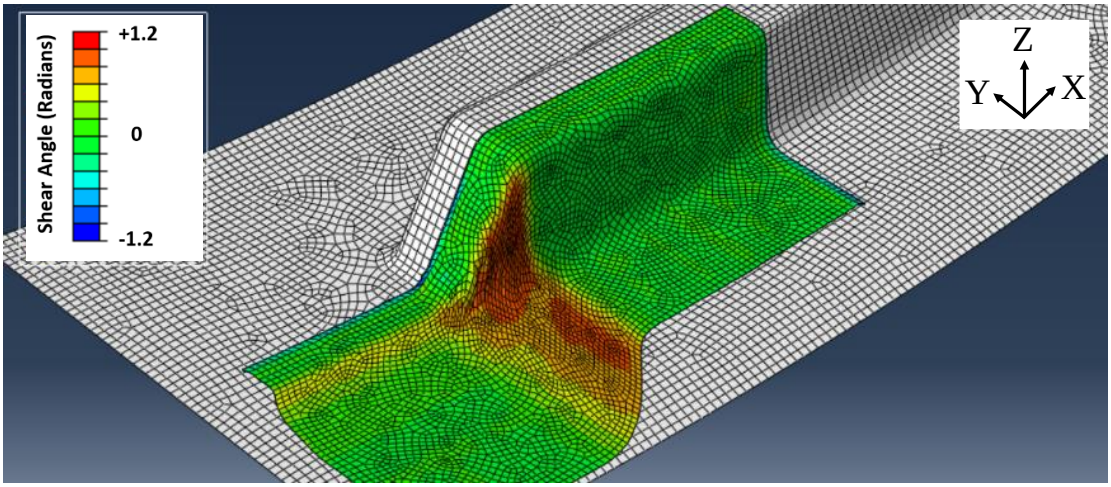

Figure 6.11: A colour deformation plot showing dry fabric formability of double curved spar, the colour gradient depicts shear angle; various wrinkles are clearly visible a) diaphragm forming b) vacuum bag forming

The diaphragm and vacuum bag simulations show a significant difference in forming output due to the entrapment of excess material in the first instance as compared to dragging fabric to the corner in the second case. This results in an improvement in the formability when less fabric is trapped which is visibly apparent but does not significantly affect the maximum or average shear angle in the critical region. This again calls into question the reliability of shear angle as a measurement of defect likelihood.

Various approaches to change the forming pattern can be envisaged as follows:

a) Force redistribution of shear by placing a stiffened zone on top of wrinkle location (this is the approach that was successful experimentally in Chapter 3).

b) Enclose the critical zone with stiffer diagonal zones to reduce the shear intensity. This is similar to (a) except the patches are not placed on top of the wrinkle site but rather as close as possible whilst outside the contours of the defect site.

c) Force redistribution of shear by stiffening edges and promoting tensile deformations in the critical zone. This is later referred to as ‘perimeter patches’.

d) Applying a pattern region to minimize local rotation of fibres without impacting the overall shear response.

Patching attempts were made to improve formability in accordance with the approach shown in section 3.2.3 and option (a) above. This approach centered around placing thin line patches at 45 degrees to the fiber direction directly on top of the critical region where the defect was occurring. The attempts to replicate this through diaphragm forming with the spar geometry were unsuccessful and

invariably led to a slight or significant worsening of the defects. As was previously stated the successful formability improvement achieved in the experimental trials of section 3.2 was not successfully demonstrated in the corresponding simulations for the same arrangement. The approach is therefore revised in favour of option (c).

The second patching strategy is to force redistribution of shear by stiffening edges and promoting tensile deformations in the critical zone. The idea is that widening shear bands may help to reduce local shear intensity and this, in turn, would result in firstly, tensile stresses in the fabric at the stage when material is drawn towards the centre, and secondly, making the central region less prone to bending and folding. The position of the patches should be such as to extend along the perimeter of the fabric at the end of the shear band slightly wider than the band itself (see Figure 6.1a). The properties of the region were artificially increased by 50 MPa compared to the properties of dry preform. The length of the shear band is chosen to be 50 mm for the wider shear band as opposed to the width of 30mm occurring naturally and 20mm for the narrow shear band as opposed to 8mm occurring naturally. This can be expected to give an average shear angle of 42.0° over the wider band. This patching strategy has been applied in application to both the diaphragm forming case and the vacuum bag forming case. It can be assumed that for the success of this strategy the prefom length over the concave corner must be shorter at some stage of the forming than the correspondent length along the tool. It also means that the edges should be put in contact with the mould prior to the corner region. Therefore two patches are placed at the perimeter of the fabric with the placement illustrated in Figure 6.12a.

Yet another patching concept (d) is to use an array of discrete point-wise patches as shown in Figure 6.12b. The hypothesis explored here is that placing these patches would encourage widening of the shear region by blocking large wrinkles from forming without excessively inhibiting shear overall.

a) 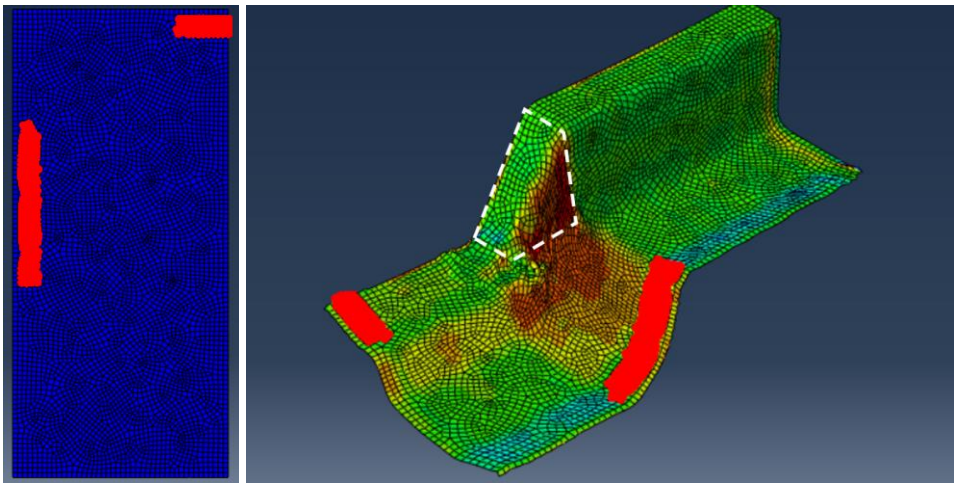

b)

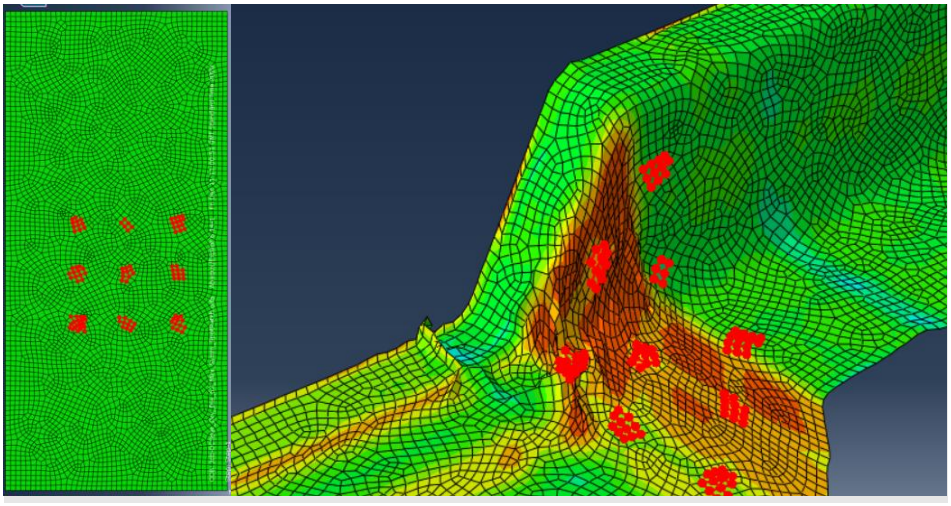

Figure 6.12: Colour plots showing the forming outcome as a result of a) perimeter patch placement locations (averaging zone highlighted in white) and b) spot patch locations; the colour gradient depicts shear angle

For the diaphragm forming simulation both of these patch arrangements successfully widened the shear band but did not visibly reduce wrinkling in the corner as shown in Figure 6.12a and Figure 6.14a. In order to quantify any impact the average shear angle over the region of interest was calculated in both the dry fabric and patched scenarios. To ensure that the average was taken of the critical region only the elements of interest were shortlisted and the shear angles extracted (see zone highlighted in white on Figure 6.12a). Again the vacuum forming run shows significantly improved formability compared to diaphragm forming. The results are summarised in Table 6.1.

a)

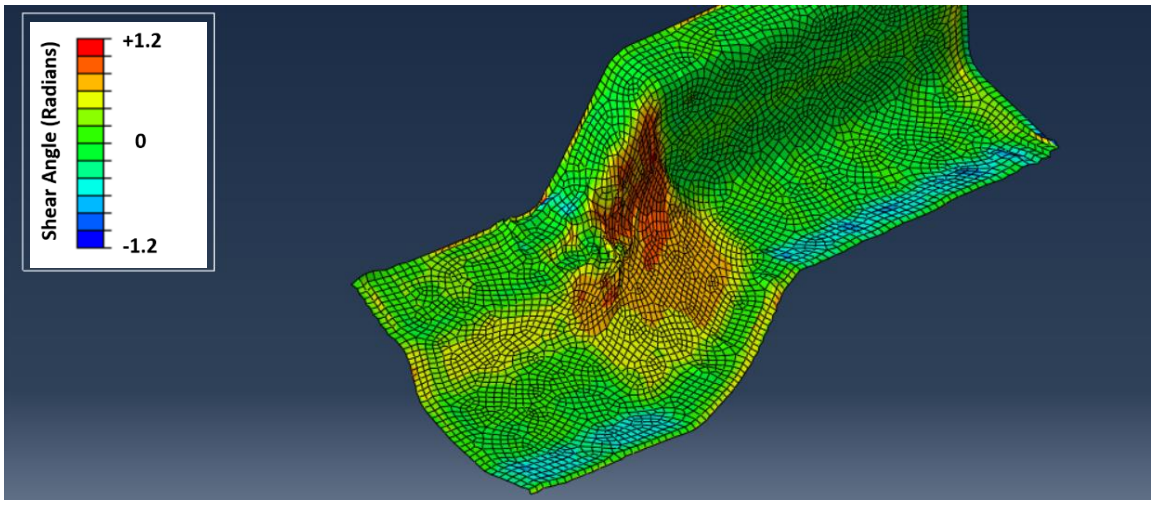

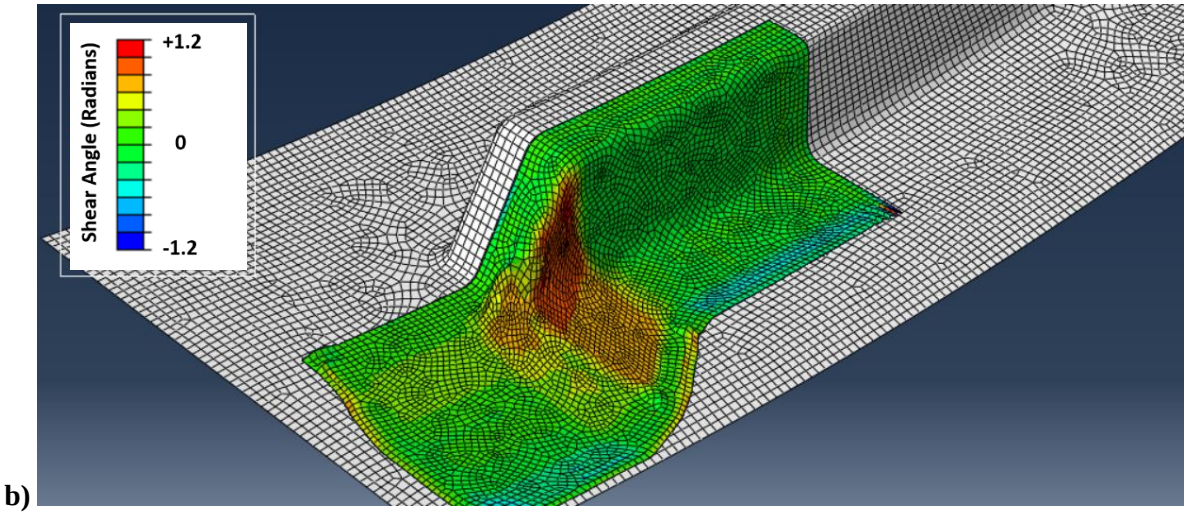

b)

Figure 6.13: Fabric deformation and shear map with perimeter patches; the colour gradient depicts shear angle, patch locations not shown a) without gravity b) with initial gravity only stage

The hypothesis behind the placement of perimeter patches was that they would introduce additional tensioning into the fabric. To assess the success of this hypothesis the in-plane stresses are plotted to observe any increases in tension. These are plotted in Figure 6.13.

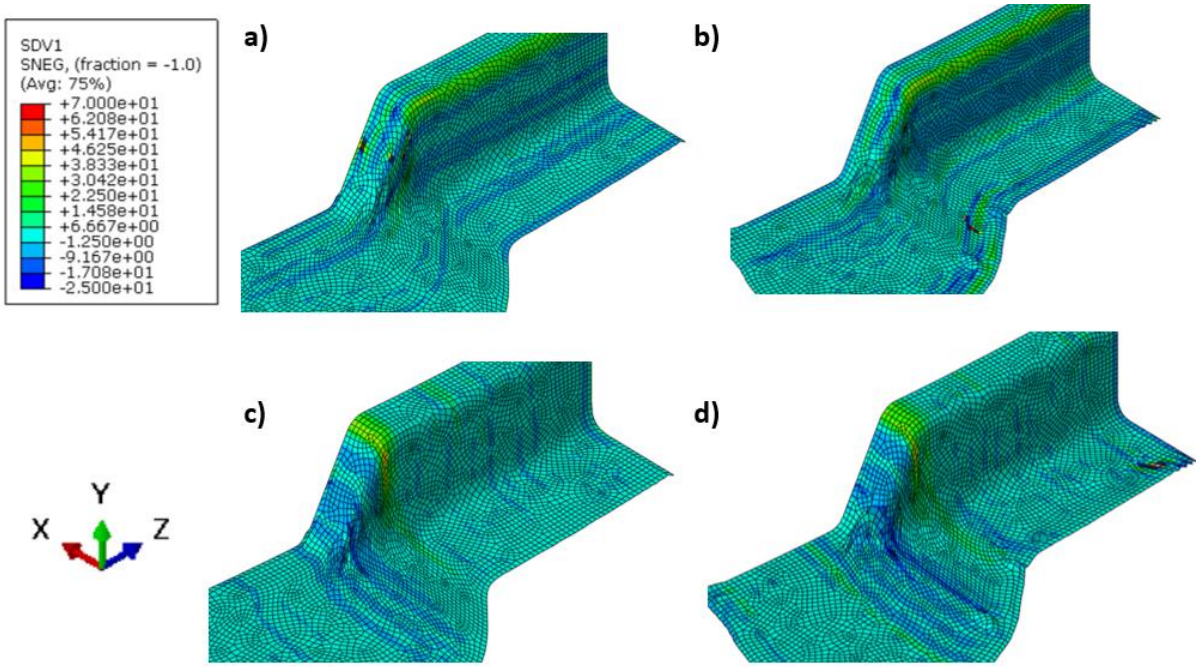

Figure 6.14: Plot of In-plane stresses for vacuum bag simulation (incl. gravity) a) no patches, x-direction, b) perimeter patches x-direction, c) no patches z-direction, d) perimeter patches z-direction

a)

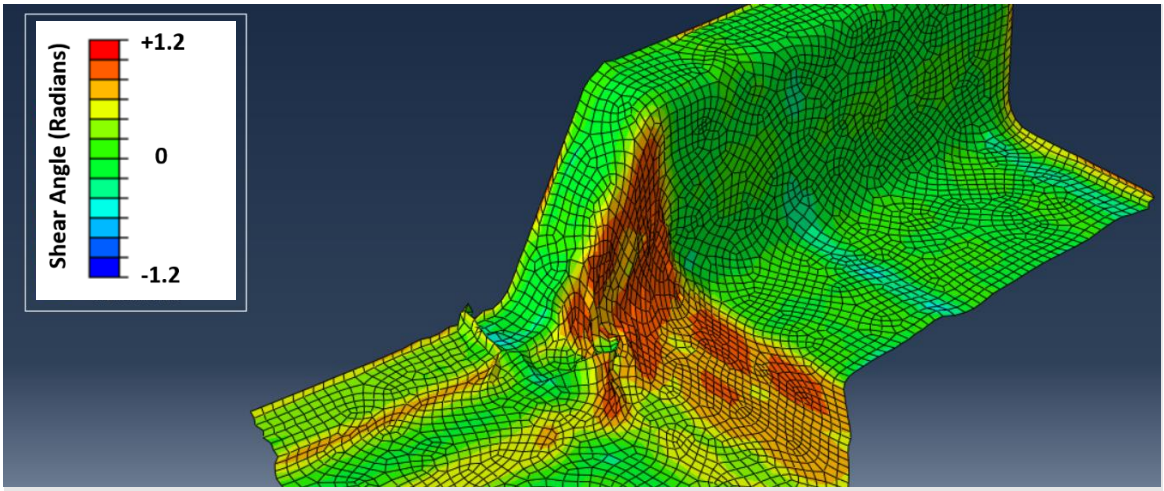

b)

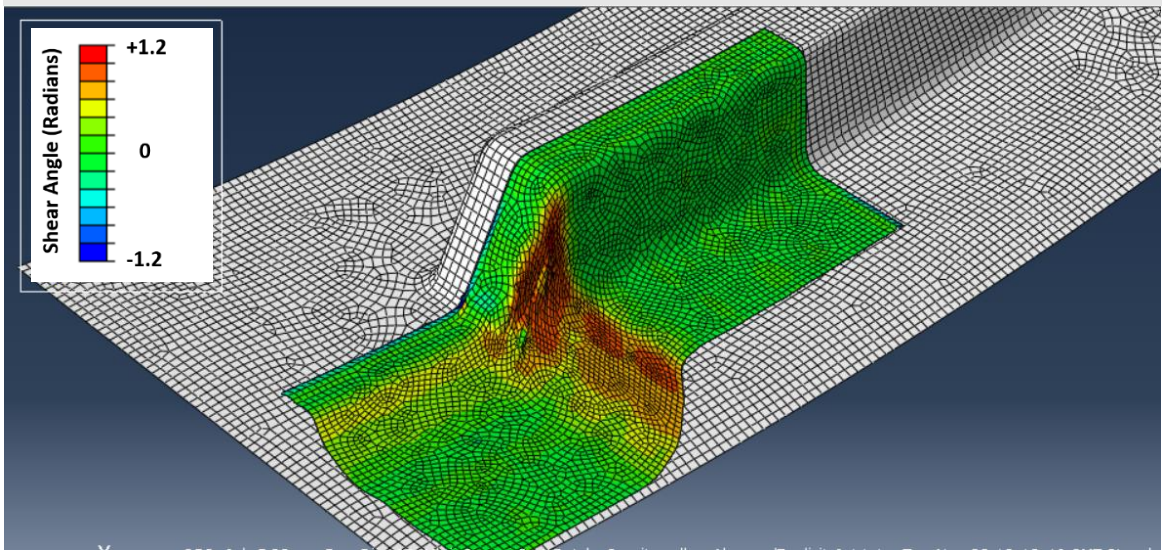

Figure 6.15: Fabric deformation and shear map with spot patches; the colour gradient depicts shear angle, patch locations not shown a) without gravity b) with initial gravity only stage

Table 6.1: Maximum and average shear angles with various patch arrangements

	Gravity Not Included		Gravity Included	
Arrangement	Maximum Shear Angle (°)	Average Shear Angle (°)	Maximum Shear Angle (°)	Average Shear Angle (°)
Dry Fabric	61.5	25.5	59.1	25.9
Perimeter Patches	62.8	24.5	66.9	24.9
Spot Patches	61.5	25.6	61.9	26.0
Perimeter Patches - Revised	-	-	64.6	25.1
Theoretical angle (Dry Fabric)	56.3	N/A	56.3	N/A
Theoretical Angle (Perimeter Patches)	42.0	N/A	42.0	N/A

It can be seen from Table 6.1 that the average shear angle is lowest for the scenario with perimeter patches both with and without gravity, however this does not lead to a decrease of the maximum shear angle. It is also well within the margins of possible numerical noise so cannot be interpreted as a confirmed improvement in formability. The expected decrease in shear angle over the band predicted by the theoretical shear angle (based on geometrical considerations) does not materialise as expected. The shear band does visually appear to widen but this does not propagate all the way to the zone of interest in the corner of the geometry, rather is widens near the patch at the perimeter but narrows again near the corner. There is also no significant introduction of tensile forces compared to baseline as shown in Figure 6.13. This suggests that patches at the perimeter are not sufficiently stiff to influence the formability positively by introducing tensile forces. Attempts were made to stiffen these patches further but this led to crashing of the simulation due to excessive over constraining of the model and could not be easily resolved, presenting a limitation of the model's usage in this fashion.

The spot patch arrangement leads to an identical maximum shear angle but does not lead to a reduction in average shear angle. Clearly each arrangement has subtly different effects on the formability.

The wrinkle detection algorithm proposed in Chapter 4 is now trialled on the same simulations as shown in Table 6.1. The wrinkles detected are weighted as previously discussed in Chapter 4, all wrinkles (node chains) not in the region of interest are discarded (i.e. beyond the contours of the final component). All wrinkles (node chains) of length < 6 nodes are then discarded, with a meshsize used of a wrinkle would therefore need to be at least 6mm long to be considered. The total number of nodes in all remaining chains are summed. The detected wrinkles > 5 nodes length are shown in Figure 6.16.

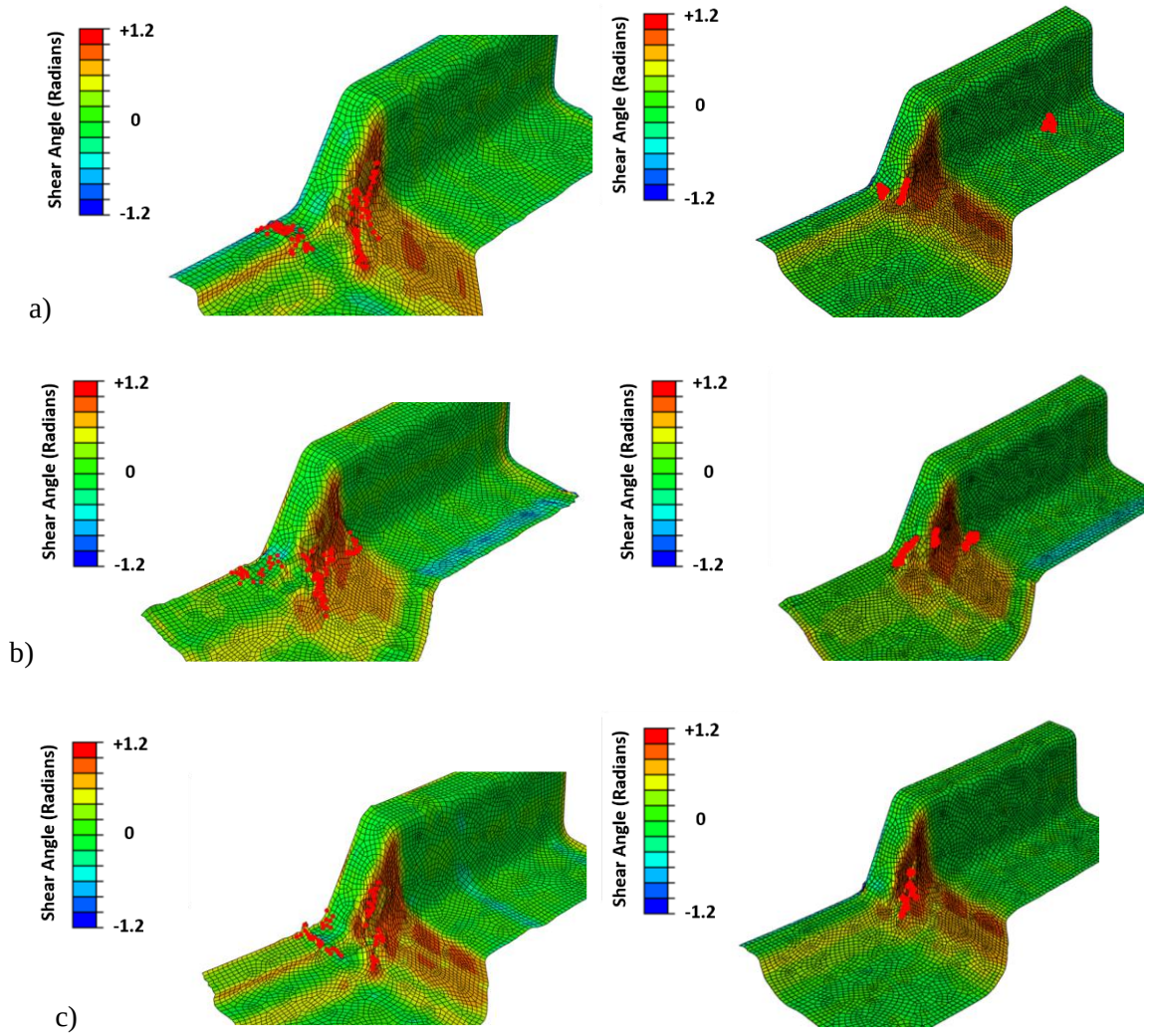

Figure 6.16: Wrinkles highlighted on the various simulation configurations trialled a) dry fabric b) perimeter patches c) spot patches; the colour gradient depicts shear angle, patch locations not shown, images on the left not including gravity, images on the right including gravity

The number of wrinkles greater than 6 length and the overall weighting is shown in Table 6.2.

Table 6.2: Number of wrinkles and overall weighting for the various combinations simulated

	Gravity Not Included		Gravity Included	
Arrangement	Number of Wrinkles	Overall Weighting	Number of Wrinkles	Overall Weighting
Untreated preform	6	97	3	20
Perimeter Patches	6	90	3	30
Spot Patches	7	64	2	19

Unlike the shear angle measurements in Table 6.1 the algorithm results in Table 6.2 suggest a formability improvement with the spot patches arrangement, this indeed appears to be the case visually as well. However, when adding gravity (i.e. vacuum bag simulation) into the simulation the margin of improvement is narrowed considerably and the overall formability is significantly improved for all scenarios compared to the diaphragm forming run (without gravity).

The hypotheses investigated as to what factors can or cannot help in mitigating defects: widening shear bands, breaking-up major defects, and introducing tensile stresses all impacted the forming behaviour but failed to demonstrate notable improvement in the overall formability. Firstly, the initial attempts to break up defects by directly placing stiffened zones on top of the occurrence site which was successful in the physical experiments of Chapter 3 led to excessive over constraining of the critical shear region in the simulation, in this case leading to larger folds forming. Secondly, attempts to widen the shear band leading to a reduction in peak shear and therefore defect likelihood, failed as the shear band could not be widened at the critical zone due to geometrical constraints leading to only a widening further towards the perimeter of the fabric. Finally introducing tensile stresses was successful in improving formability in the case of the vacuum bag forming scenario, where gravity is introduced, reducing the amount of fabric ‘trapped’, however attempts to introduce tensile forces through the use of perimeter patches failed as these could not be made sufficiently stiff without causing excessive over constraint of the model leading to crashing of the simulation.

6.5. Discussion

The results presented in this study and Chapter 3 give evidence that local stabilisation of fabric by means of reactive resin injection is a promising method that can enrich the palette of techniques available for defect mitigation in forming. Compared to other methods it has several advantages, including simplicity of implementation – no additional fabric constraints are required, flexibility and good potential for automation, and non-interference with reinforcement geometry – the yarn

architecture is not affected by resin deposition compared with through-thickness reinforcements. It was shown experimentally in Chapter 3 that fine tuning of preform properties can help to achieve a near defect free component. On the other hand, the implementation of this approach bears additional complexity. As shown in the study, forming patterns are strongly influenced not only by the patch position and geometry but also by the balance of properties between patches and bulk fabric, though varying bending rigidity of the patches in the range of 0.01 Nmm^2 to 100 Nmm^2 did not reveal a clear impact on the forming pattern. Hence, sophisticated forming process modelling tools for mapping the resin deposition, fine tuning the viscosity of deposited resin, and extensive characterisation of resin and fabric are required.

The parameters influencing the forming shape a vast design space. The two-step optimisation used in this study, although pragmatic and simple, shows how the search for an acceptable solution can be organised. The idea that the favourable position of patched regions can be dictated by the shear intensity overall agrees with conventional approaches to forming assessment, but it is clearly seen that it cannot be used alone. Defining the fine arrangement of the patch geometry requires higher fidelity simulation with direct observation of wrinkling. An essential hint in selecting patch orientation is that shearing must be impeded while the impact on bending minimised, which leads to an unusual off-fibre patch orientation.

It is important to emphasize that the simulations were used as a design tool only and direct comparison with experiments is only made in section 6.3. To have a full realistic analysis of wrinkle shape and severity all the material properties would need to match experimental reality. This leads back to the characterisation attempts of Chapter 5 which proposes a technique for establishing shear properties but does not cover bending or friction. Another limitation of the model, that prevents its direct validation in the considered cases, is that it does not take into account preform fibre slippage (laddering) – substantial defects that must be avoided in manufacturing practice.

The conclusions drawn in this study are applicable to biaxial architectures with an initially orthogonal system of fibres, i.e. single plies of woven preforms. Whether a similar technique can be applicable to multi-layer forming is yet to be explored. Due to the additional constraints and mechanisms of consolidation in the multilayer scenario this possibly represents a different challenge. On the other hand, local patching may pave the way for a different approach in manufacturing where each of the plies in a laminate can be addressed separately. It is envisaged that a manufacturing process where a multi-ply stack is used assembled from plies patched and preformed in isolation and in advance. Such pre-conditioning can also be efficiently automated and address consolidation defects as well as forming ones.

Overall, the experimental trials, informed by modelling, prove the potential of the envisaged approach. The experimental work of Chapter 3 confirmed the importance of tuning patch geometry

and properties, showed the advantage of local patching compared to powder binder stabilisation, and highlighted other essential factors where local stabilisation can play an important role – such as tool-preform friction. It was demonstrated that with careful patch parametrisation in the numerical solution, shear can be redistributed though it proved more difficult than expected to demonstrate an improved formability situation overall and none of the simulated hypothesis were successful despite the experimental success. Simulation attempts made in section 6.3 also failed to match the dry fabric (unmodified) deformation pattern to the experimentally observed deformation patterns from section 3.2.3. It was hypothesised in Chapter 5 that characterising the shear behaviour of the dry and patched fabric alone would be sufficient to obtain an accurate match to experimental results, even with the use of generic properties for other parameters such as bending and friction. The results observed suggest that this is not the case and that both bending behaviour and friction values need to be characterised for the specific textile used as well.

7. Infusion of Multi-matrix Composites

The previous chapters have been primarily focused on examining the feasibility of enhancing formability of the preform by integrating additional elements /patches in continuous preforms. In some cases, improving formability for functional materials requires somewhat a different, and to some extent, almost reverse approach. For instance, the functional materials may be fundamentally unformable, such as in the case of structural supercapacitors, where rigid nano-foam prevents any substantial shearing or bending of the preform [2], [4]. In this application, the challenge is to create formable domains, such as folding or shearing hinges, that are seamlessly connected to the rigid flat domains allocated for functional material. A particular interest presents integrating dissimilar domains in continuously-reinforced materials that would ensure the most efficient and reliable load transfer between them. This chapter explores various solutions for manufacturing of such formable multi-matrix composites. Of particular interest is how fabrics which have been modified so that bending or shearing is inhibited, can be developed to allow for the construction of complex shapes.

Two methods for the infusion of multi-matrix composites are suggested and put to test in manufacturing trials. These methods can be envisaged for various functional applications, such as repair, EMI shielding, lightning strike protection etc, but particular emphasis is put on the production of structural supercapacitors integrated to composite structures. The limitations of the current techniques are outlined and a variety of geometries and applications are trialled with various levels of complexity. Both methods are shown to be effective and consideration is given as to how to scale up the TRL to allow for more practical large scale manufacturing. Two demonstrators that have been manufactured are presented; firstly a basic C-section demonstrating the possibility of forming structural supercapacitors around corners; and secondly an L-section demonstrator showing the possibility of segmenting fabrics for multi-stage infusion with multiple plies.

Attempts to enhance the formability of dry preforms have led to a range of well-established techniques - common approaches include constraining the fabric at the boundaries [12], [17] and modifying the local properties within the preform itself [19], [23], [71]. These techniques focus primarily on how to improve the formability of a dry preform. This chapter by contrast focuses on how methods for creating multi-matrix composites can be implemented using common manufacturing techniques. Hence, this study expands the application of the previous patching method and shows further capabilities for partitioning of fabric with possible applications [112].

A key enabler for realising such multifunctional composites is the need to manufacture components which have zones of differing matrix types, whilst still maintaining continuity of the fibres (and hence efficient load-transfer) across the whole structure. The motivation for the study here was to investigate manufacturing routes to permit these components to be manufactured, such that some zones in the

component would be purely structural (i.e. monofunctional) whilst other zones would be multifunctional (i.e. structural plus another function). Our particular interest was in the development of structural supercapacitors electrodes as a practical application of multi-matrix composites [2], [112]. In particular, the need to introduce forming zones within component containing non-formable multifunctional domains.

Shear and bending response are the primary deformation mechanisms for biaxial textile fabrics. Generally speaking, the more fabric there is available to shear or bend the more formable a textile is. Where fabric is 'unavailable' due to shear or bending being inhibited this can have a significant knock on effect on formability. The manufacturing approach proposed in this chapter segments a fabric preform using two techniques – barriers or masking – to allow for the partial infusion of a preform whilst retaining a portion of the preform as dry fabric until a later stage of manufacture. This chapter describes novel experimental methods for fabric segmentation/partial infusion, to assess how much fabric can be locked before formability is inhibited, and to establish the current design limitations of the techniques used.

7.1.Motivation

The desirability of multi-matrix composites lies in maintaining continuity of fibres over the part geometry and throughout various manufacturing stages. This approach to the creation of composite components enables a range of new manufacturing options albeit at the cost of some complexity. The following applications are envisaged:

Variable strength composites – Varying matrix material in critical areas of a component to strengthen regions of high stress or wear [78]. This could be achieved through the use of additives in the resin or higher quality resins. This is potentially of benefit, for example, in large components such as wing spars, where certain regions such as bolt holes and regions of curvature tend to drive the thickness requirements of the wider part. This coupled with limitations in the ability to ramp up and down ply thickness due to the need to maintain continuous fibre paths makes localised regions of higher strength matrix highly desirable.

Thermoplastic hinges – Creating hinge regions where the shape can be adjusted by elevating the temperature and locked again by cooling. A combination of thermosetting and thermoplastic matrix materials would allow the creation of a partially re-formable component.

Selective multifunctionality – Infusing resin with additives into selected regions of the fabric [11]. This could allow for electrically conductive regions, aerogel infusion (as discussed later), sensing applications, or regions suitable for inductive curing.

Formability enhancement – Printed resin patches to enhance formability. As discussed in chapters 3 and 6 regions highly likely to lead to defects can be pre-treated to redistribute shear deformation elsewhere, assisting the forming process [71]

Continuous matrix joints – Retaining dry zones at joint locations to allow the joint to be infused as one, avoiding the need for adhesive, rather than the more conventional approach of creating two laminates and then bonding together at a later stage. It is envisaged the regions intended to be bonded can be kept dry until the bonding stage and infused as one rather than bonded – leading to a joint with discontinuous fibres but continuous matrix.

Imperial College London are pursuing the incorporation of porous aerogels to boost the storage functions of composite laminates to create structural supercapacitors [2], [112]. This project has been carried out in collaboration with ICL. Aerogels are stiff and brittle which presents a challenge for manufacturing of complex components. This part of the project is investigating the formability and manufacturability of composites when divided into structural power and purely structural areas. Areas of high shear deformation and out of plane curvature are designated as purely structural. Areas of low deformation and curvature are designated for energy storage as shown in Figure 7.1 on an example of a complex tapered spar exhibiting some characteristic features that could be observed in aerospace structures.

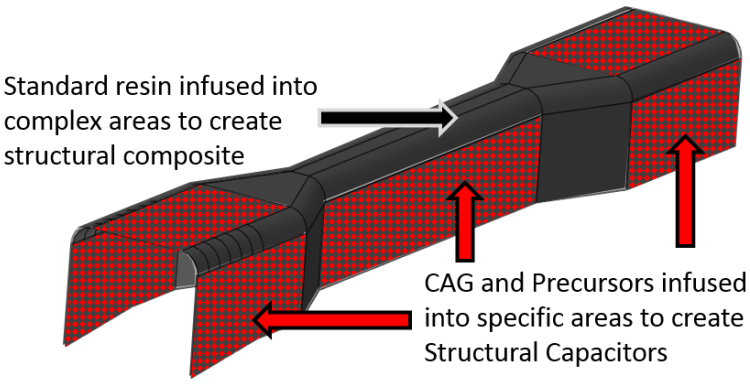

Figure 7.1: Structural and multifunctional zones segmented on a spar c-section, it can be seen how the multifunctional zones do not need to bend whilst the structural zones are formed around the corners

7.2.Methodology

In order to segment these zones without a discontinuity in the fibres it is necessary to develop a method of selective infusion. Two approaches have been taken, firstly to create a barrier out of resin as shown in Figure 7.2, this barrier is then incorporated into the bagging process, forming one of the boundaries, ready to be infused through resin transfer moulding. The design of such structures and domain allocation can be seamlessly conducted using both the numerical tools developed in previous chapters (Chapter 4 and 6), and by using experimental methodology to define shearing capabilities of the functional domains as suggested in Chapter 5.

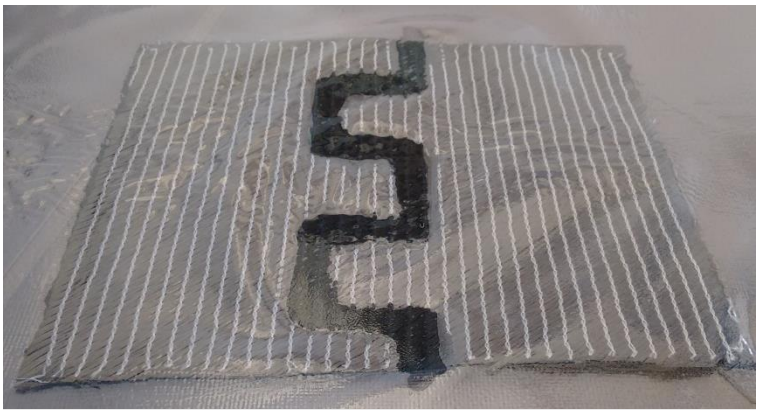

Figure 7.2: Resin barrier in non-crimp biaxial carbon fibre, it can be seen how the resolution has been partially lost due to the capillary forces in the fabric, the bagging film can also be faintly seen which is affixed to the barrier but not the rest of the fabric

The second approach is to use PLA (polylactide) to ‘mask’ the dry regions as shown in Figure 7.3 preventing resin from infusing these areas allowing for the whole sample to be bagged as usual. This is suitable either for manufacturing where the masking region can be removed in a subsequent manufacturing stage or where masking region has desirable properties from the start. The PLA is applied by cutting a thin film to the desired shape and the using a hot press to stamp the PLA into the fabric at 160 °C and 0.4 MPa, see Figure 7.3.

Figure 7.3: PLA 'mask' infused into woven carbon fibre, the unmasked area can be identified by the still visible yarns, the mask is infused into both the top and bottom of the fabric. Masking tape remains around the perimeter at this stage to prevent the fabric from unravelling

Two methods, barrier and masking, were considered for manufacturing composites with two distinct zones of different matrix, as illustrated in Figure 7.4. This process prepares the sample ready for forming.

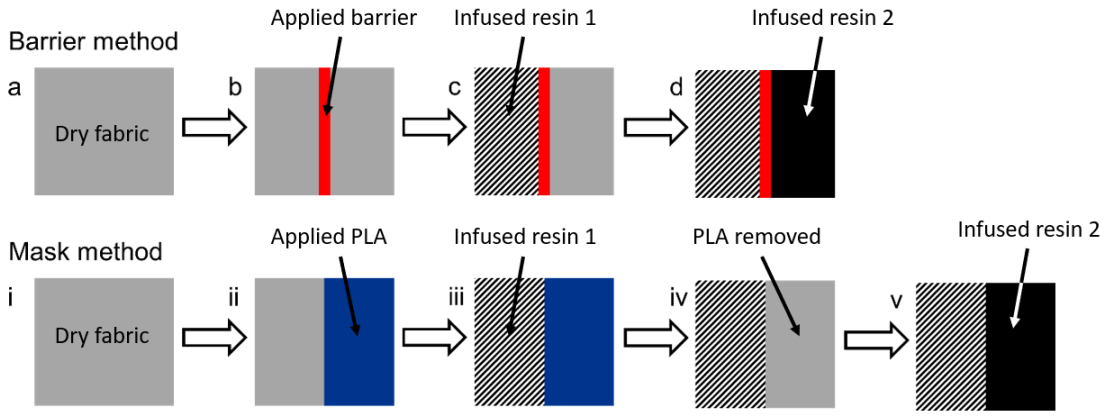

Figure 7.4: Illustration of the barrier and masking methods. On the top row (barrier method), (a) fabric (grey), (b) application of barrier (red), (c) first modification/infusion to fabric (stripes), (d) second infusion (black) to fabric in, second section, or debond barrier to bagging material and infuse whole component with another media. On the bottom row (masking method), (i) fabric (grey), (ii) application of mask (blue), (iii) first modification/infusion to fabric (striped), (iv) removal of mask, (v) second infusion (black) to whole component

Each method could be able to be applied to multiple regions, to different fabric types, without specialist equipment using conventional resins and bagging materials. There is also the potential to combine both methods together for ease of application and general uptake. Each method has benefits over the other as described in Table 7.1.

Table 7.1: Pros and cons of barrier and masking methods

Method	Pros	Cons
Barrier	- Large area zoning possible - No requirement to remove barrier before additional processing - Simple to make from commercially available matrix film	- Sufficiently wide barrier is needed to ensure robustness - Impractical for very small zoning - Co-existence and processing harmonisation needs to be done for 3 different matrices
Masking	- Able to modify small regions - Finer and complex geometries possible than the barrier method - Compatible with 3D printing patterns or sheets	- Need to remove mask before second infusion (if required) - Impractical for larger zoning - Potential residue left on fabric from mask removal - May lead to voidage if the mask is not removed

7.3. Materials

Glass fibre woven fabric E-glass ±45 biaxial NCF (200 tex with PES stitched thread) was used for proof of concept for the barrier method with vacuum bag sealant tape (Tacky Tape SM5127, 1/2″ x 1/8″) as the interior of the barrier could be observed. Epoxy adhesive Araldite® LY 3585 with Aradur® 3475 hardener was initially used to fix the fabric to the bagging material in the second development of the barrier method, but in later studies, a pre-preg adhesive film (epoxy) was used (Easy Composites XPREG® XA120 (150 gsm)) to improve handleability. Bagging materials used to bond to the fabrics were nylon based (VACtiteP) supplied from VAC Innovation (GB). The carbon fibre fabric was either ±45 biaxial 3k Carbon Fibre Cloth (non-crimp fabric, 300 gsm with polyester stitch thread) or 2x2 Twill weave (TR3523 M, 200 gsm), both using Mitsubishi Pyrofill HT Series TR-30S-3L, 3k fibres bought from Easy Composites (GB). Polylactic acid (PLA, REPREPER TECH, 9051-89-2), which is used commonly in 3D printing, was used as the masking material.

The carbon aerogel process was carried out exclusively by the staff at ICL and therefore is detailed elsewhere [2], but in summary a resorcinol-formaldehyde based sol-gel precursor was infused through flexible tooling into dry fabric, and was then aged at room temperature, 50 °C, and 90 °C. Following these steps the aerogel precursor fixed the fibres in place and modified sections are rigid. The precursor modified plies were then carbonised at elevated temperatures ca. 800 °C in an inert atmosphere. This process was required to make the carbon aerogel conductive for use as a structural electrode in a supercapacitor device. All materials were used as-received from the suppliers.

7.4. Barrier Method

The initial challenge of multi-matrix infusion is how to create a conventional vacuum bag setup whilst having one or more boundaries of the vacuum bag partitioning the fabric, rather than the more conventional approach of enclosing the entire sample. The simplest approach is to create this boundary using tacky tape (a commonly used sealant tape for vacuum sealing the tool face to the bagging film) this is effective at segmenting the fabric, though is difficult to remove afterwards. Nonetheless, it demonstrates the concept of how to keep one region of fabric dry whilst infusing the other. The trial was carried out using a single ply with tacky tape applied to both the upper and lower face of the fabric and pressed manually into the fabric, this proved sufficient to penetrate through the full thickness of the single ply. This initial sample was infused at room temperature with a low viscosity resin (Prime 20LV, Gurit (GB)) with a vacuum pressure of 95 kPa, before curing at 65° for 8 hours with the vacuum maintained throughout (arrangement before infusion). Figure 7.5a shows glass dry fibres (white), carbon fibres (grey), bagging material (green), tacky tape (black), barrier/epoxy (red), infused regions (striped), with the bleeder cloth, release film and other consumables used in the infusion process omitted for clarity. The infused and final sample is shown in Figure 7.5 and it is noted that in the final product it proved difficult to remove the tacky tape. Nonetheless, it demonstrated the concept as to how to keep one region of fabric dry whilst infusing the other, though it is worth noting that it would not be practical for multi-ply preforms..

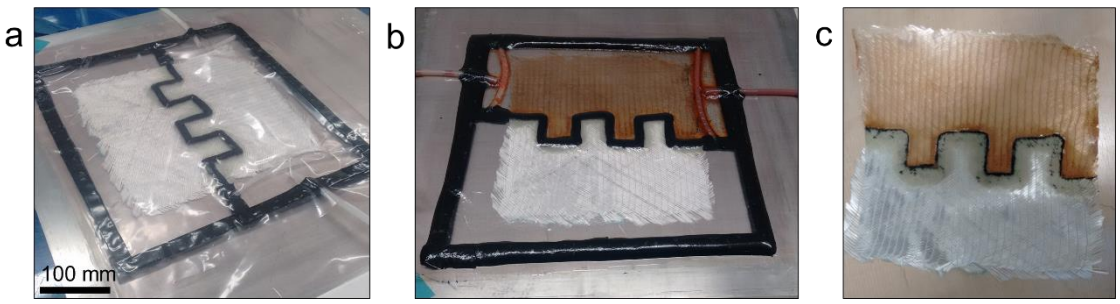

Figure 7.5: Tacky tape as barrier adhesive applied to a glass ply (a) initial arrangement, then (b) epoxy infused via resin infusion by flexible tooling (red dye used for clarity) in one region of the ply, (c) final product showing an epoxy infused region and an as-received fibre region in the opposite region. Note that the tacky tape barrier was difficult to remove as shown in (c)

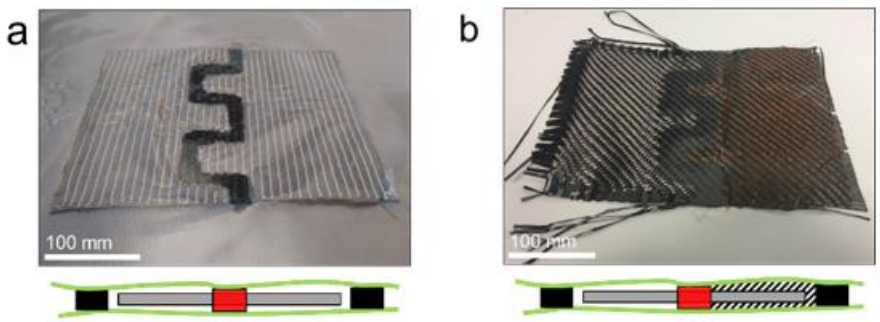

Figure 7.6: Development of the barrier method. (a) epoxy used as adhesive between infusion bags, (b) demonstration of dry fabric being modified on one side of the epoxy barrier with the barrier joined to the outer infusion bagging material; with the schematic cross-sections of their respective arrangements shown below the photographs. The barrier shape was chosen to explore the resolution and spreading of the resin in right angled corners

A more workable approach is to create the boundary using epoxy resin. The selection of the resin was made such that it was not too viscous that it would fail to penetrate the laminate, but also not too low in viscosity that it spread significantly into the interior of the fabric under the action of capillary forces. The resin also needed to be easily deposited onto the surface of a single ply and then consolidated whilst in contact with the bagging film, creating a seal (see Figure 7.6b), a commercially available two-part resin system was used initially (Prime 20LV, Gurit (GB)). The remainder of the bagging setup (such as adding the resin inlet and outlet tubes and the tacky tape perimeter) can be completed later and the sample then infused. In this arrangement there was no need to remove the resin barrier afterwards as this could remain as a constituent of the completed part. Demonstration of this approach with the aerogel precursor is shown in Figure 7.6c.

The most significant drawback of this approach was that capillary forces distorted the fidelity of the barrier leading to a poor resolution in the barrier shape and fluctuations of width of approximately ± 3mm. This necessitated the use of fairly wide barriers (10 mm), reducing the area available for CAG infusion. This has the potential to be improved using additives and partial pre-curing before consolidation to reduce barrier spreading but was not explored in this study.

Further refining the process to simplify the manufacturing, it was observed that rather than bisecting the fabric it was sufficient to simply isolate certain zones from the flow of resin during infusion (barrier still maintained through the thickness of the lamina). The previous method is developed further to return to bagging and infusing the full sample whilst certain zones are isolated and kept dry by the use of self-contained barriers sealed with bagging film (see Figure 7.7). The contrast is between a barrier that crosses the entire fabric and then joins to a tacky tape barrier (bisecting) and one where a self-contained isolated zone is fully within the perimeter of the fabric. It is shown in Figure 7.8a where carbon fibres (grey), bagging material (green), tacky tape (black), barrier/epoxy

(red), infused regions (striped), independent bagging material to outer bag (yellow), with the bleeder cloth, release film and other consumables used in the infusion process omitting for clarity. By the use of an epoxy film (XPREG XA120 Easy Composites) rather than liquid resin it was possible to pre-cut the shape of the barrier and then seal the zone to the bagging film using a hot press: 0.4 MPa at 80 °C for 1 min to soften the film, then 0.4 MPa at 150 °C for 4 min to cure and create seal. This created a good quality barrier chemically stable to commonly infused solutions and robust to those tested. In Figure 7.7 the two rectangles enclose two dry zones of fabric whilst the entire sample is infused. This geometry was chosen to provide the template for two simple c-sections (see Figure 7.8). Note that the use of a highly viscous resin film addressed the aforementioned issues attributed to capillary forces. Care had still to be taken during cure to avoid a significant drop in viscosity before the gel point was reached.

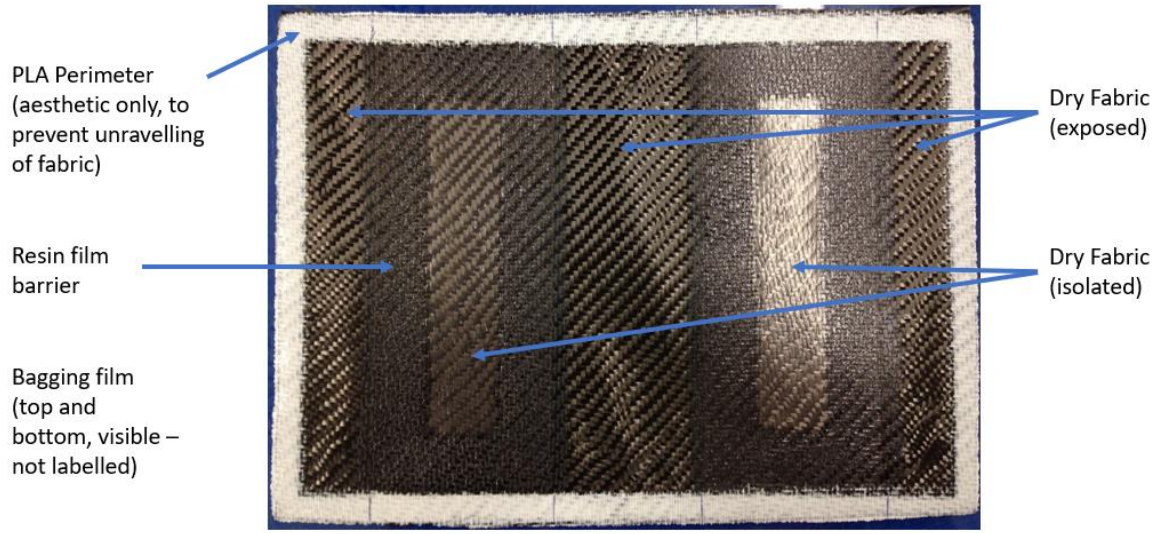

Figure 7.7: Epoxy barrier sample demonstrating isolated zones rather than full partitioning of the fabric, the bagging film is also faintly visible with a layer on the top and bottom affixed to the barrier but not the dry fabric. The perimeter of the fabric is also masked to prevent unravelling and make transportation easier

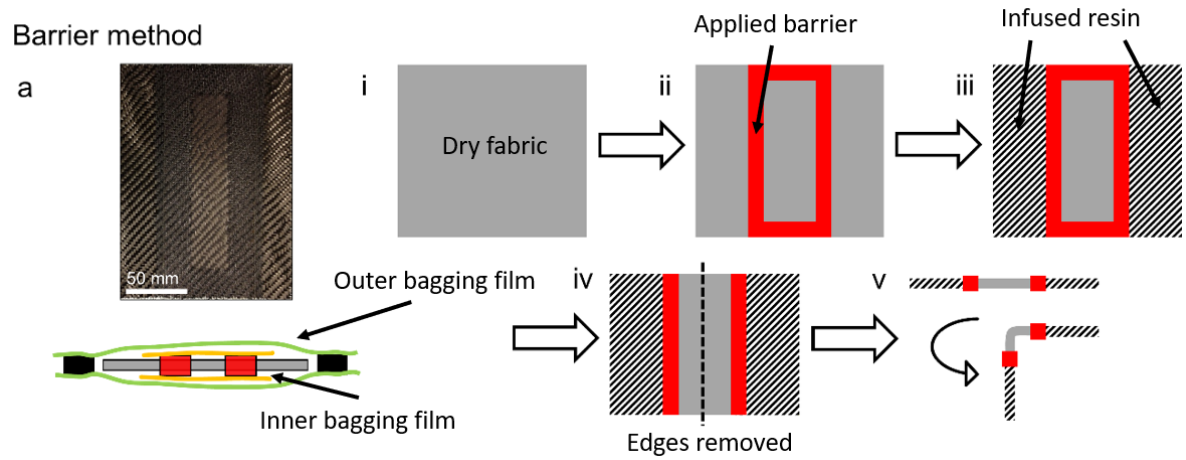

Figure 7.8: (a) Barrier method modified such that the outer most bagging material and barrier are independent. Producing a fold region using a barrier method, is as follows; (i) dry fibres, (ii) barrier applied to a specific region of the fabric, (iii) infusion of the first matrix, (iv) cutting the sample to allow for specific fold line (dotted line) to be accessible, (v) side on view of the L-shaped flexible component produced

Using this approach it is possible to design a pattern of 'dry' and 'wet' zones with barrier zones in between. The formation of a C-shaped structure with the central bendable region having a different infused resin to the flanges (shown in Figure 7.8a) is illustrated in application to c-section shape in Figure 7.8 (i) to (v). The ratio and size of these zones could be varied based on coverage and formability or zonal requirements. This method has been used to good effect to enable c-section structural supercapacitors by isolating the curved regions and infusing the flat regions with aerogel. The part is post-infused on a mould to create the final shape after the majority of fabric has been locked in shape.

One of the main challenges of this method is guaranteeing a reliable seal between the film and the epoxy barrier. Ensuring good permeation of epoxy through the thickness of the fabric presents less of a problem. It is also important to evacuate the majority of the air from the sealed region prior to curing of the barrier. If this is not done the trapped air will expand and attempt to escape during the next stage of the process (when the post-infused resin begins to cure but has not yet gelled) potentially bursting the barrier).

Due to the need for the barrier to create a strong reliable seal with the bagging film the width of the barrier is a key design driver. Thinner barriers are desirable as they allow for the optimisation of available space within the preform for infused resin, and they determine the size of component to which the method can be applied by dictating the radii that can be achieved on corners. Initial attempts with barriers created using liquid resin required widths of approximately 20mm in order to ensure a good seal, and therefore a successful infusion stage, this was partially due to the difficulties

of poor barrier resolution leading to fluctuations in width compared to the target. The move to epoxy film has enabled significant reduction in barrier width to approximately 6mm, though this is an estimate based on observations of various attempts, some of which failed, and 10mm is considered to be more reliable allowing for a slight margin for error. The barrier epoxy, when cured, creates a seal with the bagging film with ideal properties for the purpose. The film is sufficient to withstand handling and holds when under vacuum for the infusion stage, however it can be peeled off by hand with minimal effort which is important for debagging. Despite these improvements, the reliability of the barrier remains the critical stage in the process and steps to improve this warrant further work.

7.5. Masking Method

An alternative to the barrier method is to use a masking material which permeates specific regions entirely and therefore isolates the parent fabric (dry preform) from infused substances (infused resin). PLA masks were drawn in advance using 3D design software and printed in sheets. These sheets are placed coincidently on the top and bottom of the fabric and then pressed into the fabric using a hot press at 160 °C and 0.4 MPa. The printed PLA was approximately the thickness of the fabric (0.26mm compared to a fabric thickness of 0.24mm) and was adequate to fill the void space in the dry fabric, whilst avoiding loss of resolution due to polymer flow at elevated temperatures.

The primary challenge of this method was how to remove the masking material following processing in order to allow the isolated region to drape and/or be subsequently filled with the secondary matrix. PLA is readily broken down in temperatures above 400 °C in a nitrogen atmosphere [113]. For the case study of structural supercapacitor electrodes, part of the process requires high temperatures (up to 800 °C) in nitrogen to carbonise the aerogel precursor which provides a convenient point at which to burn off the mask. However, for more conventional multi-matrix systems this presents a greater challenge as burning of the mask is likely to damage the infused resin as well as potentially damaging the fabric.

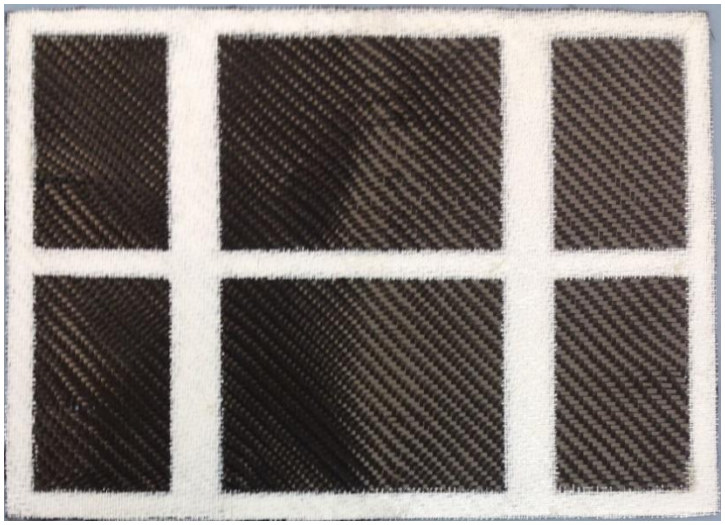

Figure 7.9: PLA masking sample created as a template to make two identical c-section parts, the masked areas will later form the corners of the c-section with the dry fabric exposed to the carbon aerogel. The perimeter of the fabric is also masked to prevent unravelling and make transportation easier

PLA has been trialled as a masking material due to the desirable properties of low melting temperature and low cost. Several samples have been successfully made (see Figure 7.10) for the purpose of protecting hinge regions during the CAG process.

PLA can be decomposed through the use of catalyst-treated polylactide at lower temperatures (order of 200 °C) in evacuated conditions [114], which might serve as an alternative method for removal for systems which cannot be heated to extreme temperatures. Development of a suitable masking material for specific resin systems is required to fully utilize this approach for the majority of conventional matrices. Examples of lamina made through the PLA mask method for structural power composite electrodes are shown in Figure 7.10. In comparison to the barrier method, the masking method is simpler and more reliable as the barrier cannot be 'breached', with an additional benefit that no regions are required to be coated by the barrier resin so smaller regions can be preserved for later matrix infusions. However, refinement of candidate masking materials and effective removal is still yet to be addressed.

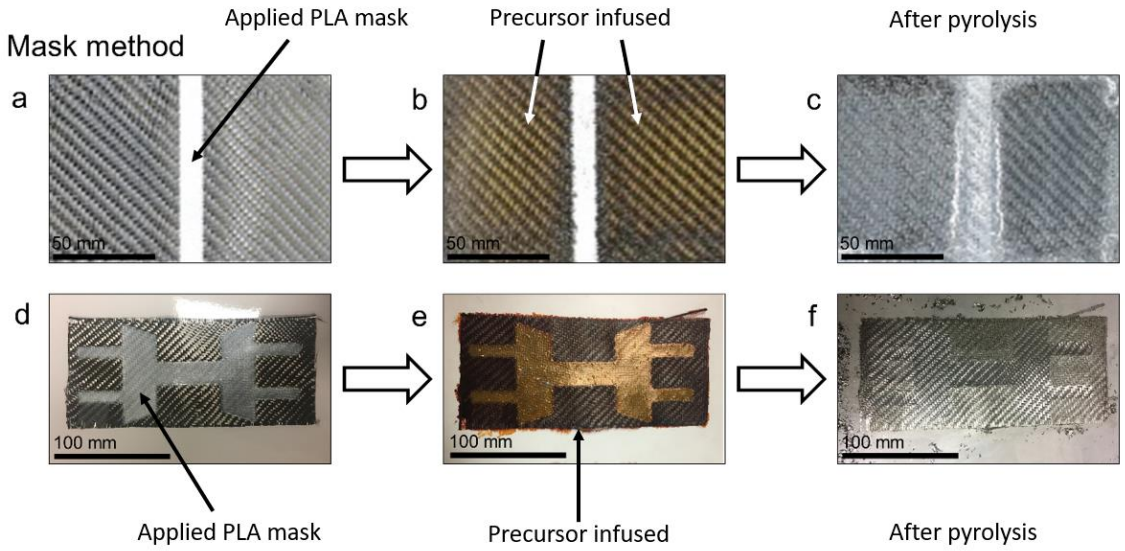

Figure 7.10: Mask method showing (a) PLA (white) hot-pressed into the fabric, (b) the fabric and PLA infused with carbon aerogel precursor, (c) carbonisation of the carbon fibre PLA showing incomplete decomposition of the PLA. (d) A more complicated PLA design was pressed into a fabric (transparent white), (e) following the same aerogel precursor procedure, (f) carbonisation and char from the PLA wiped from the surface to reveal the dry fabric surface below

7.6. C-Section Demonstrator

Demonstration elements to illustrate a simple form, in this instance a L-shaped section, are shown in Figure 7.11 for both the barrier and masking methods. These methods were successful in allowing the carbon aerogel modified fabric to be bent into a shape without inducing cracking or damage to the isolated regions (i.e. absent of aerogel). The barrier method was more successful in these initial tests with the fabric in the untreated areas able to shear without restriction in angles akin to those achievable with as-received fabric. However, a noted issue was the potential impact on structural integrity at the boundaries between the resin barriers and infused resin, since this would create discontinuities which could potentially induce stress concentrations or sites from which damage may initiate. This is an issue which should be evaluated in future studies. The masking method was more limited in its capacity to deform under shear loading, which was attributed to the PLA residue following high temperature removal: the temperature profile needs to be refined to address this issue.

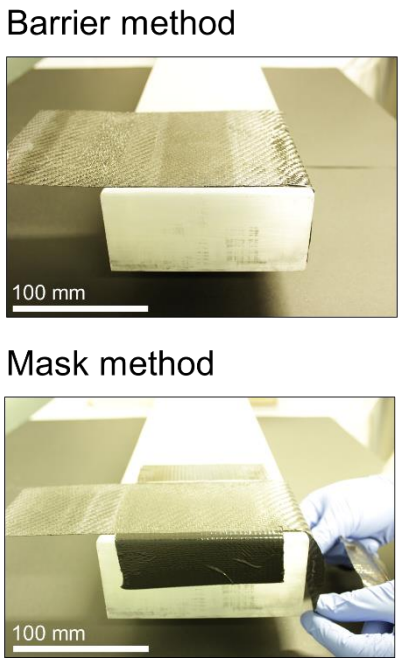

Figure 7.11: Demonstration of the formability of carbon aerogel infused carbon fibre plies using the barrier (top) and mask (bottom) methods to create small regions as fold lines about a C-section tooling piece (radius of curvature 5 mm). Note, in the masking method the addition of duct tape was used to secure the ply to the tooling piece as residual PLA caused some resistance to folding

The primary drawbacks of both the barrier and masking methods are the additional time and complexity in the manufacturing procedure as compared to the more conventional one-step processes, although these methods have been simplified to a very workable and streamlined set of operations. It is anticipated that these methods would be very amenable to automation.

To demonstrate the potential of multi-matrix infusion a small scale demonstrator was created first utilising two matrices, one resin for the corners and one PLA for the flat regions. The PLA was infused first using a printed sheet of PLA which was hot pressed into the fabric. The resin was then infused using an epoxy film applied as strips over the regions of interest. The preform was then shaped over a mould whilst the epoxy was still uncured. The preform and mould were then vacuum sealed to apply pressure and cured in the oven. Note that resin transfer moulding was not carried out as the resin was applied as a film. The completed demonstrator is shown in Figure 7.12. This demonstrator successfully shows proof of concept and allowed for a neat transition between the two matrix regions as well as a relatively simple manufacturing process. However this was a single ply component and further experimentation with multi ply infusion is required.

Figure 7.12: Multi-matrix trial demonstrator, this is only a proof of concept and therefore is not infused with carbon aerogel, however the partitioning between distinct formable and flat zones can be seen

Section 7.7 demonstrates a more complex part which gives greater detail about the manufacturing process and takes this demonstrator further.

7.7. Infusion of Multi-Ply L-Section

In order to further assess the practicality of multi-matrix infusion the barrier method described earlier in this chapter has been trialled in a multi-ply L-Section experiment. The goal of this experiment was to infuse a different matrix material over the corner zone from that of the wider part with the manufacturing goal of improving the corner strength. This investigates the idea of using a stronger matrix material in the stress critical region. Infusion was carried out using vacuum assisted resin transfer moulding (VARTM). The main problem to be addressed was whether the epoxy resin barrier method was manufacturable when multiple plys are used in contrast to the single ply approach demonstrated previously.

This geometry was chosen as it demonstrates the potential for through-thickness failure driven by the stress concentration at a corner, which is a common failure mode in composite structures and typically analysed as a corner unfolding failure mode in spars used, for example, in the aerospace industry.

7.7.1. Experimental Setup

The experiment was set up as shown in Figure 7.13. It consists of 10 plys 0.2mm thick of 320gsm biaxial glass fabric with polyester stitching at 90 degrees.

The glass fabric measuring 320mm x 200mm was formed around a right angle mould with an outer surface corner radius of 10mm. A slightly larger region than that of the fabric was marked out

spanning the corner and a barrier set around this region in accordance with the epoxy film method described in section 7.4, allowing space for a 10mm gap between the sample and the tacky tape.

An epoxy barrier (XPREG XA120 prepreg adhesive film) was embedded into dry fabric to separate the enhanced and basic resin zones similarly to section 7.4. The epoxy was embedded into the fabric using a hot press, this was set to 0.4 MPa at 80 °C. This temperature was chosen to be a low as possible to avoid premature curing whilst still allowing the hex-mesh to be removed and the resin to permeate the fabric well. The curing range for this film material was 80°C to 120°C. Ensuring an effective seal was considered to be more critical than matching exactly the thickness of film to fabric, therefore identical film barriers were embedded into the top of each ply (with the exception of the bottom ply which had one both top and bottom), with the ten ply stack used this equated to 11 matching rectangular epoxy film cutouts. Once the ten ply stack was assembled and laid over the aluminium mould the full stack was again pressed at 0.4 MPa and 80 °C to gently bond the plys together. This was done in two stages for the two flanges of the L-section.

Very careful alignment of epoxy film was required both for the top and bottom surface of the plies and between plies to ensure the barrier made a near straight vertical column through thickness. The final two exposed barrier surfaces on the top and bottom of the stack were then available to form a seal with the upper and lower bagging film, fully isolating the corner region from resin flow.

The stacking sequence was [90, 0/0, 90]5, giving a symmetric balanced layup. This resulted in the polyester stitching layup of [±45]5, which was anti-symmetric. This was unavoidable given the choice of fabric, however this is of little concern as the primary interest here is the effectiveness of the infusion process. Distribution mesh was arranged covering the first 2/3 of the infusion distance. The final third was forced to infuse through the fabric only to ensure that the resin permeates through thickness across the entire sample before reaching the exit tube. This avoids the undesirable scenario where the path of least resistance flows over the sample and never makes it through thickness to the bottom ply. Despite this, through thickness infusion still relies heavily on capillary forces, though the aformentioned precaution allows plenty of time for the resin to permeate.

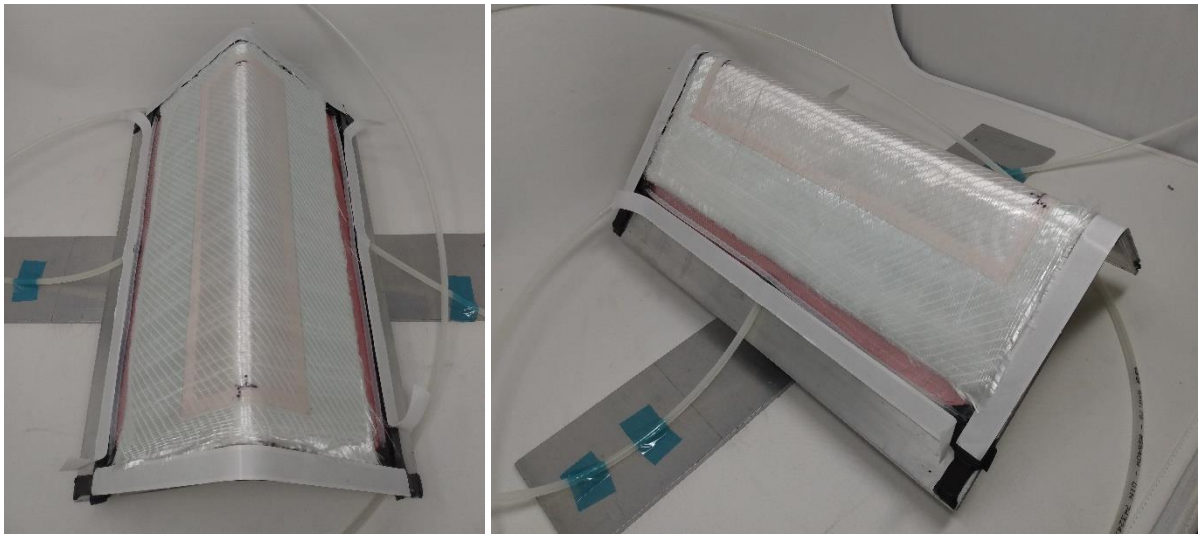

Figure 7.13: L-Section multi-ply sample prepared for infusion, it is formed over an L-section mould with no upper mould applied, resin is infused along the long edge with distribution mesh running two thirds of the distance around the corner and the remainder travelling though the fabric only to ensure through thickness penetration before the outlet is reached

Figure 7.14 provides details of the specifics of the VARTM and barrier layout.

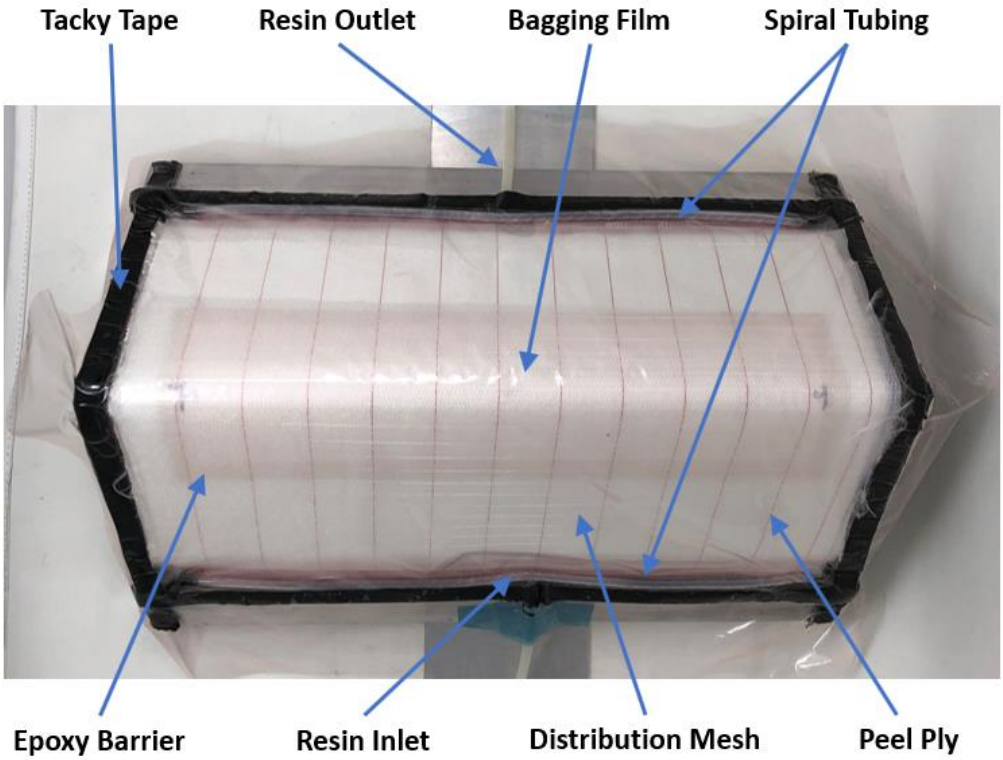

Figure 7.14: Labelled layup diagram, working from the tool face upwards there is firstly lower bagging film, followed by the fabric with integrated barrier-isolated-zone, followed by peel ply, followed by distribution mesh and finally upper bagging film. The upper and lower bagging film are sealed together with tacky tape

The sample was infused firstly with Prime 27, Gurit (GB) resin and extra slow hardener for the wider component, with the corner region kept dry. Once the primary resin was infused and cured the sample is ready for a final standard infusion of a secondary resin covering the corner only. The cure temperature to used for this experiment was 65°C. The sample was placed in the oven before infusion and the resin infused in-situ.

7.7.2. Issues Encountered

As the sample shown in Figure 7.13 was time consuming to make, various small scale tests were carried out in advance with dimensions 200mm x 70mm and just 3 plys to assess the effectiveness of the barrier, all other stages of setup were identical. This was the first time that the barrier method had been attempted with more than one ply. It can be seen in Figure 7.15 that the dry zone around the corner has remained mostly dry with a small area of leakage around the edge.

Figure 7.15: Test sample showing leakage into isolated zone, there is only partial intrusion of resin which is visible are the bottom edge of the corner, the remainder of the corner region remains dry. Sample shown after curing.

This was slightly unexpected as it was assumed that the barrier would either work fully or not at all. It appears that the barrier was not fully effective but that the lack of pressure pathway meant that after a certain amount of leakage into the dry zone the resistance to flow grew greater than the capillary forces and flow stopped. The primary problem leading to the leak appeared to be due to a weak bond between the resin film perimeter and the bagging film isolating the zone. Once the boundary is fully cured it becomes stiff leading to very easy debonding. It was observed that very narrow ‘channels’ were appearing underneath the bagging film allowing resin to seep through.

As the resin film has excellent adhesive properties and is highly viscous (it can be cut with scissors) when uncured it was decided that in further experiments the resin film barrier would be uncured

during infusion, allowing it to cure at the same time as the infused resin. This has the added advantage that it remains compressible allowing the vacuum pressure the push down on the barrier and help to seal any leaks as well as improving any thickness variations over the component. This also has the benefit that the barrier can cure at the same time as the infused resin allowing for a stronger interface [115]. As a secondary measure the width of barrier was doubled from 5mm to 10mm.

It was also noted that it was possible for air to become trapped in the isolated zone, which upon heating would expand and burst the barrier. The transition to leaving the barrier uncured significantly reduced this risk. As an additional measure the isolated zone was pressed (but not cured) one half at a time where possible allowing the majority of trapped air to escape before the barrier was sealed fully.

7.7.3. Results

Figure 7.16 shows the main sample after stage 1 of infusion. Clearly the leakage issue has not been fully resolved, though bearing in mind that the ends would be cut off this remains a functional sample.

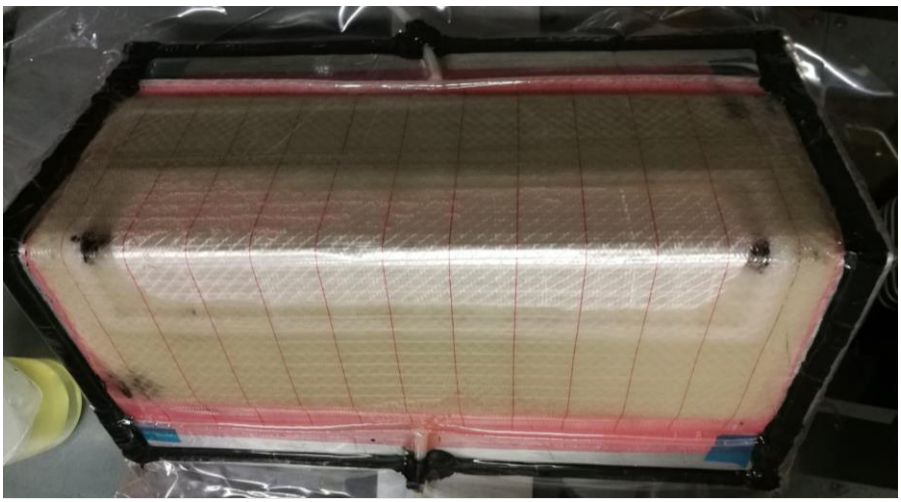

Figure 7.16: Final sample after stage 1 infusion, slight encroachment of the infused resin into the central section can be seen, however the majority of the corner region remains dry. The outline of the resin barrier can be faintly seen showing the level of ingress. Sample shown after curing.

It is most likely that the leakage occurred due to inadequate thickness of resin film being used per ply meaning that the resin barrier failed to fully permeate through thickness. To resolve this it is anticipated that using top and bottom resin film per ply (i.e. twice as many layers of resin film as fabric) would ensure better permeation.

7.8. Discussion

This manufacturing methods presented in this chapter demonstrate an effective technique for producing multi-matrix composites with minimal impact on the complexity of the manufacturing process. These methods are both reliable and simple to implement. Though there are precedents for partial infusion of dry preforms there is no established precedent for (a) making these materials by introducing barriers, (b) making continuously-reinforced TP-epoxy material, c) deploying this method for supercapacitors. Therefore these approaches enable a variety of new options for composite modifications including selective strength enhancement, localised introduction of additives and continuous matrix joints.

The method outlined below achieves the primary goal of enabling a fully repeatable process for the production of segmented composites whilst retaining formability. It is possible to create good quality partitions in terms of resolution of the barriers, and therefore, neat straight boundaries between each matrix material (see Figure 7.7). The process does not require any novel or purpose made equipment and uses conventional resins and bagging materials. The primary drawbacks of the method are the additional time and complexity of the manufacturing procedure when compared to more conventional one step processes, though the approach has been simplified to a very workable set of operations which streamline the process to a reasonable extent. An additional issue is the potential impact on structural integrity as the boundaries between resin barriers and infused resin may create structural weaknesses. However, unlike adhesively bonded interfaces … Finally the extra complexity of the manufacturing process introduced by the need to add barrier requires new automation approaches, though efforts to create the barriers with printed resin have been made.

It remains to be assessed what impact epoxy barriers have on the mechanical strength of the composite. Both the quality of the matrix-barrier interface and the strength of the barrier itself need to be assessed as these are likely to be a key driver behind the overall strength of the component.

The process used to assist with the creation of CAG infused composites for the production of structural supercapacitors has been shown to be effective for the creation of L-section joints. The exploration of more complex geometries including the use of double curvature would be a helpful next step to furthering the application of this technology. This process would itself benefit from numerical forming models to give a clearer insight into the kind of geometries achievable and the percentage CAG coverage achievable.

After careful experimentation with various possible approaches the following guidelines are recommended for the successful creation of resin film barriers:

1. Utilise an epoxy film rather than liquid resin as this significantly reduces spread due to capillary forces during pressing and curing ensuring narrow barriers and neat corners.
2. A top and bottom layer of epoxy film is required for each ply of fabric to ensure adequate permeation through thickness i.e. for a ten ply sample twenty layers of resin film will be needed.
3. Minimum workable barrier thickness is between 6mm and 10mm. Thinner barriers are more likely to fail. Note that this is specific to the NCF E-glass fabric trialled.
4. Each ply must be individually pressed at temperature before being added to the stack.
5. The full stack should be pressed at temperature before infusion to ensure adhesion between plies.
6. The barrier should not be cured prior to infusion of the matrix, this helps to ensure barrier reliability, good bonding between barrier and resin and to avoid thickness variations.
7. The first stage of resin infusion should be carried out when the barrier has achieved gelation but not fully cured.
8. The first stage of infusion should be cured at as low a temperature as possible (e.g. room temperature) to avoid a sudden drop in barrier viscosity prior to the gel point leading to spreading of the barrier into the dry zone.
9. Distribution mesh should be used to provide an easy alternate patch for the flow of resin over the isolated zone.

7.9. Outlook

The demand for processing techniques that can deliver multi-matrix zones within a component is growing, although it is recognised that such components present added complexity in their fabrication. The methods reported here have demonstrated routes to achieving such multi-matrix zoned components, and will offer new opportunities to innovate with polymer composites. For instance, introducing localised toughened or high temperature resistant zones within a component would prolong lifetimes, or allow tighter fit around hot objects (e.g. exhausts). The case study which was the motivation for the work reported here, structural power composites using aerogels as the high surface area component, clearly show a practical use for these masking or barrier methods. In particular, these methods have permitted the introduction of fold-lines allowing the production of complicated structural forms that cannot be achieved using conventional processing route for structural power laminates. These methods pave the way for developing complex structures with complex material requirements and the development and refinement of these procedures, for instance additives and partial pre-curing of the barrier, before consolidation to reduce barrier spreading could change the way in which composites used over a range of applications.

Barrier and masking manufacturing methods demonstrate an effective technique for producing multi-matrix composites with minimal impact on the complexity of the manufacturing process. These methods are and simple to implement, and there is no established precedent for achieving partial infusion of dry preforms, so this approach enables a variety of new options for composite modifications including selective strength enhancement, localised introduction of additives and continuous matrix joints.

It remains to be assessed what impact epoxy barriers have on the mechanical strength of the composite. Both the quality of the matrix-barrier interface and the strength of the barrier itself need to be evaluated, as these are likely to be a key driver behind the overall strength of the component.

A proof-of-concept demonstrator of a component of a structural supercapacitor L-section joint was produced using barrier and masked processes created by compartmentalization the laminate. The exploration of more complex geometries including the use of double curvature would be a desirable next step to furthering the application of this technology. This process would itself benefit from numerical forming models to give a clearer insight into the kind of geometries achievable; expanding the approach it could be used to determine the electrochemically active coverage that is practically attainable in structural power composites with complex geometries.

8. Conclusions and Future Work

This thesis has demonstrated various applications of multifunctional and multi-matrix composites. The overall aim being to pioneer the development of modular infusion and localised formability enhancement to aid the manufacturability of structural supercapacitors and other complex multifunctional parts. The techniques demonstrated here show the options available and are intended to inform the best approach as these advances in composites manufacture are taken up by industry and used in larger scale production, allowing for an increase in the TRL.

8.1. Notable Achievements

Chapter 3 presented the successful trail of formability enhancement using deposited resin to locally modify a preform. Through careful placement of stage-cured resin it was possible to inhibit shearing in certain critical regions and so to drive defects out of the contours of the component, improving the formability of the preform. This technique was shown to be highly sensitive to both patch location and shear stiffness so required careful characterisation of the resin to ensure the optimal shear stiffness where shearing was inhibited. Line patches were shown to be most effective orientated at 45° to the yarn direction, and it was demonstrated that these patches can remain an integral part of the final component when cured rather than requiring removal.

Chapter 4 presented a tool developed to identify the presence of wrinkles numerically, without the traditional reliance on shear angle or human observation. The tool works by comparing the angular rotations of the fabric within the simulation to the desired final angles dictated by the mould. In this way it can identify discrepancies and chain them together to identify wrinkles. It can rank the severity and length of wrinkles to present a shortlist of identified problem areas. This tool is therefore ideally suited to any set of simulations which requires iterative optimisation of forming parameters. The tool was shown to successfully identify wrinkles occurring in various trial simulations.

Chapter 5 presented two new bias extension test characterisation techniques for measuring the shear properties of patch materials. Both techniques shown in the study are promising approaches for characterising the properties of preform enhancements. They are currently demanding both in experimental and simulation time but nonetheless the viscous model especially allows for a good level of accuracy when attempting to accurately model patched fabric shear behaviour. It remains to be explored how well the technique can be carried across to other material combinations. It is clear that for high stiffness patching materials a very low percentage coverage is required in order to obtain results at higher shear angles, in the experiments presented here only the initial behaviour for the shearing of PLA was successfully obtained with the experiment failing at approximately 10°. Obtaining the viscous behaviour of resin film was considerably more successful with the simulations

matching well to the experimental results and a viscosity value was obtained, further work is needed to investigate an accurate value for experimental variability.

Chapter 6 presented simulated attempts to enhance preform formability by local modification in the form of resin patches, in order to inform the experimental process already demonstrated in Chapter 3. It is a simple and practical approach which has good potential for automation. The most challenging aspect proved to be the fine tuning of the various parameters of patch size location orientation and stiffness as well as accurate modelling of fabric behaviour. The method was trialled on two specific geometries, though it proved difficult to match the deformations observed in the experiments with those shown in the simulations, limiting the effectiveness of the simulations as a tool for optimisation. Despite the progress made in Chapter 5 towards characterising the fabric shear behaviour for both dry and patched fabric, it is concluded that the bending behaviour and friction need to be quantified before accurate formability simulation can be achieved.

Chapter 7 demonstrated the concept of segmenting a dry fabric preform using precision placed resin barriers. These allow for the partial, highly localised, liquid matrix resin infusion of a preform whilst retaining a portion of the reinforcement as a dry fabric, thus remaining highly formable until a later stage of manufacture. The challenge was to produce complex shaped engineering structures that may require quite different material inclusions. Multi-matrix composites can be used for various functional and structural applications, for example, local strengthening in the presence of stress concentrators, local conductivity improvement, incorporation of stiffening elements and supercapacitors, which may require quite specific manufacturing steps that are not compatible with the standard process routes for thermosetting matrix composites. The creation of these barriers was successfully demonstrated with both conventional RTM and the Carbon Aerogel infusion process. The technique demonstrated is simple and cheap to implement and has much potential for future larger scale manufacture. This work involved significant collaboration between the University of Bristol and Imperial College London which was a key aim of the EPSRC Future Composites Manufacturing Research Hub to improve knowledge sharing between UK research institutions.

Chapter 7 also demonstrated the successful creation of a 10ply thick L-section composite with a multi-matrix system allowing for a separate matrix resin to be infused into the formable corner section. This was the first successful trial of the epoxy barrier method using multiple plies and demonstrated a viable technique for infusing critical regions of a composite with higher strength resin, a possible alternative to pad-up regions in areas of high stress or stress concentrations such as bolt holes. Importantly this was achieved with a continuous fabric throughout.

Combined these chapters build a framework for the development of formable and defect free multi-functional composites. The novel methodology presented for partitioning fabrics to create multi-matrix composites leads to various configurations some of which restrict formability (Chapter 7).

Predictive modelling is used to anticipate these problems and identify arrangements which allow for mitigation (Chapter 6). It is demonstrated that in some cases deposited resin can also enhance formability (Chapter 3). The automated identification of wrinkles within FEA simulations is explored to maximise the benefit of the predictive models available (Chapter 4). Finally, a novel characterisation method is presented to allow for the effective identification of localised enhancement shear properties (Chapter 5), allowing for more accurate predictive modelling. These developments help to push the potential limits of multi-matrix composite manufacture by allowing for the simulated optimisation of design parameters, this significantly reduces the reliance on physical experiments, and so makes multi-matrix composites a more viable option for manufacturing challenges.

8.2.Further Work

8.2.1. Modular Infusion

The next major step in increasing the TRL of the modular infusion technique demonstrated in Chapter 7 is scaling it up for larger scale production. At present bespoke resin film barriers must be made and two of them pressed individually into each ply followed by a further press for the full stack. These barriers can be made easily using a laser cutter, however the process of removing the backing film and placing on each ply must be done manually. The two clearest paths for automation are either printing barriers onto each ply [94] or creating the full stack and then injecting highly viscous resin at various stages through the thickness. Both of these options provide great potential for streamlining the process leaving only a slightly more complex bagging procedure compared to traditional VARTM. It is anticipated that either of these techniques would provide sufficient simplification for the approach to be viable in large scale manufacturing.

Ongoing work at the National Composites Centre which has been carried out in collaboration with this project investigates the viability of creating barriers using pressure alone by creating a stamp to apply pressure where needed. It remains to be seen whether this proves to be a more time and cost effective method than using epoxy barriers.

8.2.2. Structural Supercapacitors

The largest practical manufacturing barrier to the development of structural supercapacitors is the extreme conditions which the component must be subjected to in order to pyrolyze the carbon aerogel. At present it is required to go to 750 degrees Celsius which is harmful to carbon fibre even in the controlled nitrogen environment. This leads to fibres becoming very brittle and severely compromises the mechanical properties of the finished component. It is anticipated that it will be possible to improve the process to bring the pyrolysis temperature down, making it a more viable procedure. The infused barrier or mask is sacrificed during the process so the only concern is the

structural integrity of the fabric itself. This challenge of pyrolysis temperature is an ongoing area of research at Imperial College London. The process of creating structural supercapacitors is complex, requiring many steps of manufacture and specialised equipment. At present the part must have barriers created or a mask applied, followed by infusion of aerogel and pyrolysis, followed by forming and secondary infusion of structural resin. These main steps are integral, however reduction of the pyrolysis temperature will help to make it more practical without the use of specialised high temperature equipment.

The second significant challenge is to achieve a net weight save compared to the traditional approach of having a separate structure and supercapacitor. This is currently a limitation of the practicality of the component when made. A part of this challenge is the requirement to extract charge from within the structural supercapacitor, for which various methods are being considered, the most likely being a copper wire mesh between plies. It is anticipated that this will enable rapid discharge of the capacitor rather than a gradual trickle flow.

The most valuable further work required for the production of structural supercapacitors is a large scale demonstrator, a proposed c-section design is shown in Figure 8.1. It is proposed in order to demonstrate the concept and attract further interest and investment of research effort. It is hoped that such a demonstrator will show that substantial structurally viable components can be made into commonly used geometries, whilst also having the capacity to deliver significant amounts of power. The c-section approach has been proposed as this allows for large flat regions whilst also helpfully demonstrating the formability concept trialled in this thesis, it is therefore compatible with the current pyrolysis conditions without further refinement required. Due to the relatively large radii it is anticipated that this could be manufactured without any damage to the brittle carbon fibres and subsequently mechanically tested to give a clearer idea of its relative strength compared to conventional carbon fibre composites.

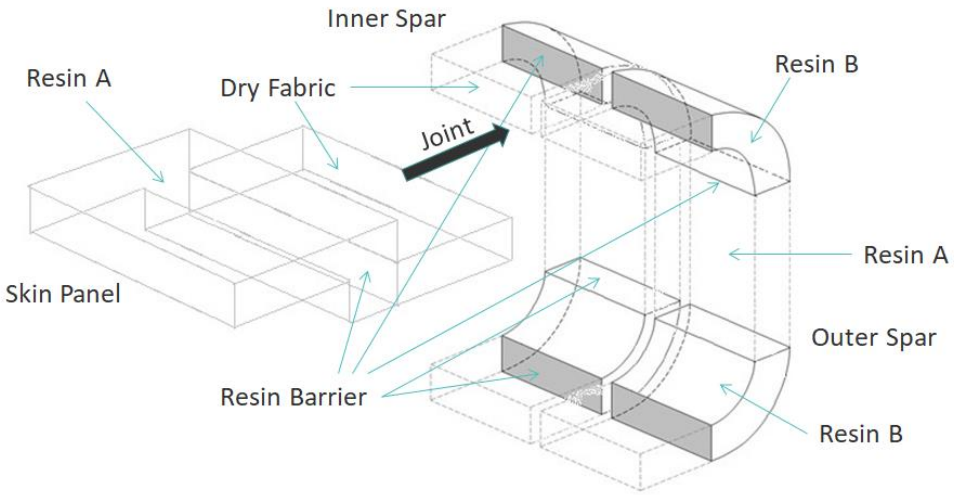

Figure 8.1: Demonstrator proposal showing a spar c-section and flange intersection with structural zones planned for all curved or joint regions and flat zones kept free for the first stage of infusion. This layout demonstrates both the potential for fabric segmentation and continuous matrix joints

From the more general perspective of construction of multi matrix composites a few hurdles still exist. The most significant of these is the need to ensure 100% barrier reliability, as for the multiply example shown in section 7.7 some leakage was still occurring. It is anticipated that this can be tackled initially by either widening the barrier or by doubling up the number of layers of resin film between each ply, this is likely to increase capillary flow of the barriers but make for more a reliable seal. Further to this is the need to ensure barriers remain robust even if they are handled or transported, it is proposed to maintain an uncured barrier allowing the sample and bagging film to be pressed firmly back together before infusion is carried out, in case of any minor leaks. This puts a requirement to either place the sample in a freezer after the barrier has been created or to minimise the amount of time between barrier creation and infusion. It would be beneficial to consider how this would work with printed resin which is considered to be more flexible than resin film but it would not be practical to use this in its uncured state due to extremely low viscosity, meaning some level of cure would be required and out life is considerably lower than that for epoxy film.

Another avenue to explore is to establish the mechanical strength of the interface between the infused epoxy and the barrier itself. A series of mechanical tests on basic shapes such as flat panels or c-sections would be beneficial and could then be compared to continuous epoxy samples to give an idea of whether this degrades the material properties. The structural cohesiveness of multi-matrix composites is an essential part of their benefit, and it is very difficult to achieve a net weight save if the structural strength is reduced significantly. It is hoped that the presence of continuous fibres throughout and the simultaneous curing of the barrier and infused resin will result in very minimal

loss in structural strength, whether this remains the case for partially cured or fully cured barriers is also of significant interest.

8.2.3. Characterisation of Enhancements

The bias extension technique demonstrated in Chapter 5 for characterising patch properties has several options for future work. For high stiffness patching materials it would be of benefit to investigate the effectiveness of the technique for a much lower percentage coverage of material such as 5%, to establish if this allows for the effective extraction of shear behaviour. The existing work hit a limit at 10 degrees for the 50% PLA coverage samples trialled. This would be a helpful step in widening the technique out to covering other types of high stiffness patch such as stitching and tufting.

In addition to the high stiffness experiments there remains some options to be explored in the area of low stiffness viscous modifications such as the resin film demonstrated. The validation of the technique would benefit from a wider data set of experimental data, due to the inherent variation in between samples. This would allow for a clearer estimation of sample spread, range and more accurate averaged results, which would help in establishing the level of accuracy that can be obtained as a viscosity value. A more accurate optical tracking technique would also be beneficial, the DIC system was not successfully used due to the impact of paint on the fabric shear behaviour, it is possible that a different type of painting technique perhaps without a base coat would allow for accurate optical tracking without this impacting the results.

8.2.4. Resin Printing

A possible further step in the process of localised property enhancement would be the transition from resin film to printed resin. This would allow for the automation of the process through pre-programmed liquid resin printer pathways. Experiments in this thesis which attempted this were held back by the lack of control over liquid resin causing poor resolution barriers and patches, and due to inadequate equipment. this step would also allow for larger scale manufacturing and better quality control if further refined. It is anticipated that nothing significant is blocking this avenue of inquiry other than the need for a high quality two part resin printer and the ability to include additives in the resin to closely control viscosity. This would potentially be a more practical approach for multi-ply samples, as resin could be injected sequentially through various depths of the fabric. A further benefit of this approach is the ability to stage cure resin so that a very specific shear stiffness can be achieved allowing the experimental conditions to be matched to simulated optimal stiffness.

One area which was not explored in this thesis is the impact of bending behaviour on the formability of fabrics. though it is generally acknowledged that shear stiffness is the dominant behaviour in the

formability trials shown, bending behaviour does have a notable impact. In this thesis generic values were used based on previous experiments and not specific to the exact fabric and weave architecture utilised. The bending stiffness of patched regions was also approximated on the basis that shear behaviour was of more importance. It would be of benefit to carry out bending stiffness experiments for any fabric used and to identify this value for patched material as well. This is considered to be a relatively simple process as the characterization does not involve any of the complexities of the bias extension test technique shown in Chapter 5.

8.2.5. Wrinkle Detection Algorithm

The wrinkle detection algorithm developed in Chapter 4 has the potential for various further research activities. It remains to be explored in detail exactly how the severity of a wrinkle should be measured. A hybrid technique based on wrinkle length and number of wrinkles was explored here, however it would be very interesting to compare this to experiments and observe the impacts of a different criterion on the behaviour of the sample. Of particular value would be a comparison between the structural impacts of many small wrinkles as opposed to one large wrinkle.

The algorithm itself would benefit from a thorough examination of its ability to cope with various geometric challenges, at present it has been trialled on two geometrical shapes and it was able to distinguish well between wrinkles and larger folds. However, its robustness in more complex geometrical situations is yet to be explored. Complex situations of double curvature are more problematic when comparing the orientation of the mesh with the orientation of the mould. Ideally it would also have the various down-select thresholds calibrated to match experimental data so that's the down select effectively eliminates minor discrepancies which in practise do not constitute a wrinkle.

8.2.6. Localised Formability Enhancement

The primary unexplored area regarding localised formability enhancement is the question of how to automate patch placement in such a way that converges to an optimal solution. The successful formability enhancements showed in this thesis all required some level of human input even though simulations were very helpful for trialling a wide range of setups and comparing their effectiveness. The iterative approach of patch placement could result in the optimization routine compounding problems rather than converging on an improved arrangement. It requires more refinement before it can be claimed to be fully automated. Of particular importance is the ability to significantly reduce the runtime from approximately one hour to nearer 5 minutes so that a significant number of runs can be completed in a small amount of time. There are two primary optimization techniques; firstly running a high number of pre-determined patch locations and honing in on the best scenario and secondly identifying critical zones and targeting patches on the zones. The first of these two techniques is the

most time consuming and could benefit most from runtime optimization. The second technique was found to be less effective as often the best way to eliminate a wrinkle was not to place the patch immediately on top of it but rather somewhere in the proximity.

8.3. Summary

Multifunctionality of composites is a wide field which has many promising areas of development ongoing at present. Overall this thesis has aimed to further the field through the development of multi-matrix structures and by enhancing the formability of dry preforms. The enhancement of preform formability with the placement of locally deposited resin patches is successfully demonstrated experimentally as well as the ability to segment fabrics allowing for multiple stages of infusion with different resins. These are developed with the ultimate goal of improving the flexibility of composite structures and providing gains in weight saving.

The multi-matrix infusion technique was developed initially with the production of structural supercapacitors in mind where formability is especially problematic. Despite this, the technique can be applied to any structure where multiple stages of infusion are beneficial. There remain significant challenges in the production of structural supercapacitors namely the excessive heat required in the pyrolysis process and the ongoing challenge of net weight saving. This thesis has however significantly furthered our understanding of how to form these structures into more complex shapes and demonstrated the concept experimentally.

In the field of formability enhancement experiments showed the effectiveness of the local modification technique for a specific geometry. Various simulation tools are developed within this thesis which complement the approach and allow for some level of optimisation before experiments are carried out. The technique requires further development to understand in detail exactly which geometries it can be effective for and the mechanism by which it acts most effectively.

Combined these advances create a framework for overcoming the additional formability limitations of multifunctional composites, where the inherent formability implications of extra complexity are a significant hindrance to development.

Bibliography

[1] Asp L E, Bouton K, Carlstedt D, Duan S, Harnden R, Johannisson W, Johansen M, Johansson M K G, Lindbergh G, Liu F, Peuvot K, Schneider L M, Xu J and Zenkert D 2021 A Structural Battery and its Multifunctional Performance *Adv. Energy Sustain. Res.* **2** 2000093

[2] Nguyen S, Anthony D B, Qian H, Yue C, Singh A, Bismarck A, Shaffer M S P and Greenhalgh E S 2019 Mechanical and physical performance of carbon aerogel reinforced carbon fibre hierarchical composites *Compos. Sci. Technol.* **182**

[3] Composites Leadership Forum 2016 The 2016 UK Composites Strategy 24

[4] Aerospace Technology Institute 2018 *Insight - Composte Material Applications in Aerospace*

[5] Boeing Commercial Airplanes 2006 Boeing 787 from the Ground Up

[6] Committee on Climate Change 2013 Fourth Carbon Budget Review – technical report *Clim. Chang. Act*

[7] Varkonyi B and Belnoue J P 2019 Predicting consolidation-induced wrinkles and their effects on composites structural performance *Int. J. Mater. Form.* **13** 907–21

[8] Akkerman R, Haanappel S P and Sachs U 2018 History and future of composites forming analysis *IOP Conf. Ser. Mater. Sci. Eng.* **406**

[9] Thompson A J, McFarlane J R, Belnoue J P H and Hallett S R 2020 Numerical modelling of compaction induced defects in thick 2D textile composites *Mater. Des.* **196** 109088

[10] Javaid A, Ho K K C, Bismarck A, Steinke J H G and Shaffer M S P 2018 Improving the multifunctional behaviour of structural supercapacitors by incorporating chemically activated carbon fibres and mesoporous silica particles as reinforcement

[11] Ivanov D S, Le Cahain Y M, Arafati S, Dattin A, Ivanov S G and Aniskevich A 2016 Novel method for functionalising and patterning textile composites: Liquid resin print *Compos. Part A Appl. Sci. Manuf.* **84** 175–85

[12] Nosrat Nezami F, Gereke T and Cherif C 2017 Active forming manipulation of composite reinforcements for the suppression of forming defects *Compos. Part A Appl. Sci. Manuf.* **99** 94–101

[13] Lee J S, Hong S J, Yu W R and Kang T J 2007 The effect of blank holder force on the stamp forming behavior of non-crimp fabric with a chain stitch *Compos. Sci. Technol.* **67** 357–66

[14] Allaoui S, Boisse P, Chatel S, Hamila N, Hivet G, Soulat D and Vidal-Salle E 2011 Experimental and numerical analyses of textile reinforcement forming of a tetrahedral shape *Compos. Part A Appl. Sci. Manuf.* **42** 612–22

[15] Zhu B, Yu T X, Zhang H and Tao X M 2011 Experimental investigation of formability of commingled woven composite preform in stamping operation *Compos. Part B Eng.* **42** 289–95

[16] Boisse P, Hamila N and Madeo A 2016 Modelling the development of defects during composite reinforcements and prepreg forming *Philos. Trans. R. Soc. A Math. Phys. Eng. Sci.* **374**

[17] Chen S, Harper L T, Endruweit A and Warrior N A 2015 Formability optimisation of fabric preforms by controlling material draw-in through in-plane constraints *Compos. Part A Appl. Sci. Manuf.* **76** 10–9

[18] Breuer U, Neitzel M, Ketzer V and Reinicke R 1996 Deep drawing of fabric-reinforced thermoplastics: Wrinkle formation and their reduction *Polym. Compos.* **17** 643–7

[19] Molnár P, Ogale A, Lahr R and Mitschang P 2007 Influence of drapability by using stitching technology to reduce fabric deformation and shear during thermoforming *Compos. Sci. Technol.* **67** 3386–93

[20] Liu L S, Zhang T, Wang P, Legrand X and Soulat D 2015 Influence of the tufting yarns on formability of tufted 3-Dimensional composite reinforcement *Compos. Part A Appl. Sci. Manuf.* **78** 403–11

[21] Döbrich O, Gereke T and Cherif C 2012 Drape simulations: Textile material model for correct property reproduction to improve the preform development process of fiber-reinforced structures *12 th Int. LS-DYNA Users Conf.* 1–10

[22] Hübner M, Diestel O, Sennewald C and Gereke T 2012 Simulation of the Drapability of Textile Semi- Finished Products with Gradient-Drapability Characteristics by Varying the Fabric Weave *Fibres Text. East. Eur.* **5** 88–93

[23] Mouritz A P, Leong K H and Herszberg I 1997 A review of the effect of stitching on the in-plane mechanical properties of fibre-reinforced polymer composites *Compos. Part A Appl. Sci. Manuf.* **28** 979–91

[24] Tam A S and Gutowski T G 1990 The kinematics for forming ideal aligned fibre composites into complex shapes *Compos. Manuf.* **1** 219–28

[25] El Said B, Green S and Hallett S R 2014 Kinematic modelling of 3D woven fabric

deformation for structural scale features *Compos. Part A Appl. Sci. Manuf.* **57** 95–107

[26] Dong L, Lekakou C and Bader M G 2001 Processing of composites: simulations of the draping of fabrics with updated material behaviour law *J. Compos. Mater.* **35** 138–63

[27] Khan M A, Mabrouki T, Vidal-Sallé E and Boisse P 2010 Numerical and experimental analyses of woven composite reinforcement forming using a hypoelastic behaviour. Application to the double dome benchmark *J. Mater. Process. Technol.* **210** 378–88

[28] Lin H, Wang J, Long A C, Clifford M J and Harrison P 2007 Predictive modelling for optimization of textile composite forming *Compos. Sci. Technol.* **67** 3242–52

[29] Boisse P, Hamila N, Vidal-Sallé E and Dumont F 2011 Simulation of wrinkling during textile composite reinforcement forming. Influence of tensile, in-plane shear and bending stiffnesses *Compos. Sci. Technol.* **71** 683–92

[30] Peng X and Ding F 2011 Validation of a non-orthogonal constitutive model for woven composite fabrics via hemispherical stamping simulation *Compos. Part A Appl. Sci. Manuf.* **42** 400–7

[31] Yu W R, Harrison P and Long A 2005 Finite element forming simulation for non-crimp fabrics using a non-orthogonal constitutive equation *Compos. Part A Appl. Sci. Manuf.* **36** 1079–93

[32] Syerko E, Comas-cardona S, Binetruy C, Syerko E, Comas-cardona S, Binetruy C, Syerko E and Binetruy C C 2018 Models for shear properties / behavior of dry fibrous materials at various scales : a review *HAL*

[33] Thompson A J, Belnoue J P H and Hallett S R 2020 Modelling defect formation in textiles during the double diaphragm forming process *Compos. Part B Eng.* **202** 108357

[34] Sharma S B, Sutcliffe M P F and Chang S H 2003 Characterisation of material properties for draping of dry woven composite material *Compos. Part A Appl. Sci. Manuf.* **34** 1167–75

[35] Harrison P, Clifford M J and Long A C 2004 Shear characterisation of viscous woven textile composites: A comparison between picture frame and bias extension experiments *Compos. Sci. Technol.* **64** 1453–65

[36] Barbagallo G, Madeo A, Azehaf I, Giorgio I, Morestin F and Boisse P 2017 Bias extension test on an unbalanced woven composite reinforcement: Experiments and modeling via a second-gradient continuum approach *J. Compos. Mater.* **51** 153–70

[37] Potter K 2002 In-plane and out-of-plane deformation properties of unidirectional preimpregnated reinforcement *Compos. Part A Appl. Sci. Manuf.* **33** 1469–77

[38] Schirmaier F J, Dörr D, Henning F and Kärger L 2017 A macroscopic approach to simulate the forming behaviour of stitched unidirectional non-crimp fabrics (UD-NCF) *Compos. Part A Appl. Sci. Manuf.* **102** 322–35

[39] Wang Y, Chea M K, Belnoue J P H, Kratz J, Ivanov D S and Hallett S R 2020 Experimental characterisation of the in-plane shear behaviour of UD thermoset prepregs under processing conditions *Compos. Part A Appl. Sci. Manuf.* **133**

[40] Dangora L M, Mitchell C J and Sherwood J A 2015 Predictive model for the detection of out-of-plane defects formed during textile-composite manufacture *Compos. Part A Appl. Sci. Manuf.* **78** 102–12

[41] Harrison P 2016 Modelling the forming mechanics of engineering fabrics using a mutually constrained pantographic beam and membrane mesh *Compos. Part A Appl. Sci. Manuf.* **81** 145–57

[42] D1388-14:2015 A 2008 Standard Test Method for Stiffness of Fabrics **i** 1–6

[43] Gereke T, Döbrich O, Hübner M and Cherif C 2013 Experimental and computational composite textile reinforcement forming: A review *Compos. Part A Appl. Sci. Manuf.* **46** 1–10

[44] Boisse P, Colmars J, Hamila N, Naouar N and Steer Q 2018 Bending and wrinkling of composite fiber preforms and prepregs. A review and new developments in the draping simulations *Compos. Part B Eng.* **141** 234–49

[45] Boisse P, Aimène Y, Dogui A, Dridi S, Gatouillat S, Hamila N, Khan M A, Mabrouki T, Morestin F and Vidal-Sallé E 2010 Hypoelastic, hyperelastic, discrete and semi-discrete approaches for textile composite reinforcement forming *Int. J. Mater. Form.* **3** 1229–40

[46] Aimene Y, Hagege B, Sidoroff F, Vidal-Sallé E, Boisse P and Dridi S 2008 A Hyperelastic approach for composite reinforcement forming simulations *Int. J. Mater. Form.* **1** 811–4

[47] Peng X, Guo Z, Du T and Yu W R 2013 A simple anisotropic hyperelastic constitutive model for textile fabrics with application to forming simulation *Compos. Part B Eng.* **52** 275–81

[48] Thompson A J 2017 Multi-Scale modelling of textile composite manufacture *PhD Thesis*

[49] Boisse P, Zouari B and Daniel J L 2006 Importance of in-plane shear rigidity in finite element analyses of woven fabric composite preforming *Compos. Part A Appl. Sci. Manuf.* **37** 2201–12

[50] Lebrun G, Bureau M N and Denault J 2003 Evaluation of bias-extension and picture-frame test methods for the measurement of intraply shear properties of PP/glass commingled fabrics *Compos. Struct.* **61** 341–52

[51] Xiong H, Guzman Maldonado E, Hamila N and Boisse P 2018 A prismatic solid-shell finite element based on a DKT approach with efficient calculation of through the thickness deformation *Finite Elem. Anal. Des.* **151** 18–33

[52] Denis Y, Guzman-Maldonado E, Hamila N, Colmars J and Morestin F 2018 A dissipative constitutive model for woven composite fabric under large strain *Compos. Part A Appl. Sci. Manuf.* **105** 165–79

[53] Vermes B, Thompson A, Belnoue J P H, Hallett S R and Ivanov D S 2018 Mitigation against forming defects by local modification of dry preforms *ECCM 2018 - 18th Eur. Conf. Compos. Mater.* 24–8

[54] Skordos A A, Monroy Aceves C and Sutcliffe M P F 2007 A simplified rate dependent model of forming and wrinkling of pre-impregnated woven composites *Compos. Part A Appl. Sci. Manuf.* **38** 1318–30

[55] Haanappel S P, Thije R Ten and Akkerman R 2010 Forming Predictions of Ud Reinforced Thermoplastic Laminates *14th Eur. Conf. Compos. Mater.* 1–10

[56] Peng X Q and Cao J 2005 A continuum mechanics-based non-orthogonal constitutive model for woven composite fabrics *Compos. Part A Appl. Sci. Manuf.* **36** 859–74

[57] Yu W R, Pourboghrat F, Chung K, Zampaloni M and Kang T J 2002 Non-orthogonal constitutive equation for woven fabric reinforced thermoplastic composites *Compos. Part A Appl. Sci. Manuf.* **33** 1095–105

[58] Xiao H, Bruhns O T and Meyers A 1997 Hypo-Elasticity Model Based upon the Logarithmic Stress Rate *J. Elast.* **47** 51–68

[59] Harrison P, Alvarez M F and Anderson D 2018 Towards comprehensive characterisation and modelling of the forming and wrinkling mechanics of engineering fabrics *Int. J. Solids Struct.* **154** 2–18

[60] Jauffrès D, Sherwood J A, Morris C D and Chen J 2010 Discrete mesoscopic modeling for the simulation of woven-fabric reinforcement forming *Int. J. Mater. Form.* **3** 1205–16

[61] Ferretti M, Madeo A, dell'Isola F and Boisse P 2014 Modeling the onset of shear boundary layers in fibrous composite reinforcements by second-gradient theory *Zeitschrift fur Angew.*

Math. und Phys. **65** 587–612

[62] Hamila N, Boisse P and Chatel S 2009 Semi-discrete shell finite elements for textile composite forming simulation *Int. J. Mater. Form.* **2** 169–72

[63] Hamila N and Boisse P 2007 A meso-macro three node finite element for draping of textile composite preforms *Appl. Compos. Mater.* **14** 235–50

[64] Xiao Z and Harrison P 2021 Design of buckling and damage resistant steered fibre composite laminates using trellis shear kinematics *Compos. Struct.* **260** 113526

[65] Gatouillat S, Barregi A, Vidal-Sallé E and Boisse P 2013 Simulation of composite forming at meso scale *Key Eng. Mater.* **554**–**557** 410–5

[66] Thompson A J, El Said B, Belnoue J P H and Hallett S R 2018 Modelling process induced deformations in 0/90 non-crimp fabrics at the meso-scale *Compos. Sci. Technol.* **168** 104–10

[67] Creech G and Pickett A K 2006 Meso-modelling of Non-crimp Fabric composites for coupled drape and failure analysis *J. Mater. Sci.* **41** 6725–36

[68] Ivanov D S and Lomov S V. 2014 Compaction behaviour of dense sheared woven preforms: Experimental observations and analytical predictions *Compos. Part A Appl. Sci. Manuf.* **64** 167–76

[69] Lomov S V and Verpoest I 2000 Compression of Woven Reinforcements: A Mathematical Model *J. Reinf. Plast. Compos.* **19** 1329–50

[70] Boisse P 2017 Simulations of Woven Composite Reinforcement Forming *Woven Fabr. Eng.* Polona Dobnik Dubrovski 978-953-307-194-7. hal-016

[71] Turk M A, Vermes B, Thompson A J, Belnoue J P H, Hallett S R and Ivanov D S 2020 Mitigating forming defects by local modification of dry preforms *Compos. Part A Appl. Sci. Manuf.* **128**

[72] Boisse P, Hamila N, Guzman-Maldonado E, Madeo A, Hivet G and dell'Isola F 2017 The bias-extension test for the analysis of in-plane shear properties of textile composite reinforcements and prepregs: a review *Int. J. Mater. Form.* **10** 473–92

[73] Zhu B, Yu T X and Tao X M 2007 Large deformation and slippage mechanism of plain woven composite in bias extension *Compos. Part A Appl. Sci. Manuf.* **38** 1821–8

[74] Pourtier J, Duchamp B, Kowalski M, Legrand X, Wang P and Soulat D 2018 Bias extension test on a bi-axial non-crimp fabric powdered with a non-reactive binder system *AIP Conf.*

Proc. **1960**

[75] Krollmann J, Snajdr R, Paz M, Zaremba S and Drechser K 2016 Hybrid-matrix approach: How to overcome the conflict of matrix selection? *AIP Conf. Proc.* **1779**

[76] Quan D, Deegan B, Alderliesten R, Dransfeld C, Murphy N, Ivanković A and Benedictus R 2020 The influence of interlayer/epoxy adhesion on the mode-I and mode-II fracture response of carbon fibre/epoxy composites interleaved with thermoplastic veils *Mater. Des.* **192** 1–10

[77] Cheng X, Xiong J, Peng B, Cheng Z and Li H 2009 Mechanical Properties of RTM-made Composite Cross-joints *Chinese J. Aeronaut.* **22** 211–7

[78] Stanier D, Radhakrishnan A, Gent I, Roy S S, Hamerton I, Potluri P, Scarpa F, Shaffer M and Ivanov D S 2019 Matrix-graded and fibre-steered composites to tackle stress concentrations *Compos. Struct.* **207** 72–80

[79] Hindersmann A 2019 Confusion about infusion: An overview of infusion processes *Compos. Part A Appl. Sci. Manuf.* **126** 105583

[80] van Oosterom S, Allen T, Battley M and Bickerton S 2019 An objective comparison of common vacuum assisted resin infusion processes *Compos. Part A Appl. Sci. Manuf.* **125** 105528

[81] Gillio E F, McKnight G P, Gillespie Jr. J W, Advani S G, Bernetich K R and Fink B K 1999 Processing and properties of co-injected resin transfer molded vinyl ester and phenolic composites *Polym. Compos.* **20** 780–8

[82] Summerscales J and Searle T J 2005 Low-pressure (vacuum infusion) techniques for moulding large composite structures *Proc. Inst. Mech. Eng. Part L J. Mater. Des. Appl.* **219** 45–58

[83] Kruckenberg T, Qi B, Falzon P, Liu X L and Paton R 2001 Experimental and predicted in-plane flow height measurements for stiffened structures made using the resin film infusion process *Sampe J.* **37** 28–34

[84] Uchida H, Yamamoto T and Takashima H 2001 Development of low-cost, damage-resistant composites using RFI processing *Sampe J.* **37** 16–20

[85] Fiedler L, Barré S and Molina J I 2003 TANGO composite fuselage platform *Sampe J.* **39** 57–63

[86] Krollmann J, Alvarado C, Carqueville P, Snajdr R, Zaremba S and Drechsler K 2016 *Hybrid-*

[87] Grancarić A M, Jerković I, Koncar V, Cochrane C, Kelly F M, Soulat D and Legrand X 2018 *Conductive polymers for smart textile applications* vol 48

[88] Turk M A, Cao H, Thompson A J, Belnoue J P, Hallett S R and Ivanov D S 2022 A New Approach to Measuring Local Properties of Preforms Enhanced for Formability *Front. Mater.* **9** 1–16

[89] Ivanov D S, White J A P, Hendry W, Mahadik Y, Minett V, Patel H and Ward C 2015 Stabilizing textile preforms by means of liquid resin print: a feasibility study *Adv. Manuf. Polym. Compos. Sci.* **1** 26–35

[90] Lightfoot J S, Wisnom M R and Potter K 2013 A new mechanism for the formation of ply wrinkles due to shear between plies *Compos. Part A Appl. Sci. Manuf.* **49** 139–47

[91] Allaoui S, Cellard C and Hivet G 2015 Effect of inter-ply sliding on the quality of multilayer interlock dry fabric preforms *Compos. Part A Appl. Sci. Manuf.* **68** 336–45

[92] Wang P, Hamila N and Boisse P 2013 Thermoforming simulation of multilayer composites with continuous fibres and thermoplastic matrix *Compos. Part B Eng.* **52** 127–36

[93] Belnoue J P H, Nixon-Pearson O J, Thompson A J, Ivanov D S, Potter K D and Hallett S R 2018 Consolidation-driven defect generation in thick composite parts *J. Manuf. Sci. Eng. Trans. ASME* **140**

[94] CIMComp 2019 EPSRC Future Composites Manufacturing Research Hub Poster Book 2019 37

[95] Cao J, Akkerman R, Boisse P, Chen J, Cheng H S, de Graaf E F, Gorczyca J L, Harrison P, Hivet G, Launay J, Lee W, Liu L, Lomov S V., Long A, de Luycker E, Morestin F, Padvoiskis J, Peng X Q, Sherwood J, Stoilova T, Tao X M, Verpoest I, Willems A, Wiggers J, Yu T X and Zhu B 2008 Characterization of mechanical behavior of woven fabrics: Experimental methods and benchmark results *Compos. Part A Appl. Sci. Manuf.* **39** 1037–53

[96] Lin H, Clifford M J, Long A C and Sherburn M 2009 Finite element modelling of fabric shear *Model. Simul. Mater. Sci. Eng.* **17**

[97] Matveev M Y, Endruweit A, De Focatiis D S A, Long A C and Warrior N A 2019 A novel criterion for the prediction of meso-scale defects in textile preforming *Compos. Struct.* **226** 111263

[98] Shen H, Yang Y, Wang P, Hong Y, Legrand X, Yang X and Wu I 2020 Effect of tufting technique on sound insulation of multi-layer glass woven fabrics *Mater. Res. Express* **7**

[99] Yu X, Cartwright B, McGuckin D, Ye L and Mai Y W 2006 Intra-ply shear locking in finite element analyses of woven fabric forming processes *Compos. Part A Appl. Sci. Manuf.* **37** 790–803

[100] ten Thije R H W and Akkerman R 2008 Solutions to intra-ply shear locking in finite element analyses of fibre reinforced materials *Compos. Part A Appl. Sci. Manuf.* **39** 1167–76

[101] Hamila N and Boisse P 2013 Locking in simulation of composite reinforcement deformations. Analysis and treatment *Compos. Part A Appl. Sci. Manuf.* **53** 109–17

[102] Wang Y, Belnoue J P H, Ivanov D S and Hallett S R 2021 Hypo-viscoelastic modelling of in-plane shear in UD thermoset prepregs *Compos. Part A Appl. Sci. Manuf.* **146** 106400

[103] Larberg Y and Åkermo M 2014 In-plane deformation of multi-layered unidirectional thermoset prepreg - Modelling and experimental verification *Compos. Part A Appl. Sci. Manuf.* **56** 203–12

[104] Coffin D, Pipes R B and Simáček P First-Order Approximations for the Effective Shearing Viscosities of Continuous-Fiber Suspensions *J Compos Mater 1995;291169–80*

[105] Favaloro A J, Tseng H C and Pipes R B 2018 A new anisotropic viscous constitutive model for composites molding simulation *Compos. Part A Appl. Sci. Manuf.* **115** 112–22

[106] Hjellming L N and Walker J S 1990 Motion of Continuous Fibers through a Newtonian Resin for High Fiber Volume Fraction *J. Compos. Mater.* **24** 853–78

[107] Wang J, Ge X, Liu Y, Qi Z, Li L, Sun S and Yang Y 2019 A review on theoretical modelling for shearing viscosities of continuous fibre-reinforced polymer composites *Rheol. Acta* **58** 321–31

[108] Harrison P, Clifford M J, Long A C and Rudd C D 2004 A constituent-based predictive approach to modelling the rheology of viscous textile composites *Compos. Part A Appl. Sci. Manuf.* **35** 915–31

[109] Faal R T, Sourki R, Crawford B, Vaziri R and Milani A S 2020 Using fractional derivatives for improved viscoelastic modeling of textile composites. Part II: Fabric under different temperatures *Compos. Struct.* **248** 112494

[110] Faal R T, Sourki R, Crawford B, Vaziri R and Milani A S 2020 Using fractional derivatives

for improved viscoelastic modeling of textile composites. Part I: Fabric yarns *J. Compos. Mater.* **54** 3245–60

[111] Lee W, Padvoiskis J, Cao J, de Luycker E, Boisse P, Morestin F, Chen J and Sherwood J 2008 Bias-extension of woven composite fabrics *Int. J. Mater. Form.* **1** 895–8

[112] Qian H, Kucernak A R, Greenhalgh E S, Bismarck A and Shaffer M S P 2013 Multifunctional structural power composites based on carbon aerogel modified high performance carbon fibre fabrics *ICCM Int. Conf. Compos. Mater.* **2013-July** 2238–43

[113] Ohkita T and Lee S H 2006 Thermal degradation and biodegradability of poly (lactic acid)/corn starch biocomposites *J. Appl. Polym. Sci.* **100** 3009–17

[114] Pety S J, Tan M H Y, Najafi A R, Barnett P R, Geubelle P H and White S R 2017 Carbon fiber composites with 2D microvascular networks for battery cooling *Int. J. Heat Mass Transf.* **115** 513–22

[115] Galvez-Hernandez P, Gaska K and Kratz J 2021 Phase segmentation of uncured prepreg X-Ray CT micrographs *Compos. Part A Appl. Sci. Manuf.* **149**

Appendix A

Python script

The python script used throughout this thesis for Abaqus model creation and wrinkle detection is available on the link below.

Data are available at the University of Bristol data repository, data.bris, at:

https://data-bris.acrc.bris.ac.uk/deposits/2erfjhmaqdv252k33b2t91xfc6